PREPARATION AND CHARACTERISATION OF BIMETALLIC CORE-SHELL NANOPARTICLES

by

NIKKI JADE COOKSON

A thesis submitted to

The University of Birmingham

for the degree of

MASTERS IN RESEARCH

School of Chemistry

The University of Birmingham

September 2009

UNIVERSITY OF
BIRMINGHAM

University of Birmingham Research Archive

e-theses repository

This unpublished thesis/dissertation is copyright of the author and/or third parties. The intellectual property rights of the author or third parties in respect of this work are as defined by The Copyright Designs and Patents Act 1988 or as modified by any successor legislation.

Any use made of information contained in this thesis/dissertation must be in accordance with that legislation and must be properly acknowledged. Further distribution or reproduction in any format is prohibited without the permission of the copyright holder.

ABSTRACT

New fields of research in chemistry and physics require improved synthetic techniques for colloidal metal particles. This work reports two novel techniques for synthesising bimetallic core-shell nanoparticles. The first technique is the chemical deposition of transition metal salts onto gold nanoparticle seeds. The transition metals used were platinum, palladium and rhodium. Gold nanoparticle seeds were produced using published methods. The gold nanoparticles were stabilised with either citrate or thiol-based stabilisers and the effects of the different stabilisers were studied. The gold nanoparticle seeds and the bimetallic core-shell nanoparticles were characterised using UV-vis spectroscopy, HAADF imaging, AFM imaging and with cyclic voltammetry.

The citrate-stabilised gold nanoparticle seeds provided a better starting material for the bimetallic core-shell nanoparticles, however this route had problems with aggregation and morphology. The thiol-stabilised gold nanoparticles had a better morphology, but the thiol-stabilisation meant that it was difficult to coat the gold nanoparticles.

The second technique studied was the use of galvanic replacement technique for producing bimetallic core-shell nanoparticles, which provides a novel and rapid technique for coating gold nanoparticle seeds with platinum.

The $Au_{(core)}$-$Pd_{(shell)}$ bimetallic nanoparticle system stabilised with citrate was the most successful of the three bimetallic systems studied, producing core-shell particles of approximately 5 nm in diameter.

ACKNOWLEDGEMENTS

I would firstly, like to thank Dr Sarah Horswell for her support encouragement and enthusiasm and for sharing her expansive knowledge with me. Many thanks as well, to the Horswell and Rayment research groups, especially Anna and Jatin, for their invaluable expertise at AFM and Andrew for always being ready to help with any problem and his witty words of wisdom.

Additionally, I would like to thank Dr Ziyou Li and Zhiwei Wang from the Nanoscale Physics Research Laboratory for their work and assistance involved in electron microscopy analysis for this study.

Lastly, I would like to thank Dan Binks for being supportive, for his no nonsense words of encouragement and for making my days brighter.

CONTENTS

LIST OF FIGURES

Chapter 3

CHAPTER 1 - INTRODUCTION

The purpose of this project was to design a synthesis route for bimetallic core-shell nanoparticles in conjunction with the characterisation of the particles. The characterisation of the bimetallic core-shell particles was carried out with Atomic Force Microscopy (AFM), UV-vis spectroscopy and scanning transmission electron microscopy (STEM) with high angle annular dark field (HAADF) detector. A potential use for the bimetallic core-shell nanoparticles is as catalysts in fuel cells. Bimetallic nanoparticles can offer additional degrees of freedom compared with monometallic nanoparticles by altering their physical properties. This can enable a wide range of applications in technologies such as catalysis [1, 2] and optical devices [3]. At present it is still a significant challenge to control the internal structures and chemical order of bimetallic nanoparticles, particularly bimetallic nanoparticles with sizes smaller than 5 nm [3]. A controlled study of synthesis of $Au_{(core)}$-$Pd_{(shell)}$ bimetallic nanoparticles via a chemical reduction route of nanoparticle seed and experiments using citrate and thiol-stabilised gold nanoparticle seeds as a starting product for $Au_{(core)}$-$Pt_{(shell)}$, $Au_{(core)}$-$Rh_{(shell)}$ and $Au_{(core)}$-$Pd_{(shell)}$ bimetallic nanoparticles is presented here. This work also includes the reproduction of gold nanoparticle synthesis as shown by Brown *et al*.[4] and Yang *et al*.[5].

This thesis consists of six chapters: Introduction, Experimental Methods, Citrate-Stabilised Particles, Thiol-stabilised particles, Electrochemical Deposition of Platinum onto Gold Nanoparticles and Conclusions.

The Introduction covers the following areas: aims of the project, a discussion of nanoparticles; including growth and nucleation, bimetallic nanoparticles, core-shell type nanoparticles, different methods for generating nanoparticles and bimetallic

nanoparticles, and different methods for characterising nanoparticles including AFM, UV-vis spectroscopy electron microscopy and electrochemistry will also be discussed.

1.2 Aims of the Project

The main aim of this project was to develop a synthesis route for the production of bimetallic core-shell type nanoparticles for use in fuel cell applications. The aim was to make bimetallic core-shell nanoparticles of between 2-10 nm in diameter and of high monodispersity. It is imperative that the particles are more catalytically active then monometallic nanoparticles, as this would have implications for the cost-effectiveness of bimetallic nanoparticles. An important part of the project is the characterisation of the particles, without which the size, monodispersity and shape characteristics could not be determined. This was carried out with first UV-vis spectroscopy and STEM. Other methods for characterizing the nanoparticles included cyclic voltammetry and AFM.

1.3 Nanoparticles

A nanoparticle is defined as a particle in the nanoscale size range. For transition metal nanoparticles, the decrease in size to the nanometre length scale increases the surface-to-volume ratio. This, together with the ability to make them in different sizes and shapes, makes them potentially useful in the field of catalysis [6]. Nanoparticles have been shown to possess structural, electronic, dielectric, magnetic, optical and chemical properties that are different from the corresponding

bulk materials. These properties exhibit strong size variations [7]. The systematic adjustment of the reaction parameters, such as reaction time, temperature, concentration and the selection of reagents and surfactants can be used to control the size and shape of the nanoparticles [6].

1.4 Nucleation and Particle Growth

The chemical growth of nanometre-size materials involves the processes of precipitation of a solid phase from solution. There are three types of nucleation processes: homogenous nucleation, heterogeneous nucleation and secondary nucleation. Homogenous nucleation occurs in the absence of a solid interface by combining solute molecules to produce nuclei. For a particular solvent, there is a certain solubility for a solute, when the addition of any excess solute will result in the formation and precipitation of nanoparticles. For nucleation to occur, the solution must be supersaturated [6].

1.5 Nanocatalysis

Nanocatalysis is when nanoparticles are used to catalyse a reaction. Many important reactions are strongly dependent on noble-metal catalysis, such as electrochemical reactions on the platinum electrode in proton-exchange membrane fuel cells (PEMFCs) [1, 8]. The application of bimetallic nanoparticles as catalysts is one of the most active areas of nanoscience [7]. The use of bimetallic nanoparticles may give rise to synergism, when the particles are used in catalysis. This is where the combination of two different metals gives rise to an enhancement of specific properties. These properties may be different to those of pure elemental particles, and can include unique size-dependent optical, electronic and catalytic effects. This has led to applications in electronics and engineering as well as catalysis [9, 10]. Bimetallic nanoparticle catalysts provide a way to utilize smaller amounts of expensive catalyst material, by using a less expensive metal for the core material.

Being of the nanoscale has an advantage over bulk materials, in that a larger portion of the atoms are used in the catalysis process, as a larger surface area is provided.[6]. Nanoparticles are used as the catalysts in fuel cells [11]. Nanoparticles have a large surface-to-volume ratio compared to bulk material, this is one of the things that makes them good catalysts. For example, the most favourable size for platinum-based electrocatalysis is in the range of 2-4 nm [8].

Bimetallic nanoparticles often improve the selectivity and rates of metal-catalysed reactions. For example, the hydrogenation rate of simple olefins is increased in the presence of palladium catalysts containing 20% gold, when compared with monometallic palladium catalysis [12].

When nanoparticles are stabilised with polymers, which leads to satisfactory particle distribution, the presence of high-molecular-weight polymers is likely to be detrimental to the catalytic properties of such particles. Citrate, however, is relatively small in size, and cannot function as a steric stabiliser; it is more likely to be stabilizing nanoparticles via electrostatic interaction [13]. Citrate stabiliser is less likely to be a hindrance during catalysis.

1.6.1 Production of Gold Nanoparticles

Gold nanoparticles are of interest as a potential core for bimetallic core-shell nanoparticles, as they are more economically viable than the metals that are generally used for catalysis. Gold particles are not difficult to synthesize. Zhao and Xu chose gold as a core for their Au-Pt core-shell nanoparticles because it is inert in acid electrolytes and its surface favours deposition of platinum [8, 14].

Brown *et al*. synthesized gold nanoparticles of mean diameter 2.6 to 100 nm, using a seeding technique. They compared the use of citrate and hydroxylamine as reductants. The citrate seeded particles were highly uniform in size; however, the hydroxylamine seeded gold colloids produced two distinct populations of large spheres and small rods [4]. They found that the 2.6 nm diameter seeds had a standard deviation of ~1 nm. The citrate method of developing gold nanoparticles was first developed by Turkevich *et al.* [15]. This is one of the best-known methods for producing gold nanoparticles and involves reducing $HAuCl_4$ with sodium citrate. The citrate acts as the reductant and as the stabiliser [2, 15].

Brust *et al*. synthesised thiol-derivatized gold nanoparticles in a two-phase liquid-liquid system. They used sodium borohydride to reduce $AuCl_4^-$ in the presence of alkanethiol, this produced particles of 1-3 nm diameter [16].

Yang *et al*. used a combination of seeding growth and digestive ripening to achieve precise control of monodispersed gold nanoparticles. They used alkyl amines to allow the stabilization and thermal reduction of $HAuCl_4$. They were able to generate gold nanoparticles of various sizes, (2.1-8.8 nm), specifically the particle sizes of 2.1±0.97 nm and 3.1±0.26 nm are of interest for this study. A change in the colours of the sols was also noted. For the particles of 2.1 nm diameter, the sol was brown, for that of 3.1 nm, the sol was red [5].

1.6.2 Production of Platinum Nanoparticles

Platinum nanoparticles have been extensively studied for their catalytic properties. For example, platinum is a highly useful industrial catalyst for reducing automobile pollutant gases, for producing hydrogen from methane and in the direct methanol fuel cell [17].

Furlong *et al*. prepared stable aqueous colloidal platinum sols by citrate reduction. They found that with increasing heat during the reaction gave an increase in particle size. They were able to make particles as small as 4 nm [18].

Henglein *et al*. produced different Pt colloidal sols by utilizing radiolysis, hydrogen reduction and citrate reduction as described by Turkevich *et al*. [19]. Radiolysis gave particles with a mean diameter of 1.8 nm, hydrogen reduction gave 7.0 nm and citrate reduction gave particles with a mean diameter of 2.5 nm. They found that citrate acts not only as a reductant, but also as a stabiliser for the Pt

colloidal sols formed [20]. This was also the case for citrate reduced gold nanoparticles [2, 15].

Lin *et al*. produced citrate-stabilised platinum nanoparticles of 2-3 nm average size, with approximately ±2 nm distribution via methanol reduction [13].

Luo and Sum devised a single-step heat-treatment method for the production of poly(vinylalcohol) (PVA) stabilised platinum nanoparticles with diameters of 2-7 nm. The PVA acted as both the reductant and the stabiliser [21].

1.6.3 Production of Palladium Nanoparticles

Palladium nanoparticles can be produced using the following methods: solution thermolysis, sonochemical methods, electrochemical methods and radiolysis [22].

1.7 Bimetallic Nanoparticles

Bimetallic nanoparticles are the combination of two metals of the nanoscale size range. This area of nanoscience is of interest in the field of catalysis as bimetallic nanoparticles can exhibit synergistic effects.

Bimetallic nanoparticles can be classified into four types of mixing patterns: core-shell nanoparticles, sub-cluster nanoparticles, mixed nanoparticles and multishell nanoparticles. Core-shell nanoparticles consist of a shell of one type of atom surrounding a core of another type of atom [9].

1.7.1 Production of $Au_{(core)}$-$Pd_{(shell)}$ Bimetallic Nanoparticles

Bimetallic nanoparticles are generally synthesized in one of two ways: simultaneous or sequential reduction of appropriate precursors [12]. A number of methods have been developed for synthesizing $Au_{(core)}$-$Pd_{(shell)}$ bimetallic nanoparticles.

Cao *et al*. investigated kinetically controlled platinum deposition onto colloidal gold particles that self assembled onto substrates, to produce $Au_{(core)}$-$Pt_{(shell)}$ nanoparticles. Hydroxylamine hydrochloride was used as the reducing agent. They found that the platinum deposition was isotropic and uniform on each particle, with a standard deviation of approximately 10% for core-shell particles of 13 and 16 nm. They found that the deposition was kinetically controlled and that kinetic analysis revealed that the growth rate of the core-shell nanoparticles depends on the concentration of platinum salt ($PtCl_6^{2-}$), the molar mass and density of the platinum metal, as well as a constant associated with the surface reaction [23].

Knecht *et al*. have discussed different ways of forming Au-Pd bimetallic nanoparticles. The reduction of metallic precursors can either by initiated by the polyol method or by addition of borohydride. The polyol reduction often results in the formation of $Au_{(core)}$-$Pd_{(shell)}$ nanoparticles, because of the difference in the reduction potentials of gold and palladium. The gold is easier to reduce and provides a seed for the palladium to be reduced on. The sizes of the core and shell can be controlled by the ratio of gold:palladium used during synthesis [12].

Kim *et al*. synthesized $Au_{(core)}$-$Pd_{(shell)}$ by first producing monodispersed gold-core particles having approximately 75 nm diameters, by conventional citrate

reduction. These cores were coated with palladium to give core-shell particles with diameters in the range of 100 to 600 nm, with controllable palladium shell thickness [22].

1.7.2 Production of $Au_{(core)}$-$Pt_{(shell)}$ Bimetallic Nanoparticles

Xhao and Xu deposited very small platinum particles onto gold particles, which were then loaded on to a conventional carbon support, for use as an electrocatalyst in PEMFCs. The deposition of platinum onto gold nanoparticles was carried out by reducing $K_2[PtCl_6]$ with hydrogen in a colloidal solution of gold nanoparticles with a narrow size distribution (10 nm ±1.2 nm), in the presence of polyvinylpyrrolidone (PVP) stabiliser [8].

Kumar and Zou prepared 3 nm diameter colloidal gold as demonstrated by Brown *et al*. [4]. They then used 3-aminopropyltrimethoxysilane to attach the colloidal gold to ITO glass slides via surface derivatization. Platinum films were deposited on to the colloidal gold by means of the galvanic replacement technique [11].

Henglein produced $Au_{(core)}$-$Pt_{(shell)}$ and $Pt_{(core)}$-$Au_{(shell)}$ bimetallic nanoparticles using hydrogen reduction and radiolysis techniques. These particles are of interest due to their catalytic properties [24].

Akita *et al* produced $Au_{(core)}$-$Pd_{(shell)}$ bimetallic nanoparticles with a diameter of 13±3.2 nm via a sonochemical technique [1].

1.8 AFM – Atomic Force Microscopy

Atomic force microscopy (AFM) was invented in 1986 by G. Binnig and co-workers at Stanford University. AFM is an offshoot from the scanning tunnelling microscope (STM) [25]. The use of AFM has an advantage over electron microscopy, as it can be done in ambient conditions and does not require the samples to be placed under vacuum

Tapping mode was chosen for imaging samples in this study as it is a good technique for imaging fragile samples. The use of tapping mode can overcome problems associated with friction, adhesion and electrostatic forces by alternately placing the tip in contact with the surface to provide high resolution and then lifting the tip off the surface to avoid dragging the tip across the surface [26].

1.8.1 The Principles of AFM

The principles behind AFM are very straightforward. An atomically sharp tip is scanned over a surface with feedback mechanisms that enable the piezo-electric scanners to either maintain the tip above the sample surface at a constant force or a constant height, to obtain height or force information respectively. AFM can be classified into 3 modes by the interaction of the tip and the sample surface: contact mode, non-contact mode and tapping mode [27].

The nanoscope AFM head utilises an optical detection system in which the tip is attached to the base of a reflective cantilever. A diode laser is focused onto the back of a reflective cantilever. As the tip scans the surface of the sample, moving up and down with the contour of the surface, the laser beam is deflected off the attached

cantilever into a dual element photodiode. The photodetector measures the difference in light intensities between the upper and lower photodetectors, and then converts to voltage [28].

1.8.2 Tapping Mode

Tapping mode allows high resolution topographic imaging of sample surfaces. Tapping mode prevents the tip from sticking to the surface and causing damage during scanning. Unlike other modes, when the tip contacts the surface, it has sufficient oscillation amplitude to overcome the tip-sample adhesion forces and the sample surface is not pulled sideways by shear forces since the applied force is always vertical.

Tapping mode imaging is conducted in air by oscillating the cantilever assembly at or near the cantilever's resonant frequency using a piezoelectric crystal. The piezo motion causes the cantilever to oscillate with a high amplitude when the tip is not in contact with the surface. The oscillating tip is then moved toward the surface until it begins to tap the surface. During scanning, the vertically oscillating tip alternately contacts the surface and lifts off. As the oscillating cantilever begins to intermittently contact the surface, the cantilever oscillation is necessarily reduced due to energy loss caused by the tip contacting the surface. The reduction in oscillation amplitude is used to identify and measure surface features [26].

1.8.3 AFM in Characterising Nanoparticles

Kumar and Zou used AFM in the characterisation of their platinum-overlayer-coated gold nanoparticles, which were produced by deposition of platinum onto 3 nm diameter gold nanoparticles, by galvanic displacement technique. They used the AFM technique to visually assess the platinum loading onto the gold nanoparticles [11]. Joseph *et al*. used AFM to determine film thickness and morphology of 1,9-nonanedithiol and doceylamine stabilised nanoparticles [29].

1.9 UV-vis Spectroscopy in Nanoparticle Characterisation

Michael Faraday was the first to identify finely divided metal particles as the source of the colour of colloidal solutions, specifically gold solutions [30]. Colloidal dispersions of metals exhibit absorption bands or broad regions of absorption in the ultra-violet/visible range. These arise because of excitation of plasmon resonances or interband transitions and are a characteristic property of the metallic nature of the particles [31]. The surface plasmon resonance was explained by Mie in 1908, including linear optical properties such as extension and scattering of small metal particles [32].

UV-vis spectroscopy can be used to determine size and elemental information from colloidal sols of metallic nanoparticle systems. The UV-vis absorption spectra of a metal nanoparticle systems is dependent on the size of the nanoparticles [6]. A good example of this is gold. Gold nanoparticles display distinctive optical plasmon absorbances in the visible range, with size and shape dependent properties [3, 33]. Optical spectroscopy has been widely used to characterise Au-Ag nanoparticle

systems [3]. Creighton and Eadon have calculated UV-vis absorption spectra for metallic nanoparticles of between 3 and 20 nm. These calculations have been performed for metals including gold, platinum, palladium and rhodium. This was achieved by using the optical constants of the metals according to Mie theory. They noted that rhodium and platinum exhibit only rather broad absorption continua that extend throughout the visible-near ultraviolet range and that the colloids of these metals are brown or grey [31]. The size range used by Creighton and Eadon (3-20 nm diameter) was chosen as within this range there is not a strong dependence of the absorption spectra on the particle size. However, they did note that for experimental colloids there are likely to be broadenings of the spectra due to polydispersity, partial aggregation or irregular-shaped particles [31].

1.9.1. UV-vis Spectra of Nanoparticles

Turkevich et al. have demonstrated that colloidal gold has an absorption maximum at 522 nm, which falls to half the value of the maximum at 470 nm and steadily rises into the ultraviolet to the limits of detection at 210 nm. The gold colloid sols were observed to have “a ruby red colour”. It was also shown that as the size of the gold nanoparticles increased, the absorption maximum gradually shifts to the red. When Turkevich et al. examined gold nanoparticles with irregular shapes, the absorption band becomes flattened [31]. Henglein states that colloidal dispersions of gold have a red colour when the particles are larger than about 3 nm [34]. Brown *et al*. found that the λ_{max} increases with increasing particle size, however, this increase is not dramatic. For example, they found that with a size increase from 19 nm to53 nm a red-shift of only 14-nm λ_{max} was observed [4].

Henglein *et al.* used the calculations performed by Creighton and Eadon [31] to show that there should be a peak in the absorbance of colloidal platinum at about 215 nm. For platinum nanoparticles produced by a radiolysis method, the peak at 215 nm was observed. However, for platinum nanoparticles produced using citrate sols the peak was not observed, just a continuous absorbance into the visible-near ultraviolet range [20, 24].

Kim *et al*. recorded a λ_{max} at 230 nm for their palladium particles, which is characteristic for palladium nanoparticles less than 10 nm in size. They also recorded a plasmon absorption band at 560 nm for the citrate reduced gold nanoparticles ~75 nm in diameter. They found that the gold absorption band disappeared completely as the palladium shell formed [22].

Lopez-Sanchez *et al*. recorded UV-vis spectra for Au and Pd sols in water. For the Au sols, they found a plasmon resonance band at 505 nm, characteristic of gold nanoparticles of a size below 10 nm. The Pd sols displayed no surface plasmon band [35].

1.9.2. UV-vis Spectra of Bimetallic Nanoparticle Systems

Henglein has described Pt-Au and Au-Pt core-shell type bimetallic nanoparticles, prepared using reduction and radiolysis techniques. Optical absorption spectra were recorded for varying ratios of Au:Pt and Pt:Au. The core particles were found to have a narrow size distribution of approximately 12 nm. Henglein found that the spectrum of the Pt particles exhibited an increasing absorption toward shorter wavelengths until a maximum is reached at around 215 nm. When gold was deposited onto the platinum particles, the plasmon band of gold appeared at 504 nm,

and this band increased in absorbance as more gold was deposited. A similar scenario was seen for the $Au_{(core)}$-$Pt_{(shell)}$ particles. It was seen that with increasing deposition of Pt the plasmon band of gold was damped and moved towards a shorter wavelength, until it is positioned at 510 nm. The increased deposition of Pt eventually results in the disappearance of the gold plasmon band, indicating that the unstructured behaviour of the Pt dominates [8, 24].

A similar scenario was found by Ferrer *et al*. when they analysed their $Au_{(core)}$-$Pd_{(shell)}$ bimetallic nanoparticles with UV-vis spectroscopy. A very pronounced absorption peak, characteristic of gold, was obtained, but by increasing the concentration of palladium, the intensity of the surface plasmon resonance peak associated with gold faded away [36].

Lopez-Sanchez *et al*. found that when they mixed the Au and Pd sols they had produced, the spectrum of a mixture of the two metal sols indicated the disappearance of the Au surface plasmon band [35]. This indicated that the palladium was dominating the optical properties of the mixture.

1.10 Electron Microscopy

Electron microscopy is widely used to characterise nanoparticles. The particles generated by this study were analysed using Scanning Transmission Electron Microscopy (STEM). This is a mode of transmission electron microscopy in which the electron beam is scanned across the sample. STEM was used in conjunction with the High Angle Annular Dark Field (HAADF) technique (also known as “Z-contrast”), to determine the internal structure of the bimetallic nanoparticles, based on the different electron scattering powers of different elements [1, 9]. Akita

and co-workers characterised their $Au_{(core)}$-$Pd_{(shell)}$ nanoparticles using the Z-contrast of the particles (Au:79 and Pd:46) from ADF-STEM [1].

High Resolution TEM (HRTEM) was also used to analyse some of the particles created during this study. HRTEM offers resolution down to the angstrom scale and allows information to be obtained on the structure of the nanoparticles [9].

1.11 Electrochemical Underpotential Deposition (UPD)

Depending on the substrate, a platinum monolayer can have a higher reactivity than bulk platinum, which can be a useful feature for nanocatalysis [11] and cost effectiveness. The deposition of metals in the UPD process occurs as a spontaneous irreversible redox process in which a Cu adlayer, obtained by UPD, is oxidised by more noble metal cations, which are reduced and simultaneously deposited. It is important that the substrate metal is more noble than the metal undergoing deposition, to avoid being oxidised in the redox reaction [37].

Kumar and Zou used the galvanic replacement technique to coat 3 nm diameter gold nanoparticles immobilised on ITO glass slides with a platinum film. They found that with increasing platinum coating thickness, by repeating the galvanic replacement cycle, the hydrogen adsorption/desorption peak grows, indicating the surface area is increasing with successive cycling [11, 14].

Mrozek *et al* prepared platinum films on roughened gold electrodes by utilising spontaneous redox replacement of an underpotential deposition copper or lead monolayer [14].

Cavalleri *et al*. studied the electrochemical Cu deposition on Au (111) surfaces covered by self-assembled monolayers. They found that the presence of the thiols strongly interfered with the Cu deposition process [38].

CHAPTER 2 - EXPERIMENTAL METHODS

2.1 Introduction to Experimental Methods

This chapter details the experimental methods used in this work to produce bimetallic core-shell nanoparticles of less then 10 nm diameter in size.

The bimetallic core-shell particles were produced by sequential reduction. Initially gold seeds were produced. Gold was chosen for the core material as it is relatively inexpensive and is suitable for metallic reduction on its surface. The first gold nanoparticle seeds were produced as described by Brown *et al*. [4], who reported a particle size of 2.6±1 nm for citrate-stabilised gold seeds. The gold seeds produced were in the size range of 2-8 nm. These gold seeds were coated using an adaptation of the chemical deposition method developed by Cao *et al*. [23]. The gold seeds were coated individually with platinum, palladium and rhodium salts respectively. This method did produce bimetallic core-shell nanoparticles; however the particles were of poor monodispersity and they were highly agglomerated. Further studies were carried out using the citrate-stabilised gold seeds and it was found that by increasing the amount of palladium used during the chemical deposition reaction, that the shell thickness of the $Au_{(core)}$-$Pd_{(shell)}$ bimetallic nanoparticles was increased.

As the monodispersity of bimetallic product was poor, it was decided to use gold seeds with a better monodispersity, in the hope that a more uniform starting product would result in better monodispersity and shape of the bimetallic end product

Thiol-stabilised gold seeds with a diameter of 3.1 nm (standard deviation of 0.26) were produced as reported by Yang and co-workers [5]. The gold seeds

produced had a size of 3.6±0.7 nm and looked very similar in appearance to those described by Yang and co-workers. The method designed by Yang *et al*.[5] is primarily a seeding method, with various growth stages, which involve more gold being coated onto the seeds to create larger particles. This method was adapted to produce $Au_{(core)}$-$Pd_{(shell)}$ by replacing the gold salt in the growth stage for a palladium salt. Also, this method was adapted to try and produce platinum and rhodium nanoparticles by replacing the gold salt in the seeding stage for either platinum or rhodium respectively.

In addition to these experiments, platinum was coated on to the citrate-stabilised gold nanoparticles and the thiol-stabilised gold nanoparticles using the galvanic replacement technique as described by Kumar and Zou [11].

2.2 Reagents

Sodium hexachlororhodate (III) ($Na_3RhCl_3 \cdot 12H_2O$) 99.99% , potassium tetrachloroplatinate (II) (K_2PtCl_4) 99.99%, dihydrogen hexaxhloroplatinate (IV) (H_2PtCl_6) 99.999%, potassiumtetrachloropalladate (II) (K_2PdCl_4) 99.99%, hydrogen tetrachloroaurate (III) trihydrate ($HAuCl_4 \cdot H_2O$) 99.999%, and trisodium citrate dihydrate ($C_6H_5Na_3O_7 \cdot 2H_2O$) 99%, were obtained from Alfa Aesar. Analytical reagent grade absolute ethanol (C_2H_5OH) 95%, toluene ($C_6H_5CH_3$), sulphuric acid (H_2SO_4) >95%, and nitric acid (HNO_3) 70%, were obtained from Fischer Scientific. Potassium chloride (KCl) and hydrogen peroxide (H_2O_2) were obtained from BDH. Perchloric acid ($HClO_4$) (70% distilled) was obtained from Sigma-Aldrich. Nafion, perfluorinated ion-exchange resin 5% wt. in mixture of lower aliphatic alcohols and H_20 (45%)), 1-

dodecanethiol ($C_{12}H_{25}SH$) and trioctylamine ($C_{24}H_{51}N$) were obtained from Aldrich. Copper (II) sulphate pentahydrate ($CuSO_4 \cdot 5H_2O$) (99%) was obtained from Fluka.

All glassware was cleaned using hot concentrated acid (1:1 H_2SO_4/HNO_3) and rinsed with ultrapure water. Water was purified using a tandem Elix Milli Q Gradient A10 Millipore system (resistivity >18.2 MΩ cm, TOC <5 ppb). Teflon pieces were cleaned with piranha solution, followed by rinsing with copious amounts of ultrapure water. Rotating disk electrode surfaces were cleaned by polishing sequentially with 1.0, 0.3 and 0.05 μm alumina slurry in water, followed by electrochemically cycling in 0.05 M sulphuric acid. This solution was prepared from Arista grade sulphuric acid (BDH) and Milli Q water. All aqueous solutions were prepared using Milli-Q water from the Millipore purification system.

2.3 Instrumentation

Transmission electron microscopy was performed with a 200kV Tecnai F20 TEM-STEM. UV-vis absorption spectra were obtained with a CamSpec M550 double beam spectrophotometer. Silica cells were used, with water as a reference except for those samples from methods 5-7, where ethanol was used, as the samples were redispersed in ethanol. Atomic force microscopy (AFM) images of nanoparticles assembled on mica were obtained using a PicoPlus II scanning probe microscope (Molecular Imaging). Cyclic voltammograms were recorded in a conventional three-electrode glass cell using a rotating disk electrode (RDE) (Pt, Au or glassy carbon) as the working electrode (WE), a Pt wire (99.995%) as the counter electrode and a Ag/AgCl/3M KCl electrode as the reference electrode. All measurements were performed at room temperature. The potentiostat was a PG580 (Uniscan

Instruments) controlled by a PC. The characterization of $Au_{(core)}$-$Pt_{(shell)}$ bimetallic nanoparticles and gold seeds was carried out in 0.05 M sulphuric acid.

2.4 Gold Sol Preparation - Method 1

Brown *et al*. prepared gold nanoparticles using a seeding method. However, the particle sizes after seeding were larger than 10nm, which is too large for the purpose of this project. It was decided that the seeds generated to make the nanoparticles from this article would be used for the initial studies instead. They were used as core material for bimetallic core-shell nanoparticles. A brief description is as follows; 1.00 ml of 1% $HAuCl_4$ was added to 90.00 ml of water at room temperature (20-23ºC). After 1 minute of stirring, 2.00 ml of 38.8 mM sodium citrate was added. One minute later, 1.00 ml of fresh 0.075% $NaBH_4$ in 38.8 mM sodium citrate was added. The colloidal solution was stirred for an additional 5 minutes and stored in a dark bottle at 4ºC [4].

2.5 Coating Method - Method 2

Cao and co-workers [23] described a chemical deposition method of coating platinum on to gold nanoparticles, which were placed on a silicon wafer substrate. As the particles generated in accordance with Brown *et al.* [4] were suspended in solution, this method was adapted for solutions. It follows in brief; 50 ml of H_2PtCl_6 (0.01%) was added to 50 ml of the previously made gold solution (section 2.4) along with 0.9 ml of $NH_2OH.HCl$ (1%). The resulting dark red solution was heated under magnetic stirring at 60ºC for varying times.

Various adaptations were made to this method. Palladium and rhodium salts were also used (potassium tetrachloropalladate (II) and sodium hexachlororhodate (III) respectively, these were treated in the same way as the platinum salt, as a 0.01% solution). Also, varying amounts of sodium citrate (38.8mM) were added in an attempt to stabilise the core-shell particles, especially as it was discovered that they were not very stable under the electron microscope beam. The initial experiments, were conducted at approximately 40ºC, consequently, further experiments were carried out at 60ºC. The final adaptation that was made was that for one series of experiments, the amount of palladium solution was increased to 0.04% to increase the palladium shell thickness.

2.6 Bimetallic Core-Shell Nanoparticles with extra Citrate Stabiliser – Method 3

These nanoparticles were made as according to method two, with the addition of 1% sodium citrate added at the time of mixing the two metal solutions. This was to see if the aggregation and stability of the nanoparticles was improved with an increasing amount of stabiliser. This method was applied to the gold nanoparticle seeds produced from method 1 and palladium and platinum salts, to produce $Au_{(core)}$-$Pd_{(shell)}$ and $Au_{(core)}$-$Pt_{(shell)}$ bimetallic nanoparticles.

2.7 $Au_{(core)}$-$Pd_{(shell)}$ Bimetallic Nanoparticles with a 1:4 Metal Ratio and 10% Citrate Stabiliser – Method 4

This method is similar to method 2. A 0.04% solution of potassium tetrachloropalladate (II), 2% hydroxylamine hydrochloride and 10% sodium citrate solution added at the time of the mixing of the two metal solutions.

2.8 Thiol-Stabilised Gold Nanoparticles – Method 5

Thiol-stabilised gold nanoparticle seeds were produced using a seeding and growth method as described by Yang *et al*. [5].

2.8.1 Seed Preparation

Hydrogen tetrachloroaurate (III) was dispersed in water. 3 ml of this aqueous solution (0.042 mol l^{-1}) was dried at 60ºC to completely remove the water and 45 ml of toluene and 4 g of tri-n-octylamine were added. The mixture was sonicated for 30 minutes until a clear yellow solution was obtained, indicating that hydrogen tetrachloroaurate (III) was fully dissolved in toluene. 0.5 ml of aqueous solution containing 0.02 g sodium borohydride was then added under vigorous magnetic stirring to reduce the hydrogen tetrachloroaurate (III). The colour of the solution quickly turned from yellow to red. After 3 hours, 2 ml of dodecanethiol was added to stabilize the particles and the reaction left to proceed for 2 hours. The excess toluene was removed by vacuum distillation until 1 ml remained. Then 20 ml of ethanol was added to precipitate the gold nanoparticles. After washing the precipitate several times with ethanol and water, the nanoparticles were dried at 54ºC for 24 hours.

2.8.2. Growth Solution Preparation

After different amounts of hydrogen tetrachloroaurate (III) aqueous solution were dried completely following the above-described procedure, 0.4 ml of decyl amine and 2 ml of toluene were added under magnetic stirring to solubilize $HAuCl_4$. The obtained yellow solution was used as the growth solution.

2.8.3 Seeding Growth Process

Gold nanoparticle seeds were redispersed in 3 ml of toluene and mixed with the growth solution. The solution was slowly heated to 120ºC under magnetic stirring and kept at this temperature for 2 hours. During heating, the colloidal solution changed from red to a deeper red, indicating that gold nanoparticles with larger diameters were formed. Excess dodecanethiol (0.5 ml) was added to stabilize the gold nanoparticles. After 30 minutes, the colloidal solution was slowly cooled to room temperature. Lastly 15 ml of ethanol was added to precipitate the gold nanoparticles. These were collected and purified according to the same procedure as for the seed preparation.

2.9 $Au_{(core)}$-$Pd_{(shell)}$ Bimetallic Nanoparticles – Method 6

This method is largely similar to method 5, however; a palladium growth solution was prepared using potassium tetrachloropalladate (II) in place of hydrogen tetrachloroaurate for the growth solution.

2.10. Rhodium and Platinum Seeds – Method 7

These methods are identical to method 5, however, for platinum seeds potassium tetrachloroplatinate was used instead of hydrogen tetrachloroaurate, and for rhodium seeds sodium hexachlororhodate (III) was used instead of the hydrogen tetrachloroaurate. The only difference to method 5 was that prior to rotary-evaporation both the platinum and rhodium seeds solutions were sonicated for 30 minutes to help fully disperse the solutions.

2.11 Platinum Coating – Galvanic Replacement Technique – Method 8

The galvanic displacement technique as described by Kumar and Zou [11] was used to coat gold seeds with platinum. This was performed on both thiol stabilised and citrate stabilised gold seeds. The thiol stabilised gold seeds were redispersed in ethanol, due to the volatility of ethanol. Nafion was initially used to deposit the gold nanoparticle sols on to the electrode surface; this was tried by both depositing the gold nanoparticle sols directly onto a Nafion film on the electrode surface and as a dispersion of gold nanoparticle sols in the Nafion. Both of these techniques were found to be unsuccessful for coating of the electrode surface. However, bare deposition was utilized with much more success. In between depositions the gold nanoparticles sol-coated electrode was placed in an oven at 60ºC until the surface appeared dry. Up to 5 depositions were carried out in this manner to increase metal loading on the electrode surface.

2.11.1 Deposition of Platinum onto Gold Nanoparticle Seeds – Method 9

Platinum films were deposited on to the gold nanoparticle seeds by means of the galvanic replacement technique. This was achieved by depositing an atomic layer of Cu onto Au nanoparticles with underpotential deposition (UPD) at -0.02 V in 1 mM copper sulphate + 0.1 M sulphuric acid for 2 minutes. The Cu-coated Au nanoparticles were then immersed in a vigorously deaerated 5 mM K_2PtCl_4 + 0.1 M $HClO_4$ solution for 10 minutes. In this process, the Cu adlayer was replaced by Pt through a galvanic replacement process, forming an atomic layer of Pt on the Au

nanoparticles. Repeated cycling at -0.2 – 0.8 V increases the amount of Pt deposited onto the Au nanoparticles [11].

CHAPTER 3- CITRATE-STABILISED NANOPARTICLES

3.1 Introduction to Citrate-Stabilised Particles

This chapter discusses the results from the experiments carried out with aqueous based citrate stabilised nanoparticles. The citrate-stabilised seeds were produced according to Brown *et al*. [4], who reported a diameter of 2.6±1 nm for their gold nanoparticle seeds. The gold nanoparticle seeds produced following Brown and co-workers method in this work (method 1, section 2.4) were in the size range 2-8 nm with a mean diameter of 3.7 nm. These gold nanoparticle seeds were the starting product for subsequent bimetallic core-shell nanoparticle systems. Those systems are as follows: $Au_{(core)}$-$Pt_{(shell)}$, $Au_{(core)}$-$Pd_{(shell)}$ and $Au_{(core)}$-$Rh_{(shell)}$.

The $Au_{(core)}$-$Pd_{(shell)}$ system was used for further investigations, as it was the most stable system. The further investigations entailed altering the amount of citrate-stabiliser and palladium metal salt used during the reaction to see if this would improve the stability of the system and increase the palladium shell thickness.

3.2.1 UV-vis Spectroscopy Analysis of Gold Nanoparticle Seeds

The five preparations of the gold nanoparticle seed sols were analysed by UV-vis spectroscopy (Figure 3.1). The spectra show peaks in the 235 and 520 nm region of the UV spectrum. This agrees with published data for gold nanoparticles [4, 29, 31]. An absorbance at 520 nm corresponds to a gold nanoparticle size of between 6-20 nm [3, 31].

3.2.2 AFM Analysis of Gold Nanoparticle Seeds

Figure 3.2 shows an AFM image of a 5 μm^2 area of the citrate-stabilised gold nanoparticle seeds. The average lateral particle size is 8.7 nm, this size is larger than the actual size of the particles due to tip convolutions. Each particle appears to be an agglomeration of several smaller particles.

3.2.3 Cyclic Voltammetry of Gold Seeds

The cyclic voltammogram for the citrate stabilised gold nanoparticles adsorbed on carbon shown in Figure 3.3 has a small oxidation onset at 1 V. Hydrogen evolution is observed below -0.3 V. The citrate appears not to be blocking the HER.

3.2.4 HAADF Analysis of Gold Seeds

Figure 3.3 is visually similar to those in the paper by Brown *et al*. [4]. There are three images of the gold sample, at different magnifications. The mean size is 3.7 nm in diameter. The sample is polydisperse and some particles appear to stick together. The particles are mostly spherical in shape.

Figure 3.1

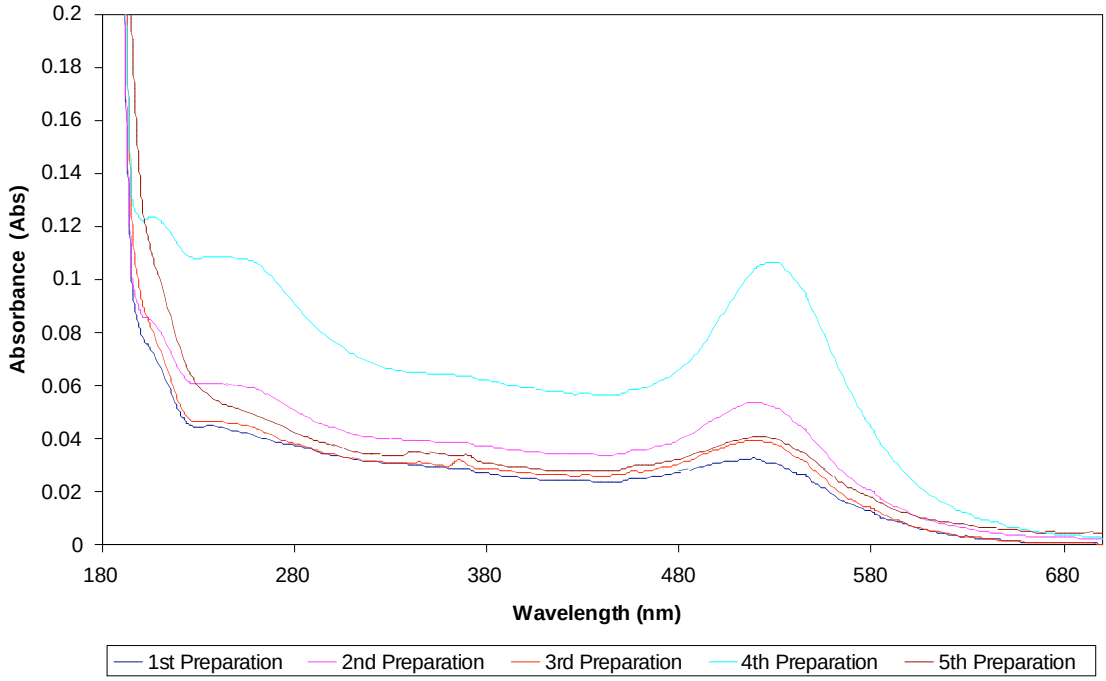

UV-vis absorption spectra of citrate-stabilised gold nanoparticles.

Figure 3.2

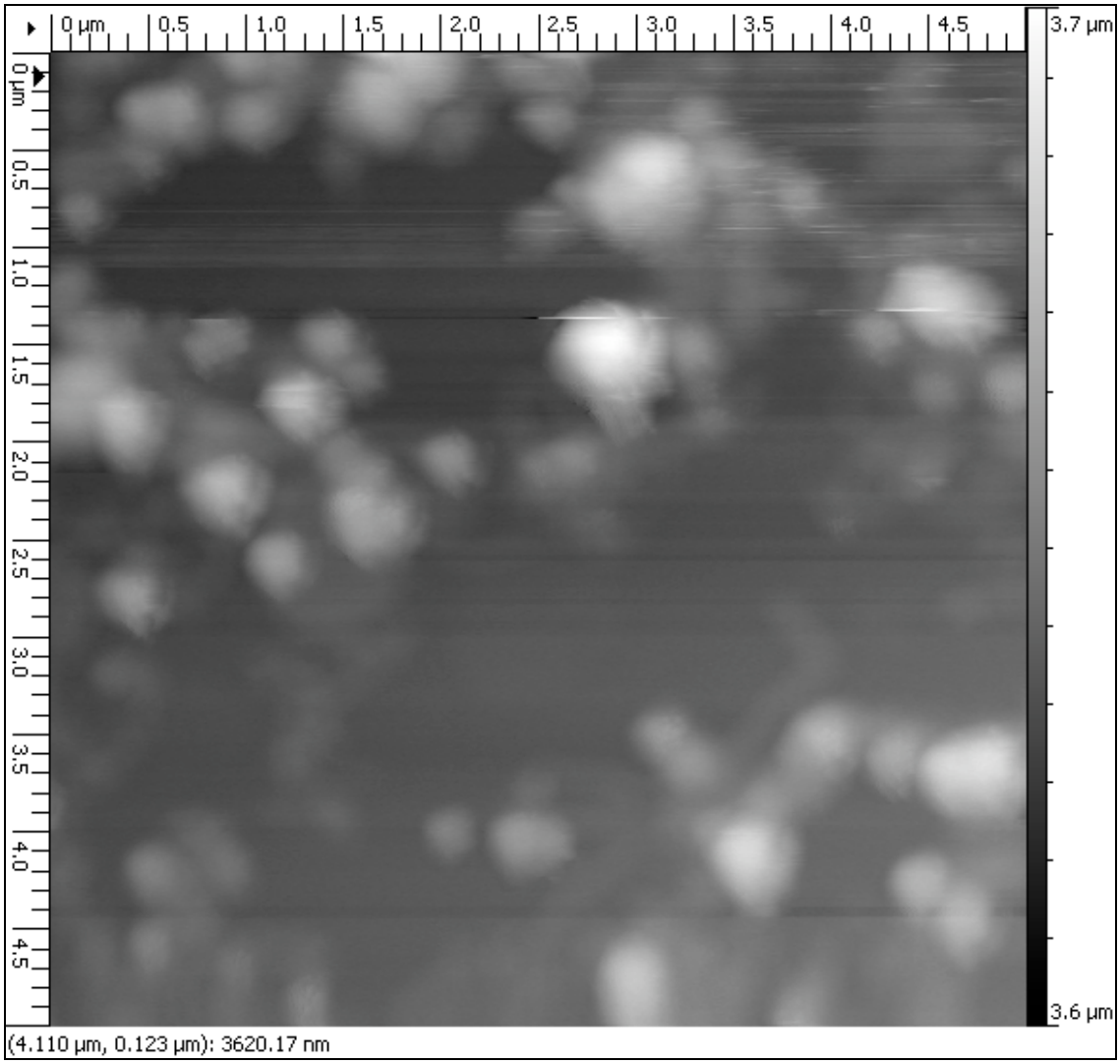

AFM topography image (5 µm x 5 µm) of citrate-stabilised gold nanoparticle seeds on mica.

Figure 3.3

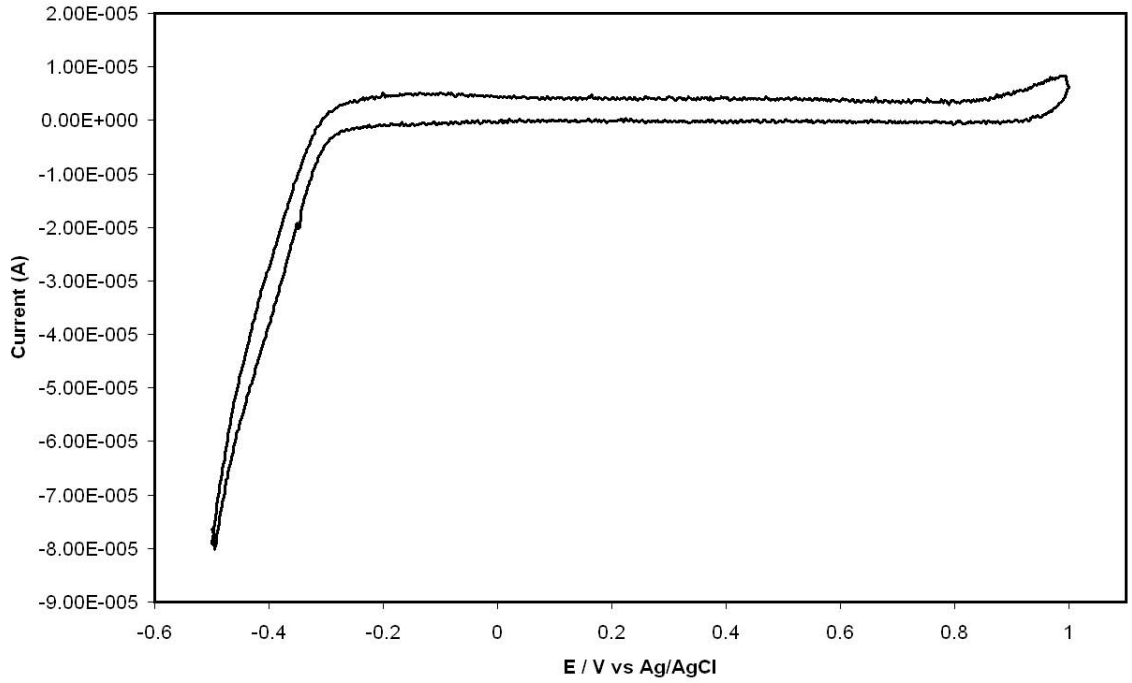

Cyclic voltammogram of citrate-stabilised gold nanoparticle seeds loaded on to GCE, in 0.05 M H_2SO_4 at a sweep rate of 0.1 V s^{-1}.

Figure 3.4

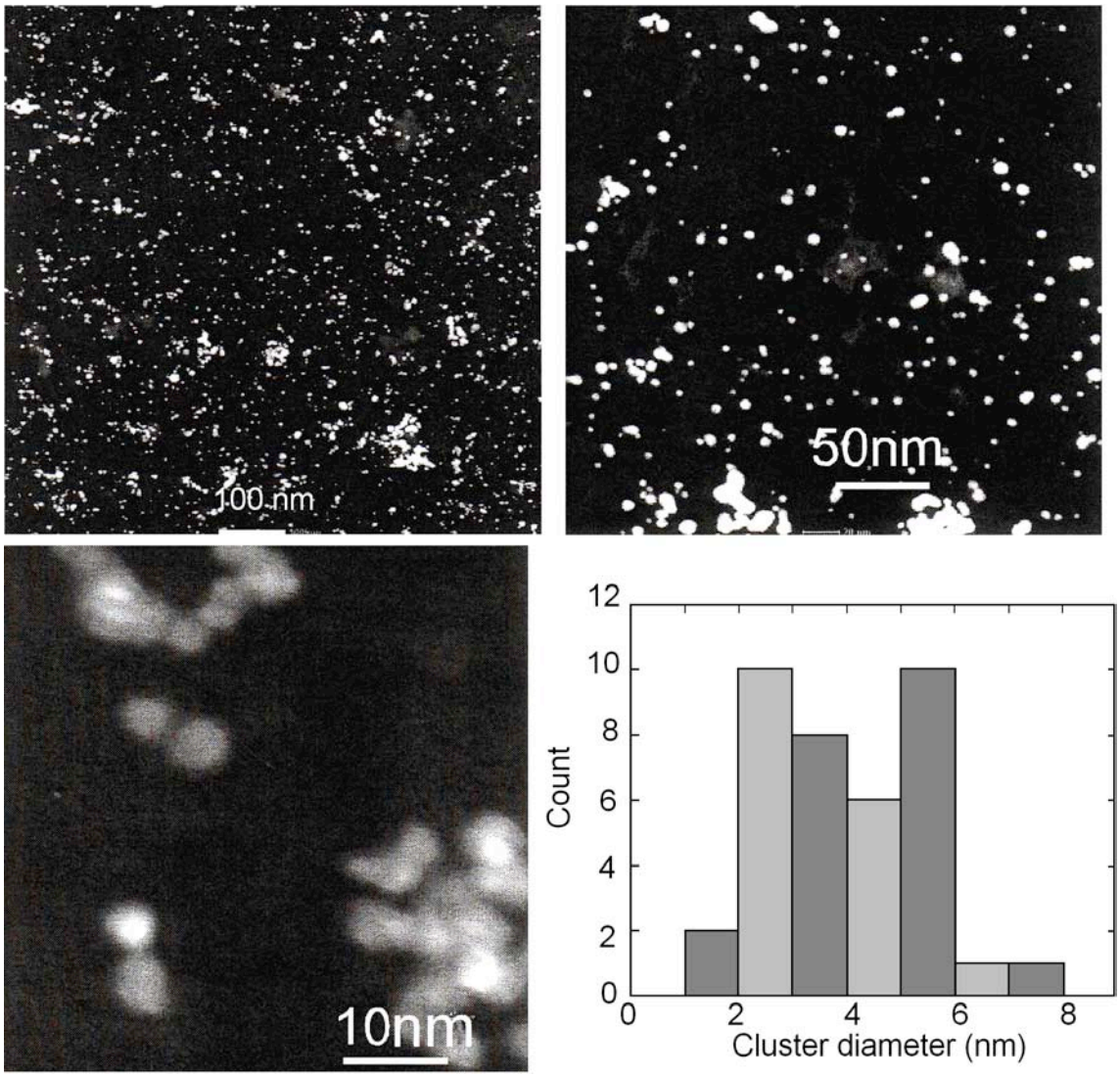

HAADF images of citrate-stabilised gold nanoparticles including a graph to show the distribution of particle sizes.

3.2.5 Discussion of Gold Seeds

The gold nanoparticle seeds produced according to Brown *et al*. [4] did differ from the published results. The gold nanoparticle seeds had a mean diameter of 3.7 nm which is larger than the 2.6±1 nm reported. This could be due to a subtle difference in conditions employed during the reaction. The HAADF images of the gold nanoparticle seeds appear similar to those reported [4].

The UV-vis spectroscopy analysis of the gold nanoparticle sols agrees with the literature [4, 29, 31]. The particles produced are indeed gold nanoparticles. However, it is difficult to use the published data to accurately measure size of the gold nanoparticles, as although the plasmon band is related to size, it can be affected by the stabiliser used and the absorption band can be broadened by particle aggregation

AFM analysis of the gold nanoparticle size differs with that of the HAADF analysis. This may be due to tip convolutions when measuring lateral size. The AFM images do give a quick overview of sample distribution. The AFM image (Figure 3.2) does reflect what is shown in the HAADF images (Figure 3.4). The HAADF image gives a much clearer view of what the gold nanoparticles actually appear like.

3.3 $Au_{(core)}$-$Pt_{(shell)}$ Bimetallic Nanoparticles

$Au_{(core)}$-$Pt_{(shell)}$ bimetallic nanoparticles were produced using method 2, which involves chemical deposition of platinum salt on to the gold nanoparticle seeds. These $Au_{(core)}$-$Pt_{(shell)}$ bimetallic nanoparticles were characterised using UV-vis spectroscopy, AFM and HAADF.

3.3.1 UV-vis Spectroscopy Analysis of Bimetallic $Au_{(core)}$-$Pt_{(shell)}$ Nanoparticles

The UV-vis spectra of $Au_{(core)}$-$Pt_{(shell)}$ nanoparticles (Figure 3.7) show no evidence of an absorption peak at 520 nm, which was visible for the gold nanoparticle seeds (Figure 3.1), which is indicative of the platinum having covered the gold seeds to create a bimetallic core-shell configuration nanoparticle. This reflects the published data, the disappearance of the gold plasmon band indicates that the surface behaviour of the particles is dominated by that of the platinum [8, 24]. There is a visible absorption band at 195 nm. This is consistent with the absorption spectra of platinum [31]. The absorbance of these samples is low as they were diluted. The spectra of the $Au_{(core)}$-$Pt_{(shell)}$ bimetallic nanoparticles all appear very similar, indicating that thirty minutes heating duration is sufficient to quench the gold plasmon band, which may imply a good coverage of the gold seeds with platinum within the first thirty minutes of the reaction.

3.3.2 AFM Analysis of Bimetallic $Au_{(core)}$-$Pt_{(shell)}$ Nanoparticles

Figures 3.6 and 3.7 show a 3.35 µm x3.35 µm area of mica coated with $Au_{(core)}$-$Pt_{(shell)}$ bimetallic nanoparticles. The 3D image is to help visualise the sample. These images have had their data levelled by mean plane subtraction, as the mica was not entirely flat on the AFM sample holder. The average particle size from visual observation is 13.3 nm. However, the raised areas are not flat; they appear to be a collection of aggregated particles. The particles appear mainly monodisperse, although there are a few larger particles, indicating that there could be two different sized populations of particles. Figure 3.8 is of a smaller area (1.28 µm x1.28 µm). In this image the population of smaller particles is clearer. This image is in false-colour mapping.

3.3.3 HAADF Analysis of Bimetallic $Au_{(core)}$-$Pt_{(shell)}$ Nanoparticles

The images (Figures 3.9. and 3.10) of the $Au_{(core)}$-$Pt_{(shell)}$ bimetallic nanoparticles appear to show some core-shell structures, however, as the Z contrast for this system is so small (Au:79, Pt:78), these images alone are not conclusive evidence of core-shell structures. The samples are very aggregated and polydisperse. Some particles are spherical, but most are not regular in shape. The particles are too agglomerated to make accurate size measurements. The samples heated for 30 minutes are very similar in appearance to those that have been heated for 8 hours, implying that the reaction is complete after 30 minutes, and that extended heating has not affected shell thickness.

Figure 3.5

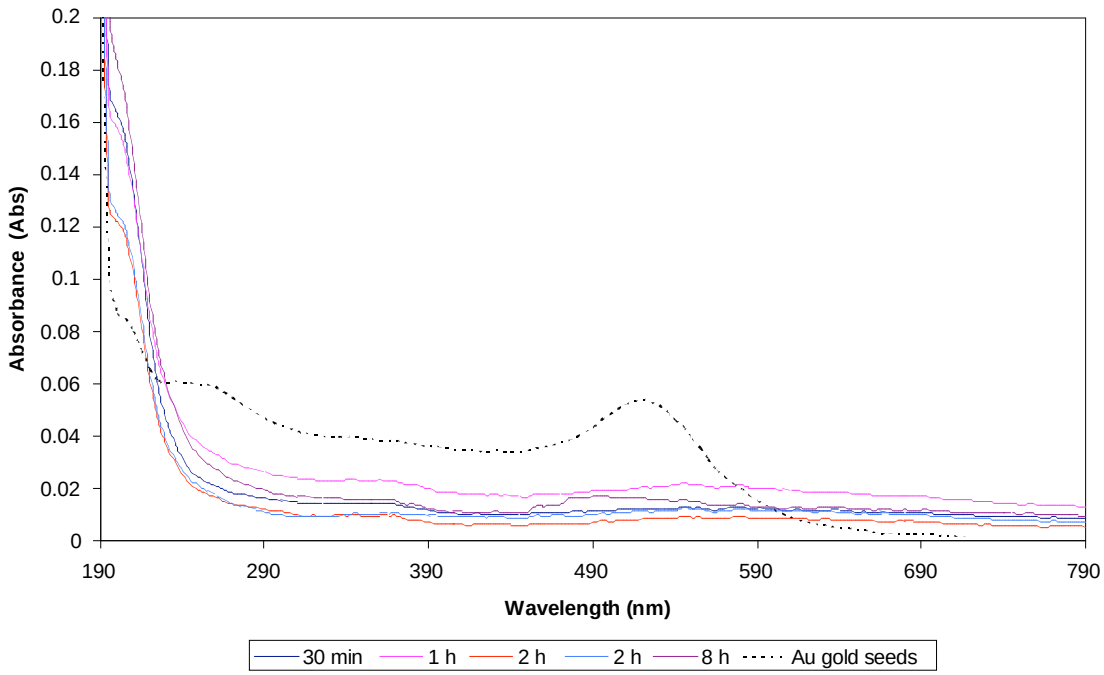

UV-vis absorption spectra of $Au_{(core)}$-$Pt_{(shell)}$ nanoparticles and gold nanoparticle seeds.

Figure 3.6

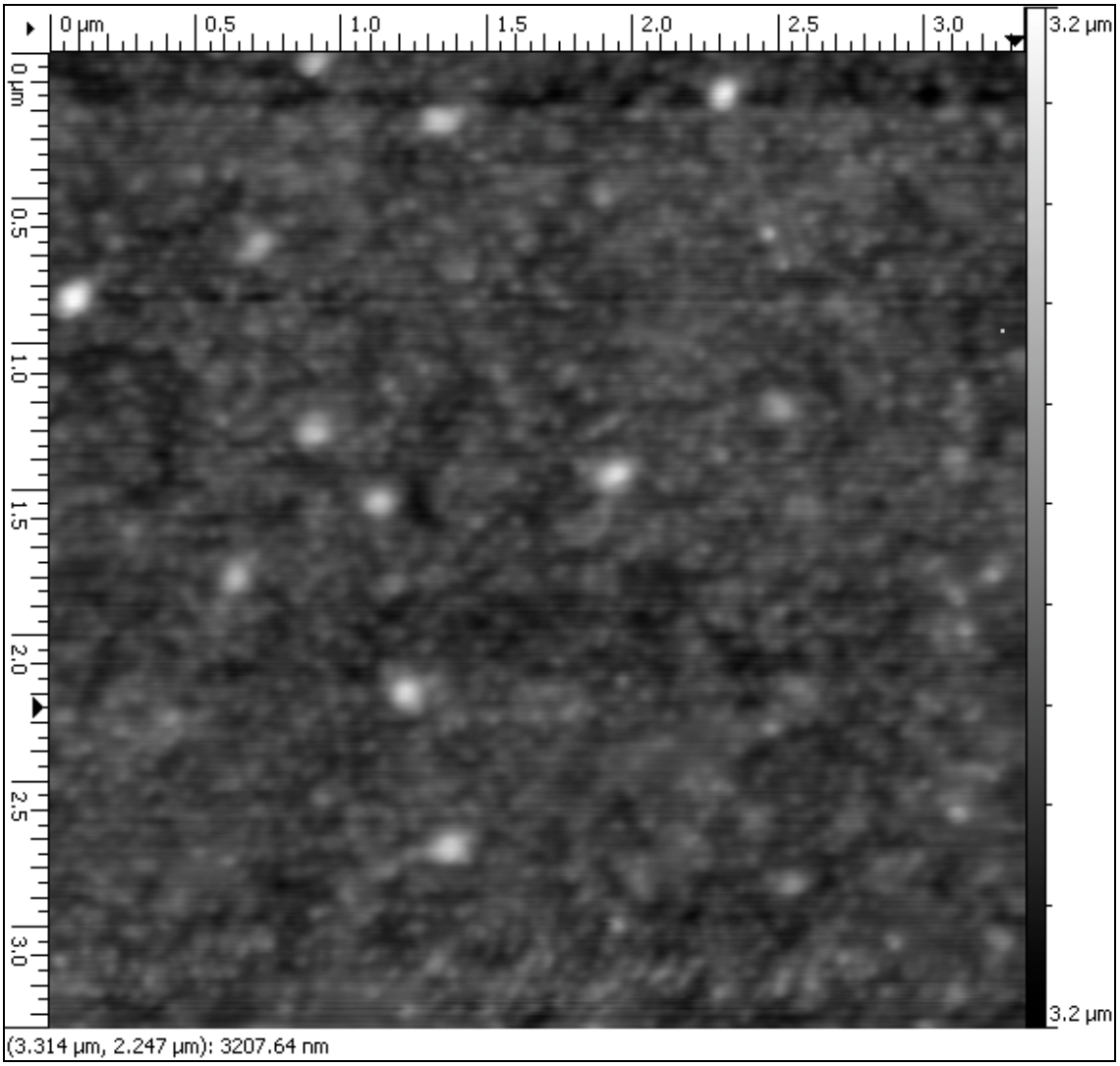

AFM topography image (3.35 µm x 3.35 µm) of $Au_{(core)}$-$Pt_{(shell)}$ nanoparticles on a mica surface (data levelled by mean plane subtraction).

Figure 3.7

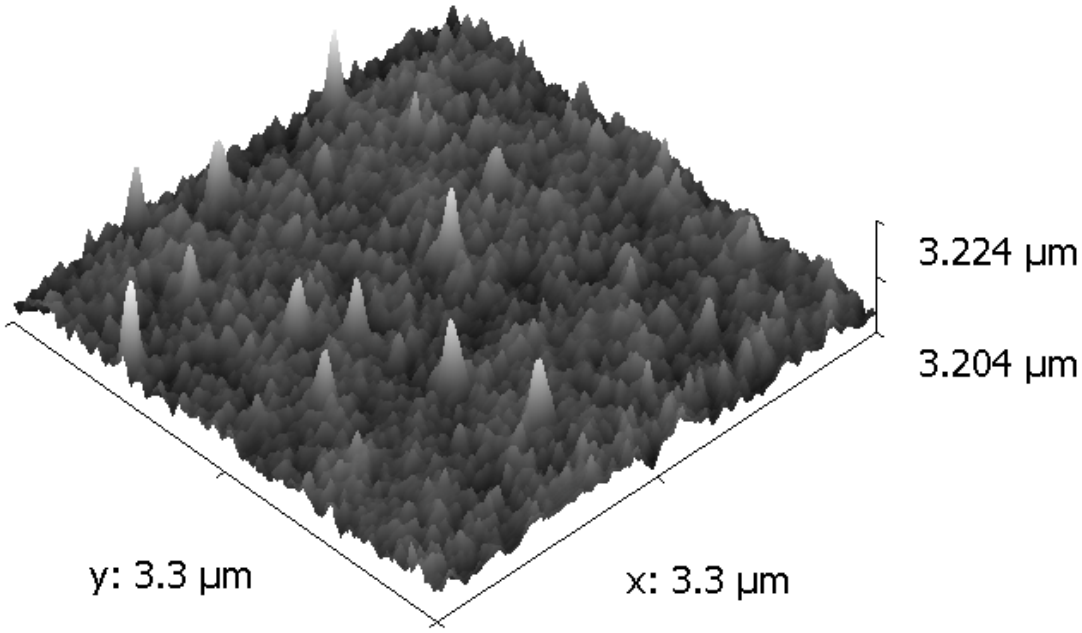

AFM 3D topography image (3.35 µm x 3.35 µm) of $Au_{(core)}$-$Pt_{(shell)}$ nanoparticles on mica (data levelled by mean plane subtraction).

Figure 3.8

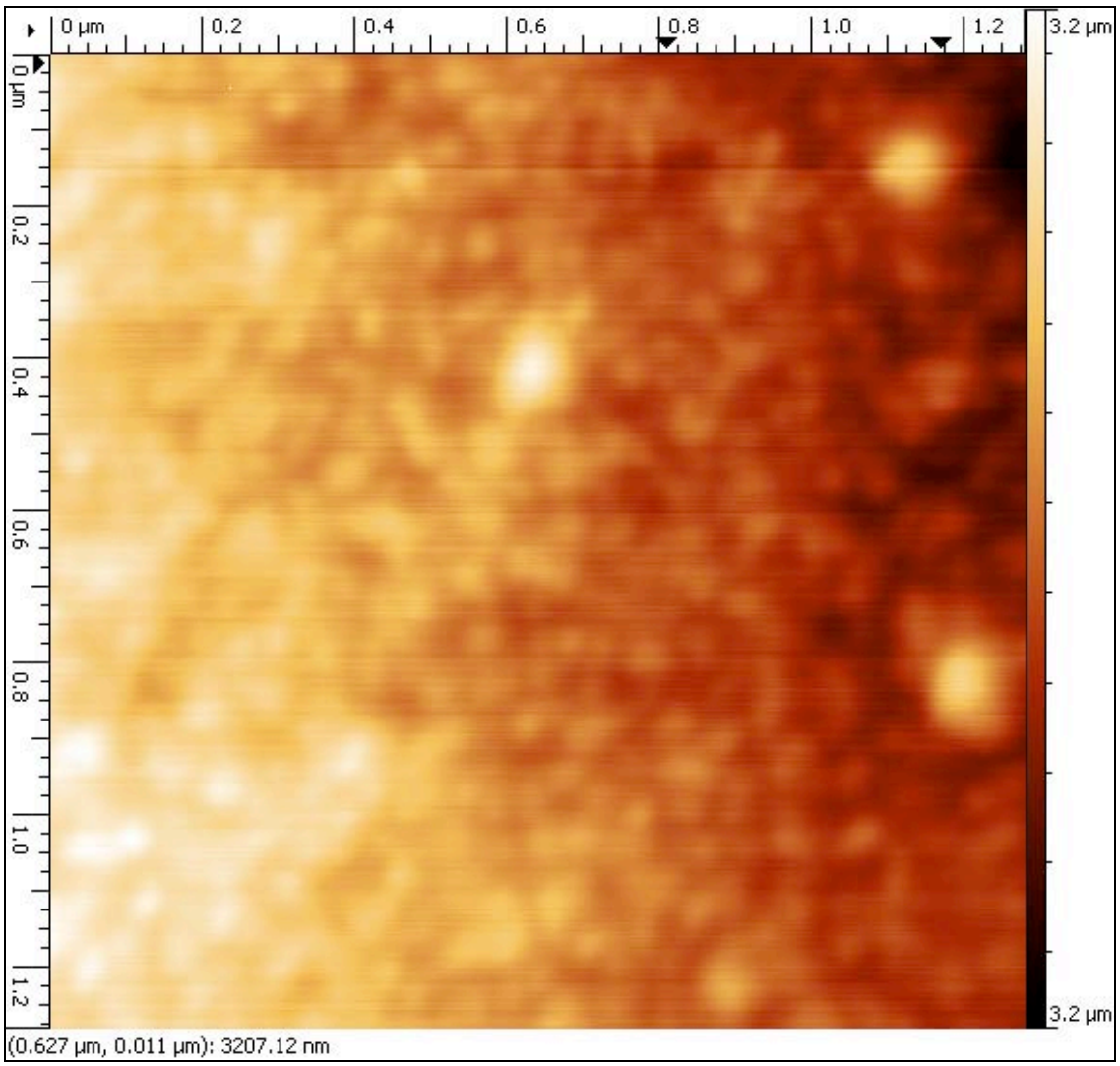

AFM topography image (1.28 µm x 1.28 µm) of $Au_{(core)}$-$Pt_{(shell)}$ nanoparticles on mica.

Figure 3.9

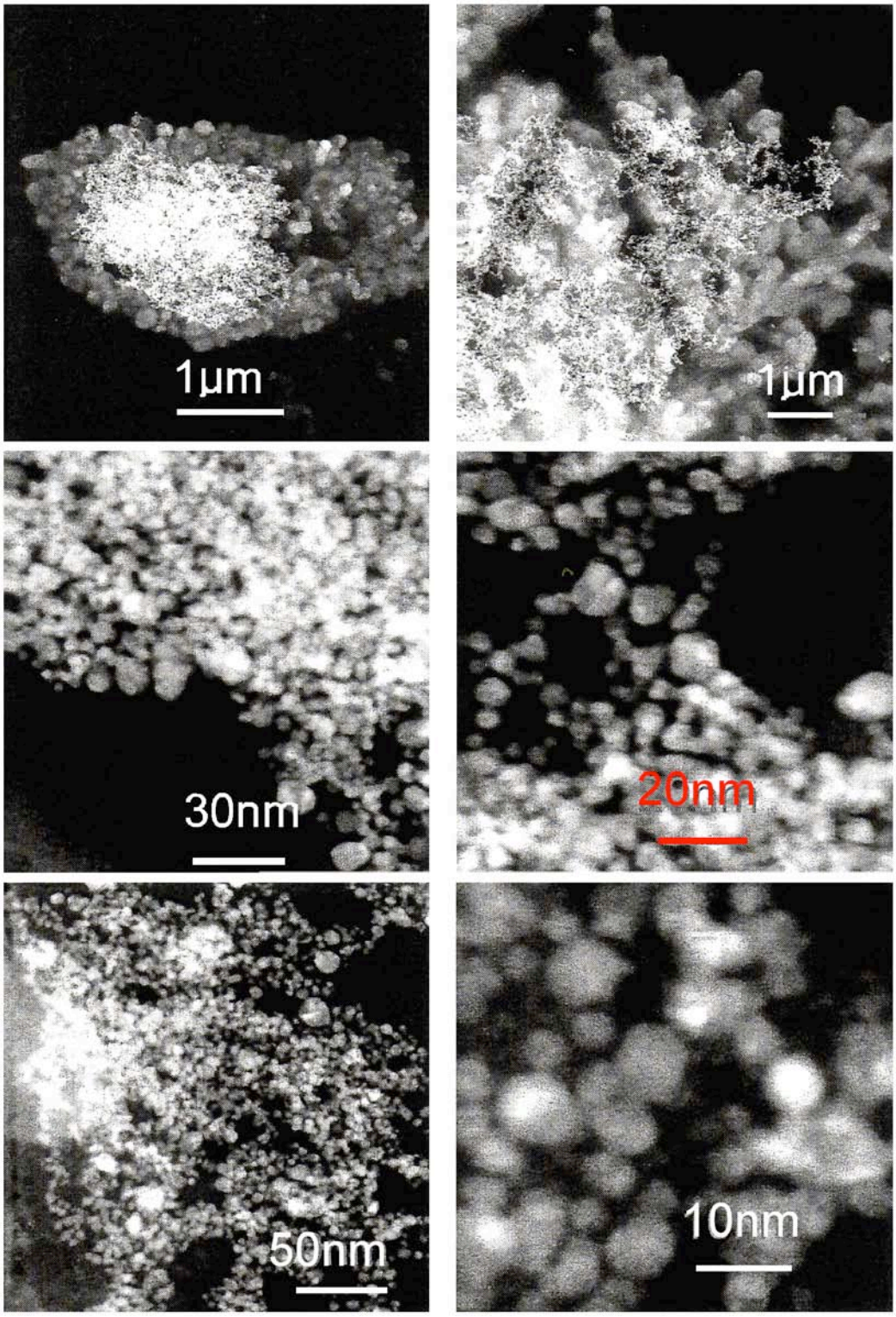

HAADF images of $Au_{(core)}$-$Pt_{(shell)}$ bimetallic nanoparticle solution which has been heated for 30 minutes.

Figure 3.10

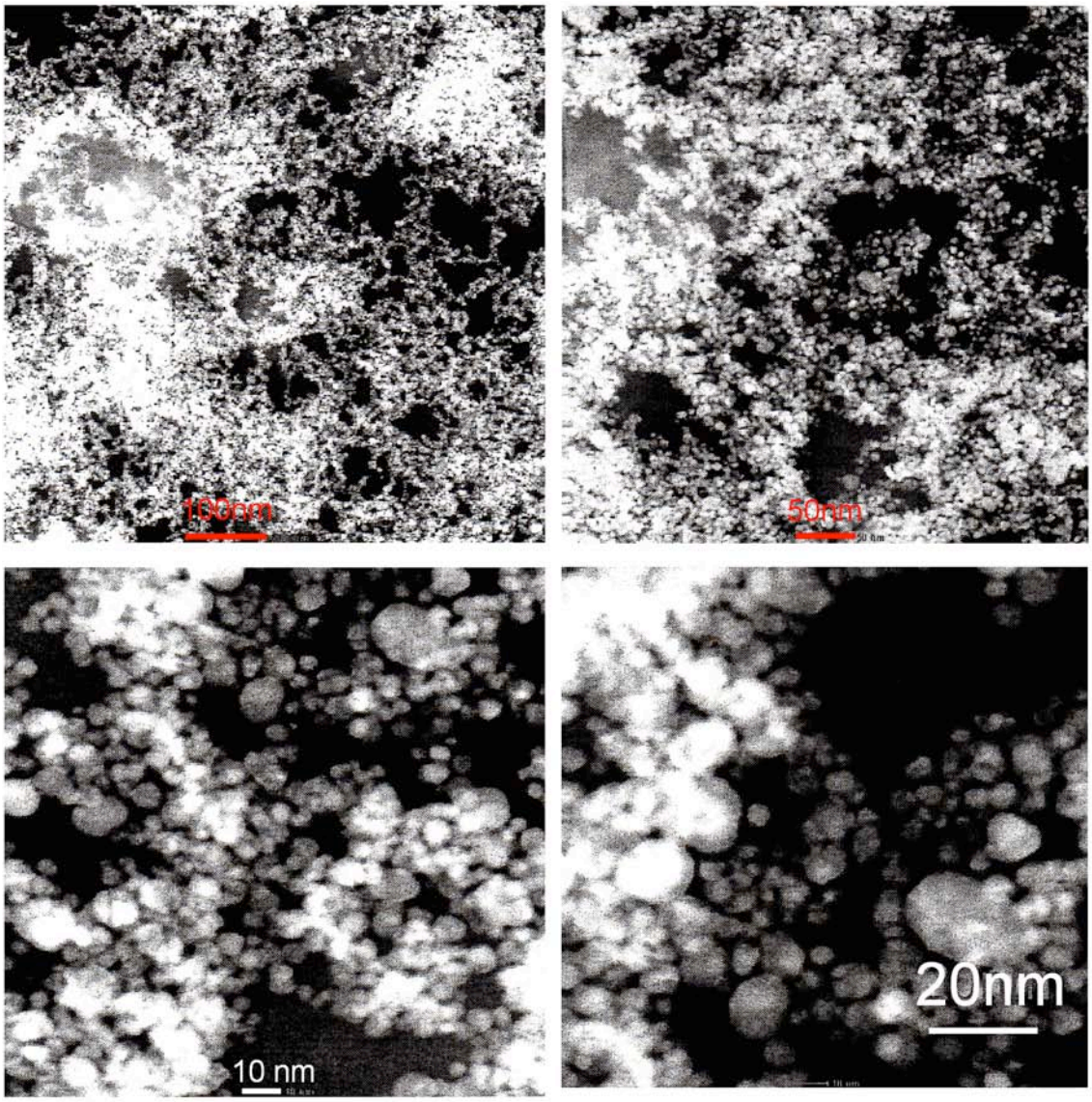

HAADF images of $Au_{(core)}$-$Pt_{(shell)}$ bimetallic nanoparticle solution which has been heated for 8 hours.

3.3.4 Discussion of Bimetallic $Au_{(core)}$-$Pt_{(shell)}$ Nanoparticles

These bimetallic $Au_{(core)}$-$Pt_{(shell)}$ nanoparticles were produced by chemically depositing platinum onto gold nanoparticle seed as described by method 2 (section 2.5). Analysis has shown that although core-shell particle behaviour has been observed, there are also monometallic particles and a high rate of agglomeration. The agglomeration has made measuring the particles unfeasible. The agglomeration could be due to the fact that citrate is a mild stabiliser.

The UV-vis spectra of the $Au_{(core)}$-$Pt_{(shell)}$ bimetallic nanoparticles do not show the absorbance band at 520 nm, which is associated with the gold particles (Figure 3.5). There is a shoulder visible on the continua of the $Au_{(core)}$-$Pt_{(shell)}$ bimetallic nanoparticles spectra at 195 nm which could be caused by a combination $Au_{(core)}$-$Pt_{(shell)}$ bimetallic nanoparticles and Pt nanoparticles. It is clear that platinum is dominating the optical activity of the particles [24].

The AFM analysis reveals that the sample is highly agglomerated; this is reflected in the HAADF analysis.

It seems that the different heating durations (at 40ºC) has not affected particle size or agglomeration, as the images of the particles that were heated for 30 minutes (Figure 3.9) look very similar to those that were heated for 8 hours (Figure 3.10). This is reflected in the UV-vis spectra.

Overall this method has not been very successful for producing bimetallic $Au_{(core)}$-$Pt_{(shell)}$ nanoparticles. Although core-shell behaviour was seen, the agglomeration of the sample was too high to facilitate use as a nanocatalyst.

3.4 $Au_{(core)}$-$Rh_{(shell)}$ Bimetallic Nanoparticles

These bimetallic $Au_{(core)}$-$Rh_{(shell)}$ nanoparticles were prepared in the same way as the $Au_{(core)}$-$Pt_{(shell)}$ bimetallic nanoparticles in section 3.3, using method 2. As well as bimetallic core-shell particles, large triangular and square-shaped particles were observed in the initial HAADF investigation of these particles, which were further investigated using HRTEM.

A control experiment was conducted, to elucidate if the rhodium salt alone would produce these large crystals under the same reaction conditions. A second batch of bimetallic $Au_{(core)}$-$Rh_{(shell)}$ nanoparticles was also produced to see if the results could be repeated. However, the control experiment and second batch of $Au_{(core)}$-$Rh_{(shell)}$ nanoparticles did not produce the large particles. These samples were analysed using UV-vis spectroscopy, HAADF and HRTEM.

3.4.1 UV-vis Spectroscopy Analysis of $Au_{(core)}$-$Rh_{(shell)}$ Bimetallic Nanoparticles

The spectra of the $Au_{(core)}$-$Rh_{(shell)}$ nanoparticles (Figure 3.11) show no peak in the 520 nm region of the UV spectrum, which would be consistent with the optical behaviour of the gold dominating the optical behaviour of the sample; this indicates that the gold cores are coated with rhodium. The difference in heating duration does not appear to have affected the spectra for the $Au_{(core)}$-$Rh_{(shell)}$ nanoparticles, indicating that the reaction was complete within 30 minutes. The spectrum of the bimetallic $Au_{(core)}$-$Rh_{(shell)}$ nanoparticles sample is similar in appearance to the spectra for rhodium as calculated by Creighton and Eadon [31]. However, there are no distinct absorption bands in the calculated spectrum of rhodium nanoparticles, just a

rather broad absorption continuum which extends throughout the visible-near ultraviolet range The spectra of the control samples is different to that of the $Au_{(core)}$-$Rh_{(shell)}$ nanoparticles, it lacks a shoulder at about 200 nm that is visible in the spectra of the $Au_{(core)}$-$Rh_{(shell)}$ nanoparticles, indicating that the shoulder is a change in the optical behaviour of the rhodium, due to the rhodium being coated on to nanoparticle seeds.

Figure 3.11

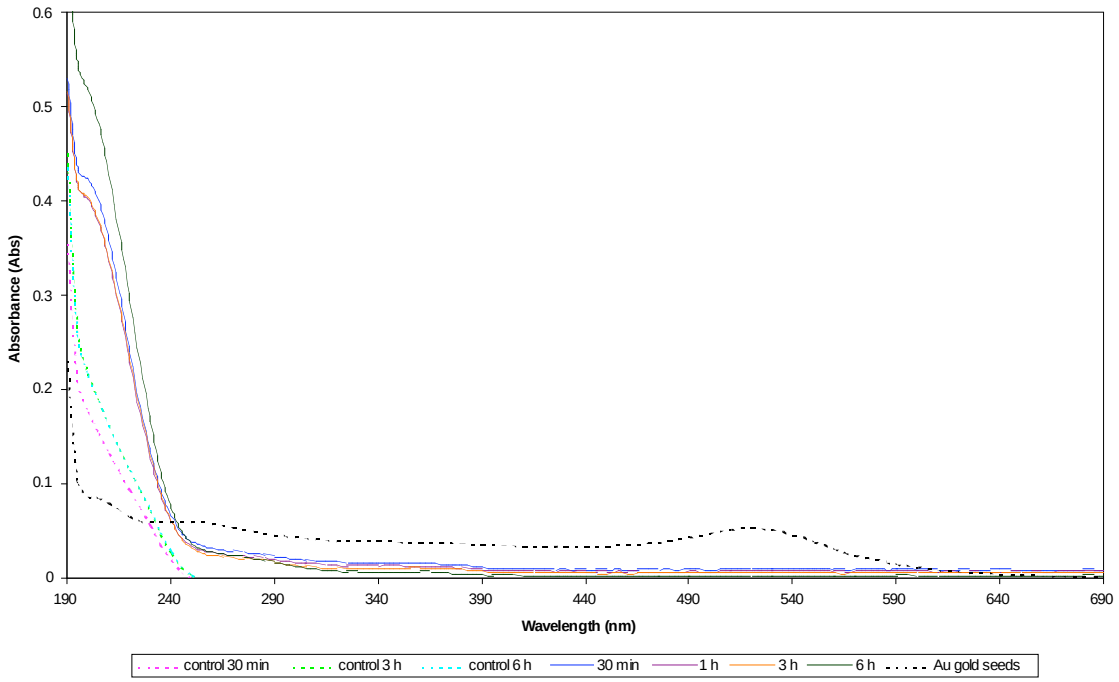

UV-vis absorption spectra of $Au_{(core)}$-$Rh_{(shell)}$ bimetallic nanoparticles, Rh control sample and citrate-stabilised gold nanoparticle seeds.

3.4.2 HAADF Analysis of $Au_{(core)}$-$Rh_{(shell)}$ Bimetallic Nanoparticles

Figures 3.12-3.14 are HAADF images of $Au_{(core)}$-$Rh_{(shell)}$ bimetallic nanoparticles. These images show evidence of core-shell structures; this can be seen due to the difference in Z contrast of gold and rhodium (79 and 45 respectively). The shells are thin, approximately 0.5-1 nm in thickness. The approximate size of these nanoparticles is 5 nm. The particles are roughly spherical in shape, although there are many oblong particles. This could be partially due to the irregular shape of the gold seeds (see Figure 3.4). These particles also form chain like structures. In addition to the small particles showing core-shell structure, there are also some large regular, triangular and square crystals which are approximately 200 nm in size. These larger crystals are well separated. Lattice spacing is visible in the larger particles, which was investigated further with HRTEM. The smaller particles in this sample have agglomerated, although the extent was rather less than for $Au_{(core)}$-$Pt_{(shell)}$ bimetallic nanoparticles

When the reaction duration is extended to 6 hours, large dendritic chains grow (Figure 3.13). It would seem that the longer reaction duration gives a longer chain length. The larger nanocrystals are not visible in the samples that were heated for 6 hours.

The second batch of Au-Rh core-shell nanoparticles (Figure 3.14) was also examined by HAADF analysis. This batch has again agglomerated and is a mixture of spherical and non-ordered shapes. The images show small clumps of clusters and no triangular or square shaped particles were found. However, the second batch does have some circular particle clusters. It appears that the $Au_{(core)}$-$Rh_{(shell)}$ nanoparticle system prefers to stick together to form larger clusters of nanoparticles.

Figure 3.12

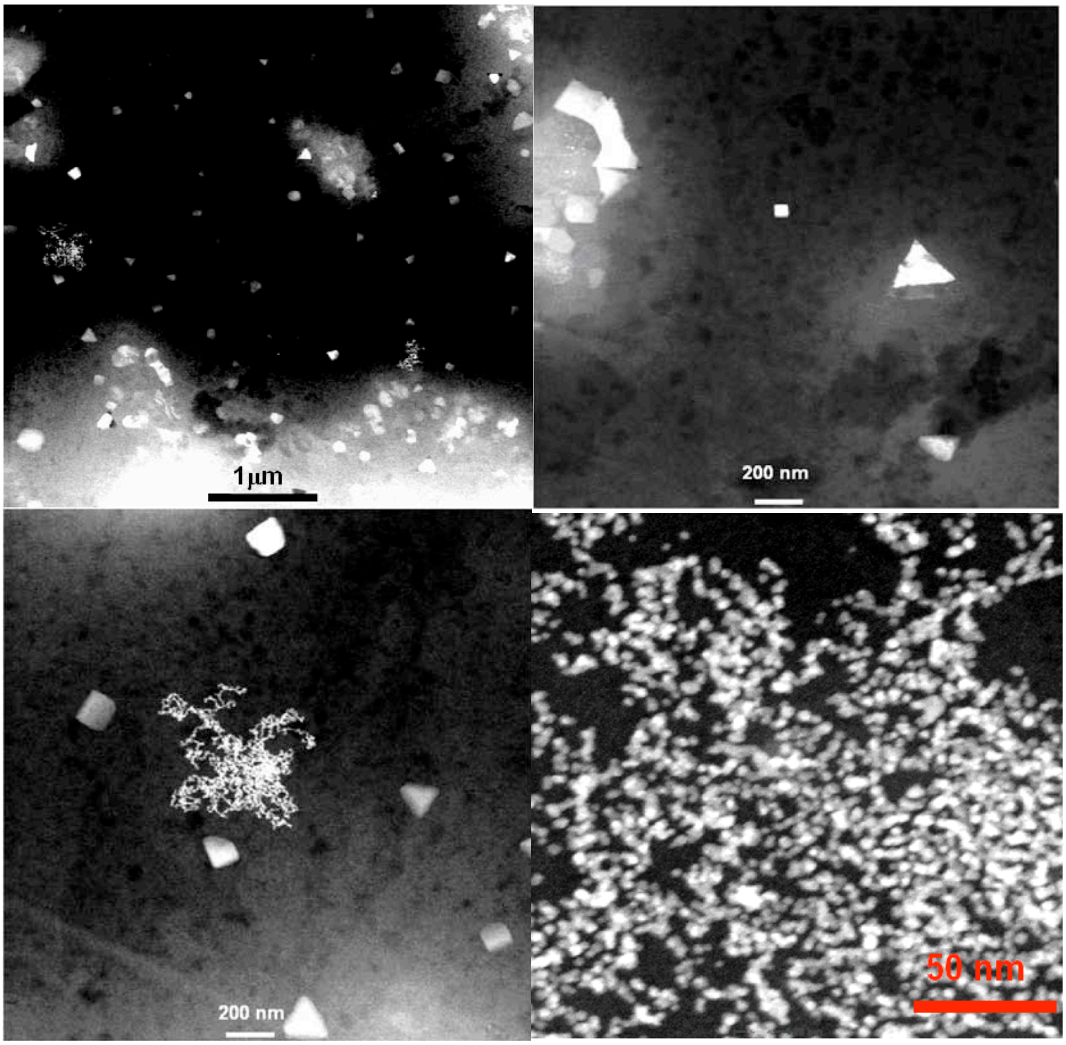

HAADF images of $Au_{(core)}$-$Rh_{(shell)}$ bimetallic nanoparticle solution which has been heated for 30 minutes.

Figure 3.13

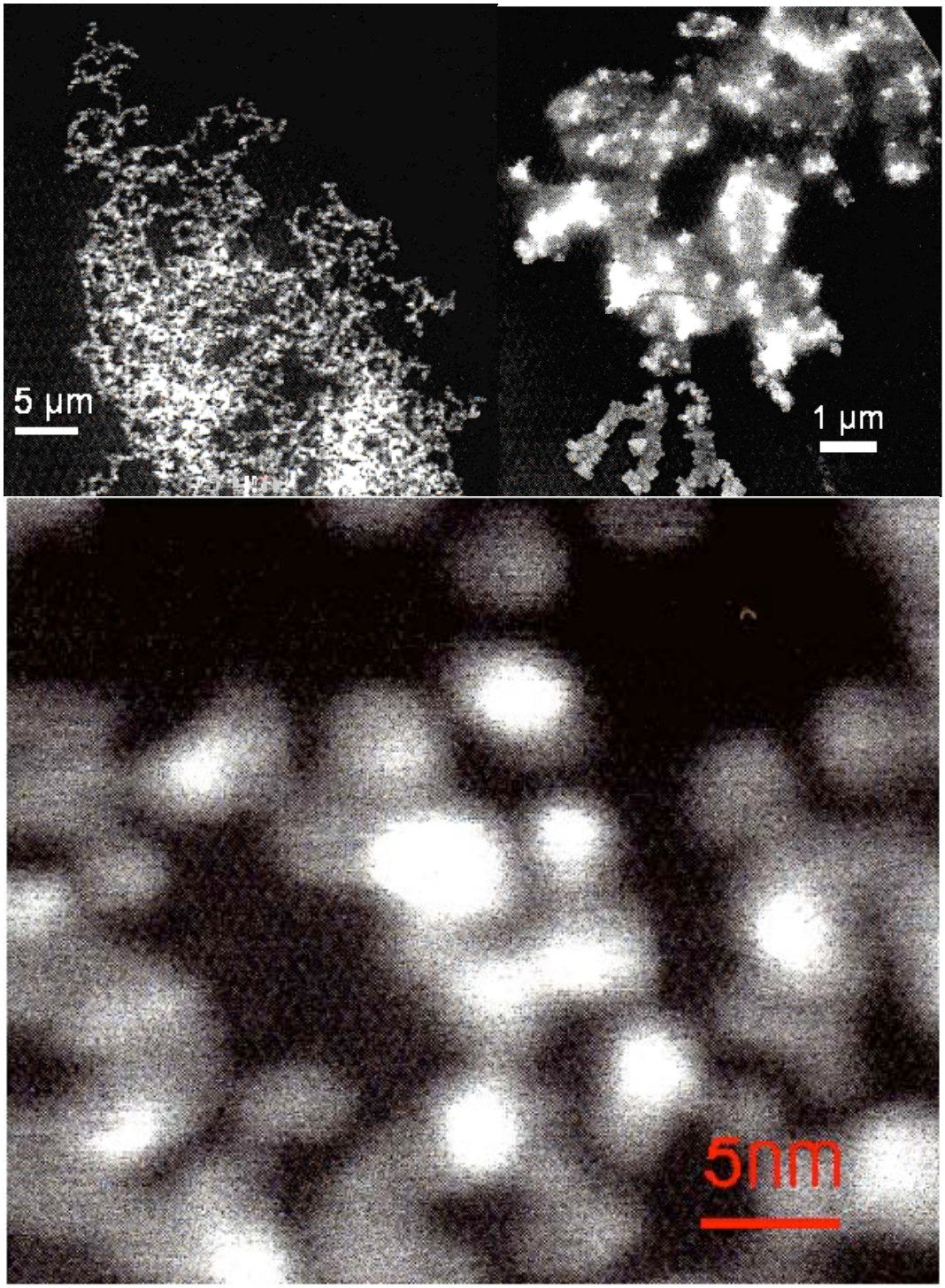

HAADF images of $Au_{(core)}$-$Rh_{(shell)}$ bimetallic nanoparticle solution which has been heated for 6 hours.

Figure 3.14

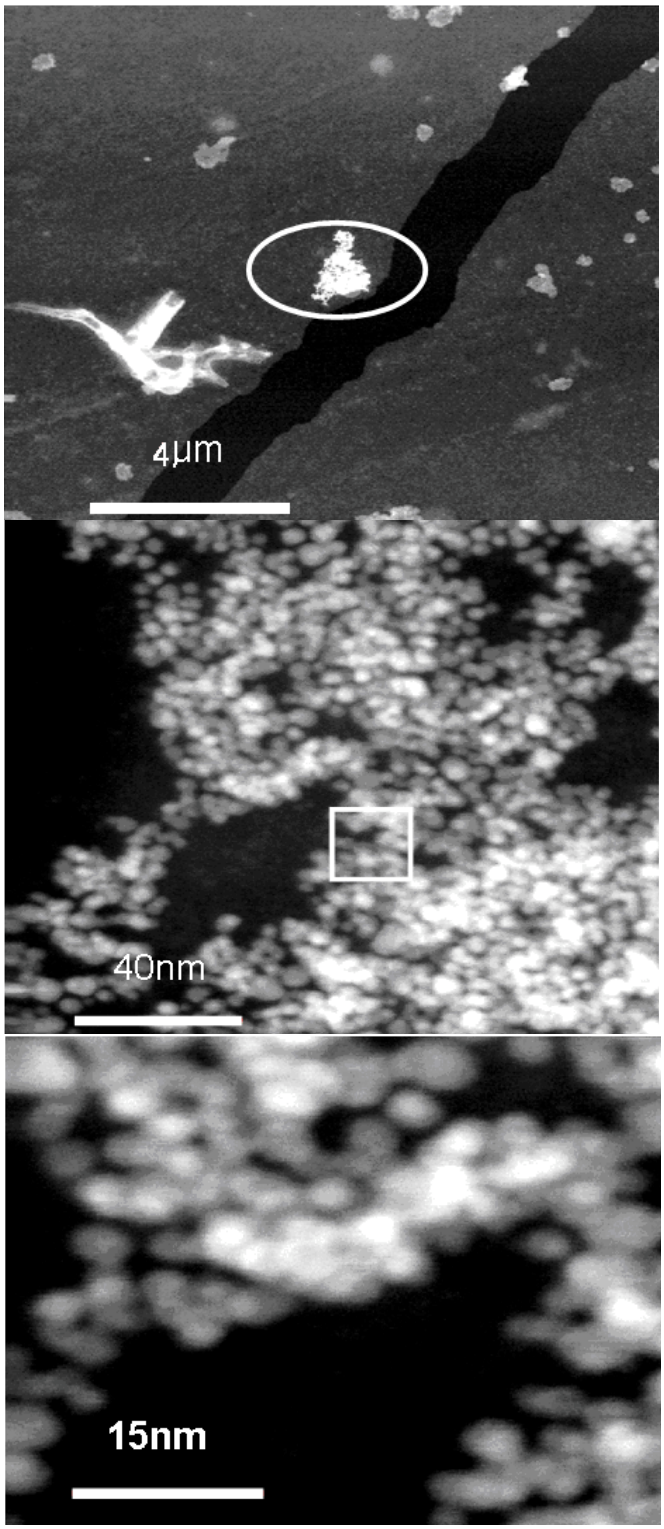

HAADF images of the second batch of $Au_{(core)}$-$Rh_{(shell)}$ bimetallic nanoparticle solution which has been heated for 30 minutes.

3.4.3 HRTEM Analysis of $Au_{(core)}$-$Rh_{(shell)}$ Bimetallic Nanoparticles

The HRTEM analysis in Figures 3.15 and 3.16 shows that there are two sets of diffraction in the aggregated nanoparticles, (111) and (200), as seen in the ring diffraction pattern (fig 3.16). This indicates FCC structure. The image (Figure 3.17) of the square large nanocrystal shows an overall BCC structure (a = 2.82 Å, b = 2.81 Å) and FCC structure (a = 2.04 Å, b = 1.98 Å) at the circled area at the edge of the nanoparticle. The square nanoparticle has a zone axis of <001>. Figure 3.18 shows enlarged sections of Figure 3.17, demonstrating the zone axis, also shown is the spot pattern of the $Au_{(core)}$-$Rh_{(shell)}$ bimetallic nanoparticles.

Figure 3.15

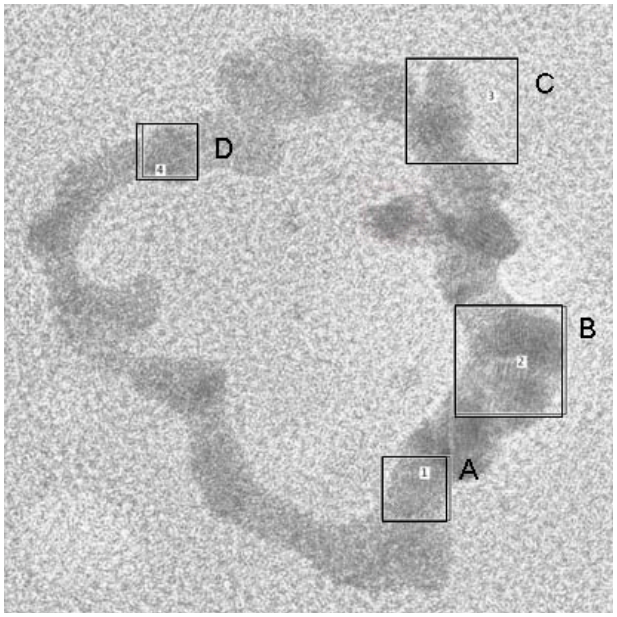

HRTEM image of aggregated $Au_{(core)}$-$Rh_{(shell)}$ bimetallic nanoparticles.

Figure 3.16

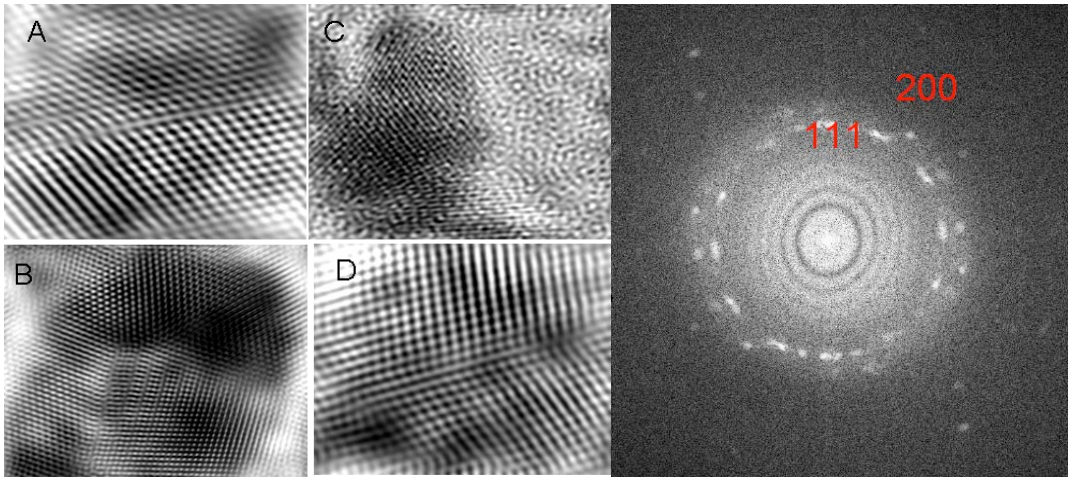

Left: HRTEM image of aggregated $Au_{(core)}$-$Rh_{(shell)}$ bimetallic nanoparticles (enlarged sections of fig. 3.15).
Right: Ring diffraction pattern of aggregated $Au_{(core)}$-$Rh_{(shell)}$ bimetallic nanoparticles.

Figure 3.17

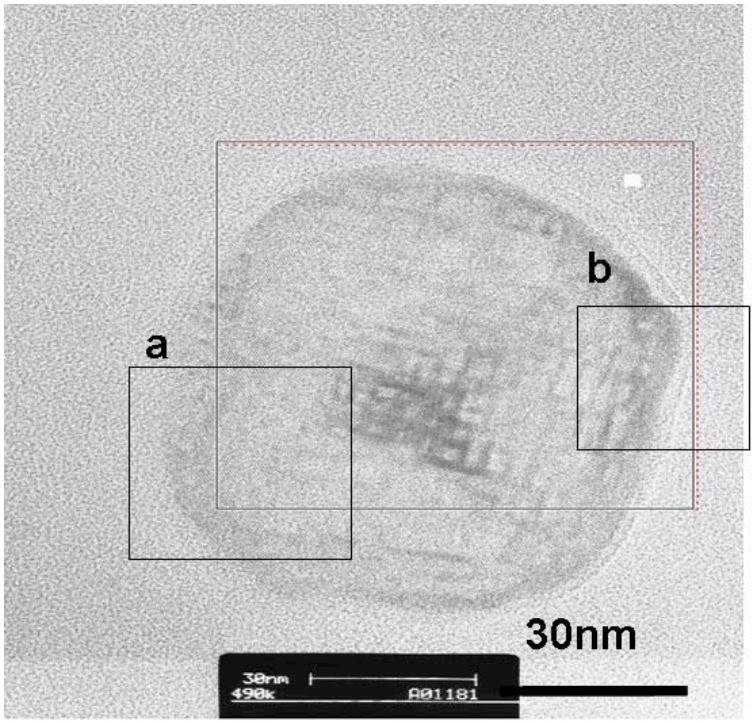

HRTEM image of square shape crystal.

Figure 3.18

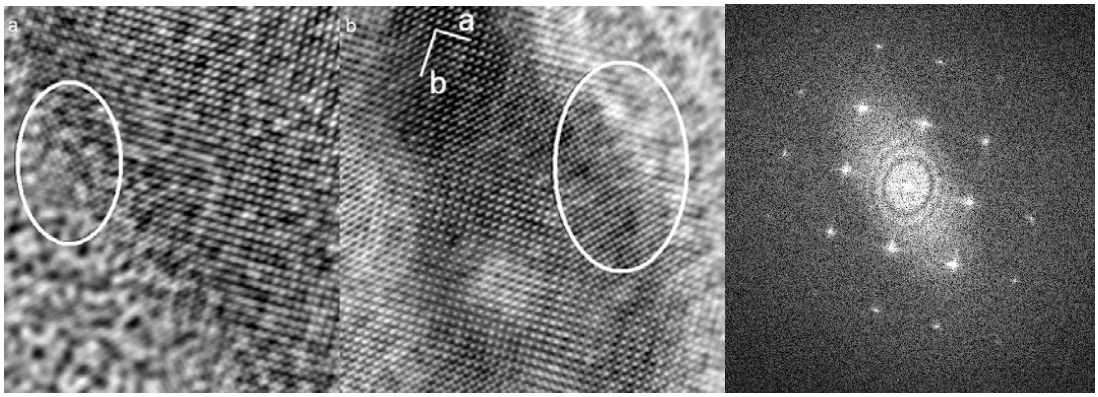

Left: HRTEM images of $Au_{(core)}$-$Rh_{(shell)}$ bimetallic nanoparticles. Enlarged sections of a & b from fig. 3.17 showing the zone axis.
Right: Spot pattern of $Au_{(core)}$-$Rh_{(shell)}$ bimetallic nanoparticles.

3.4.4 Discussion of $Au_{(core)}$-$Rh_{(shell)}$ Bimetallic Nanoparticles

The UV-vis spectra of the $Au_{(core)}$-$Rh_{(shell)}$ bimetallic nanoparticles do not show an absorption band for the Au nanoparticle seeds. This is consistent with the gold nanoparticle seeds having been coated with rhodium. The spectra of the $Au_{(core)}$-$Rh_{(shell)}$ bimetallic nanoparticles is similar to the spectra calculated for rhodium nanoparticles by Creighton and Eadon. However, this is not really conclusive as the calculated rhodium nanoparticle spectrum does not show any distinct absorption bands. The spectra of the control samples are different to those of the $Au_{(core)}$-$Rh_{(shell)}$ bimetallic nanoparticles, as the shoulder at 200 nm that is present in the $Au_{(core)}$-$Rh_{(shell)}$ bimetallic nanoparticles spectra is not observed in the control sample spectra. The control sample was also analysed by HAADF analysis and no large particles were observed.

The HAADF analysis of the $Au_{(core)}$-$Rh_{(shell)}$ bimetallic nanoparticle solution shows evidence of core-shell structure in particles of about 5 nm with a shell thickness of 0.5 -1 nm. However, the HAADF analysis also reveals that the samples are highly agglomerated. The particles appear to form chains that cluster together. It would seem that citrate stabiliser does not cause enough electrostatic repulsion to separate these particles efficiently.

The large triangular and square particles were not reproducible. The reasons for their formation are unknown. It was observed during the reaction that the nanoparticle solution had crashed out, which could be related to the cause of the large particle formation.

The TEM images show that there are two sets of diffraction in the aggregated nanoparticles, (111) and (200), as seen in the ring diffraction pattern (Figure 3.16).The image of the square large nanocrystal shows BCC and FCC faces.

The duration of heating appears to have made no difference in the appearance of the $Au_{(core)}$-$Rh_{(shell)}$ bimetallic nanoparticles, as shown by the HAADF images and the UV-vis spectroscopy.

Overall this experiment produced bimetallic $Au_{(core)}$-$Rh_{(shell)}$ nanoparticles, but like the previous experiment, the sample agglomeration was high. This could possibly be improved by adding extra citrate stabiliser in method 2, when adding the rhodium solution to the Au nanoparticle seeds solution.

3.5 $Au_{(core)}$-$Pd_{(shell)}$ Bimetallic Nanoparticles

These bimetallic $Au_{(core)}$-$Pd_{(shell)}$ nanoparticles were formed in the same way as the $Au_{(core)}$-$Pt_{(shell)}$ and $Au_{(core)}$-$Rh_{(shell)}$ bimetallic nanoparticles as described previously. This set of samples was considered to be the best of the method 2 experiments, as they are less agglomerated and show core-shell nanoparticle structure. These particles were analysed by UV-vis spectroscopy and HAADF imaging.

3.5.1 UV-vis Spectroscopic Analysis of $Au_{(core)}$-$Pd_{(shell)}$ Bimetallic Nanoparticles

Figure 3.18 shows the spectra of $Au_{(core)}$-$Pd_{(shell)}$ bimetallic nanoparticles, displaying a peak at 205 nm. No peak is observed for gold nanoparticle seeds (520 nm); this indicates that the gold nanoparticle seeds are covered with a palladium shell. Lopez-Sanchez *et al.* also found that when they mixed Au and Pd together to produce $Au_{(core)}$-$Pd_{(shell)}$ bimetallic nanoparticles, that the palladium damped the absorption band of the gold. The spectra of the $Au_{(core)}$-$Pd_{(shell)}$ bimetallic nanoparticles are similar to that reported [35]. There is no visible trend between reaction heating time and absorbance in the UV-vis wavelength range.

3.5.2 HAADF Analysis of $Au_{(core)}$-$Pd_{(shell)}$ Bimetallic Nanoparticles

The HAADF images in Figures 3.19 and 3.20 show that the $Au_{(core)}$-$Pd_{(shell)}$ bimetallic nanoparticle system prefers to form chains of particles rather than aggregating more extensively. These particles are mostly spherical, however it is clear that the gold cores are not entirely spherical and this causes the coating not to

be spherical. In some cases it would appear that a few gold seeds have agglomerated together and the palladium has coated the clump as a whole.

Figure 3.19

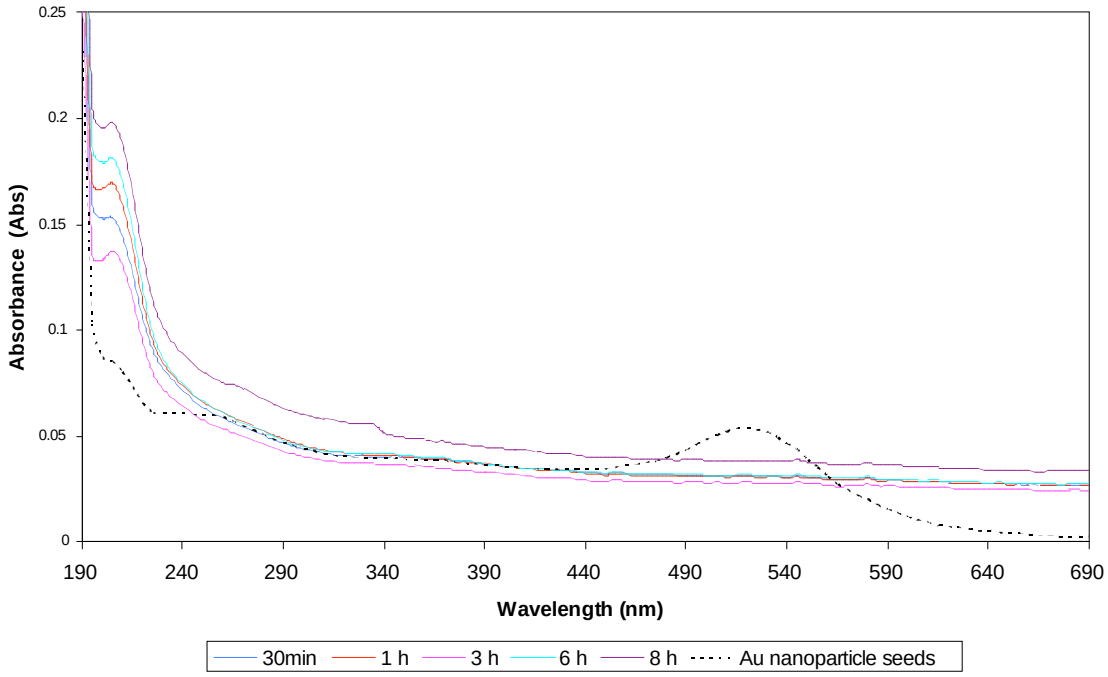

UV-vis spectra of $Au_{(core)}$-$Pd_{(shell)}$ bimetallic nanoparticles and Au nanoparicle seeds.

Figure 3.20

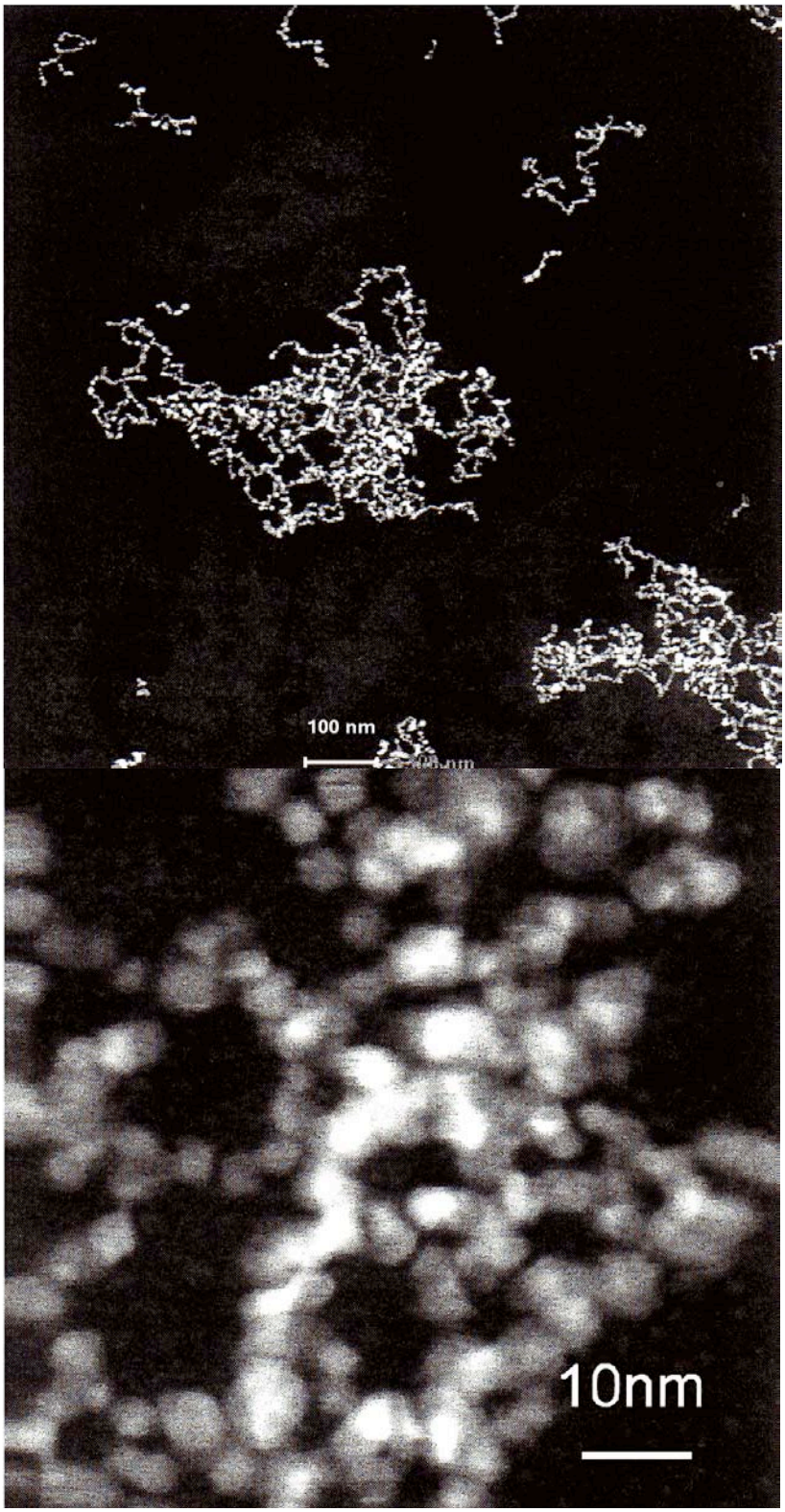

HAADF images of $Au_{(core)}$-$Pd_{(shell)}$ bimetallic nanoparticle solution which has been heated for 30 minutes.

Figure 3.21

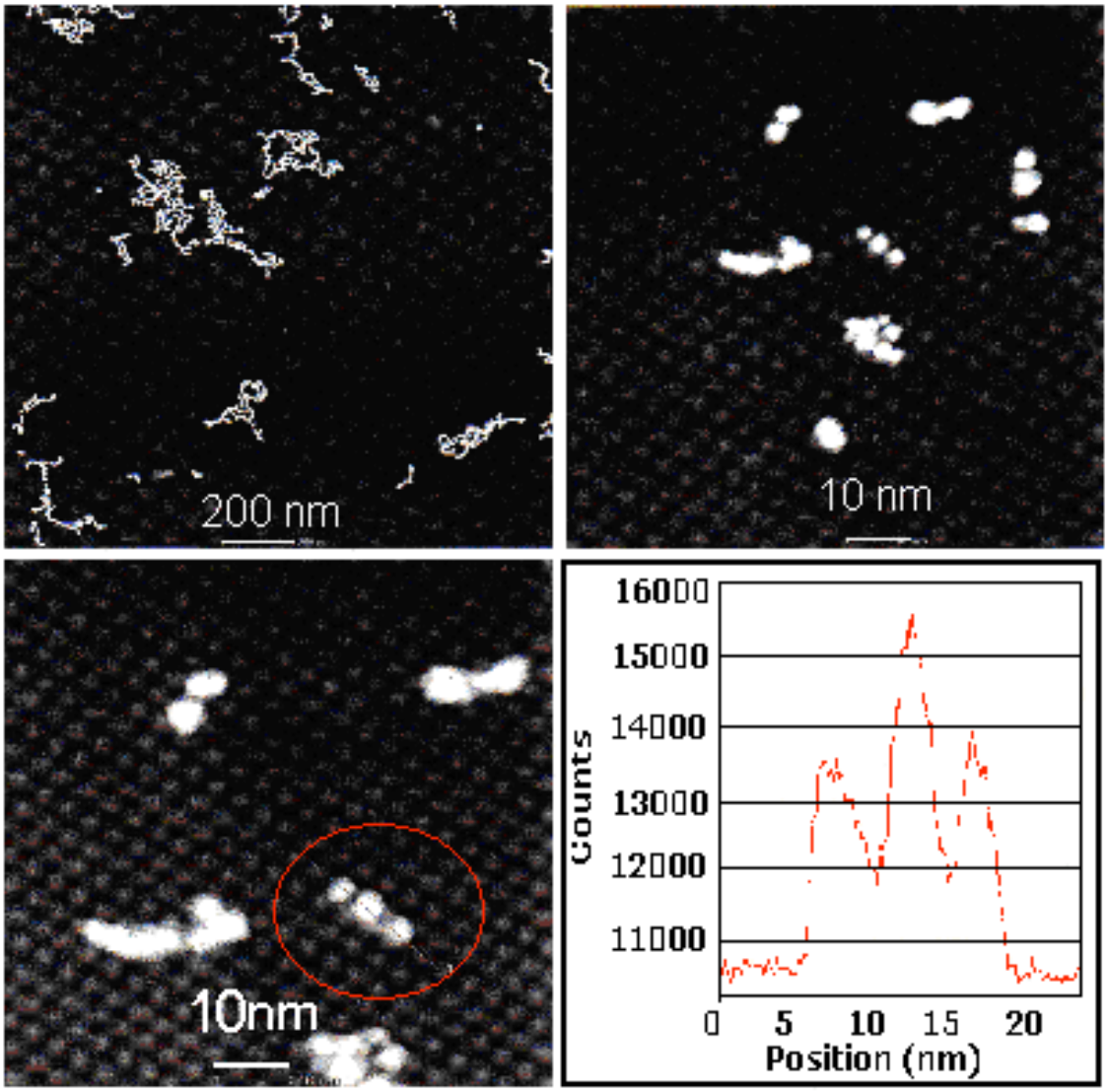

HAADF images of $Au_{(core)}$-$Pd_{(shell)}$ bimetallic nanoparticle solution which has been heated for 8 hours, including a line profile of three particles indicated in the circle in the bottom left-hand image.

3.5.3 Discussion of $Au_{(core)}$-$Pd_{(shell)}$ Bimetallic Nanoparticles

The UV-vis spectra for the $Au_{(core)}$-$Pd_{(shell)}$ bimetallic nanoparticle solution are consistent in appearance with the literature. However, the reported peak for $Au_{(core)}$-$Pd_{(shell)}$ bimetallic nanoparticles is 230 nm. This difference could be due to the different stabiliser used (PVA) in that work and the reported particles being immobilised on activated carbon [35].

These $Au_{(core)}$-$Pd_{(shell)}$ bimetallic nanoparticle solutions are less agglomerated than the $Au_{(core)}$-$Pt_{(shell)}$ and $Au_{(core)}$-$Rh_{(shell)}$ bimetallic nanoparticle systems The $Au_{(core)}$-$Pd_{(shell)}$ bimetallic nanoparticle system shows the core-shell like structure most clearly. These particles are mostly spherical, although it is clear from the HAADF analysis that the gold seed nanoparticles are not entirely spherical and this could cause the coating to be uneven. In some cases it would appear that a few gold cores have agglomerated together and the palladium has coated the agglomerated particles as a whole.

3.6 $Au_{(core)}$-$Pt_{(shell)}$ Bimetallic Nanoparticles with extra Citrate-Stabiliser

The $Au_{(core)}$-$Pt_{(shell)}$ bimetallic nanoparticles described in chapter 3.3 show poor dispersity and have a high rate of aggregation. They are also unstable under the electron microscope beam. In an attempt to improve this, additional stabiliser was added during the reaction (method 3, section 2.6).

These $Au_{(core)}$-$Pt_{(shell)}$ bimetallic nanoparticles were made using the gold seeds from method 1 and then coated via chemical deposition, as illustrated in method 3. At the time of mixing the two metal solutions, sodium citrate solution was added to stabilise the nanoparticles. These $Au_{(core)}$-$Pt_{(shell)}$ bimetallic nanoparticles were characterised by UV-vis spectroscopy, and cyclic voltammetry.

3.6.1 UV-vis Spectroscopy Analysis of $Au_{(core)}$-$Pt_{(shell)}$ Bimetallic Nanoparticles with extra Citrate Stabiliser

Figure 3.21 shows a visible Au absorption band at 515-540 nm in the spectra of $Au_{(core)}$-$Pt_{(shell)}$ bimetallic nanoparticles. There is also a peak at about 205 nm. The spectra are similar to that of Henglein for $Au_{(core)}$-$Pt_{(shell)}$ bimetallic nanoparticles with a 1:0.25 Au:Pt ratio [24].This demonstrates that the optical properties of gold nanoparticle seeds have been changed; however, the presence of the 520 nm peak indicates that some gold cores may not be coated with platinum entirely, and some may not be coated at all.

3.6.2 Cyclic Voltammetry of $Au_{(core)}$-$Pt_{(shell)}$ Bimetallic Nanoparticles with extra Citrate Stabiliser

$Au_{(core)}$-$Pt_{(shell)}$ bimetallic nanoparticles produced by method 3 were deposited on a carbon electrode and voltammograms were recorded in sulphuric acid. The voltammetry is plotted in Figure 3.23, along with a voltammogram of a bulk Pt polycrystalline electrode for comparison.

The $Pt_{(poly)}$ electrode displays two pairs of peaks af negative potentials, corresponding to reductive adsorption (cathodic sweep) and oxidative desorption (anodic sweep):

$$H^+ + e^- \leftrightarrows H_{ads}$$

The positive current between 0.8 V and 1 V is due to the formation of surface platinum oxide and the cathodic peak at 0.4 V corresponds to the reduction of this oxide.

The $Au_{(core)}$-$Pt_{(shell)}$ bimetallic nanoparticle cyclic voltammogram exhibits hydrogen evolution and oxidative deposition. The single peak is partly because of the extended potential range to more HGR current and perhaps partly because of the covering of the electrode surface by stabiliser. At positive potentials, oxidative current is difficult to discern, but shallow peaks at 0.9 V and 0.4 V are apparent. These are indicative of the reduction of gold oxide and platinum oxides respectively. The $Au_{(core)}$-$Pt_{(shell)}$ bimetallic nanoparticle cyclic voltammogram would thus indicate the presence of gold and platinum sites, although the loading on the carbon substrate is not very high.

Figure 3.22

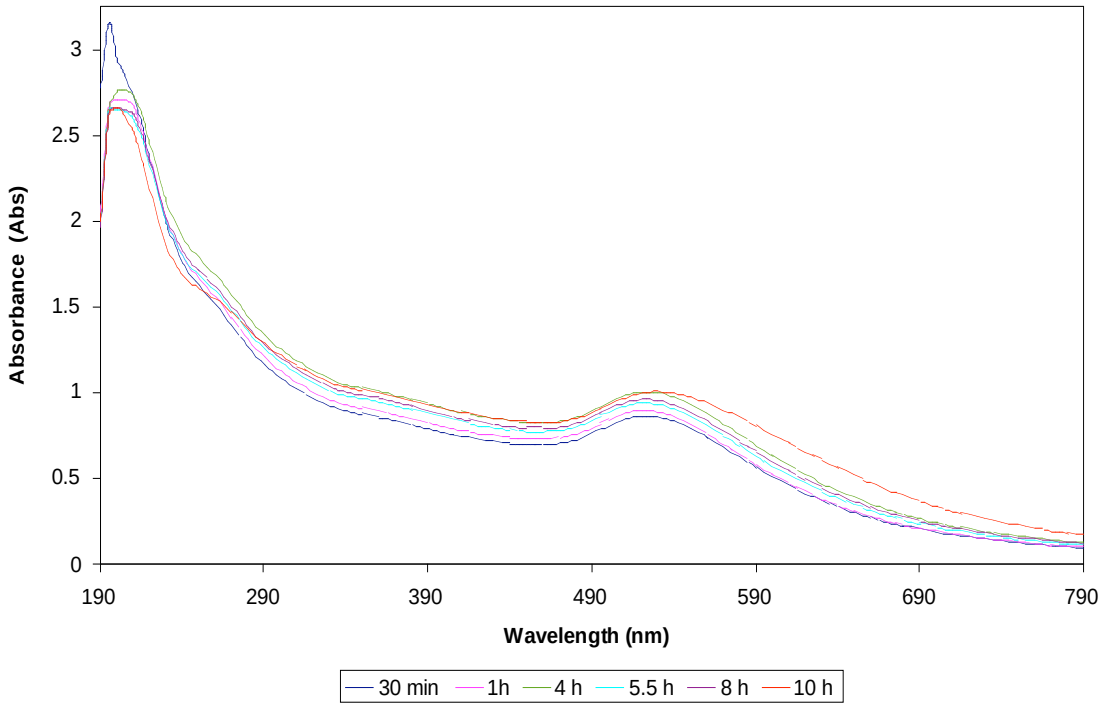

UV-vis spectra of $Au_{(core)}$-$Pt_{(shell)}$ bimetallic nanoparticles with extra citrate stabiliser.

Figure 3.23

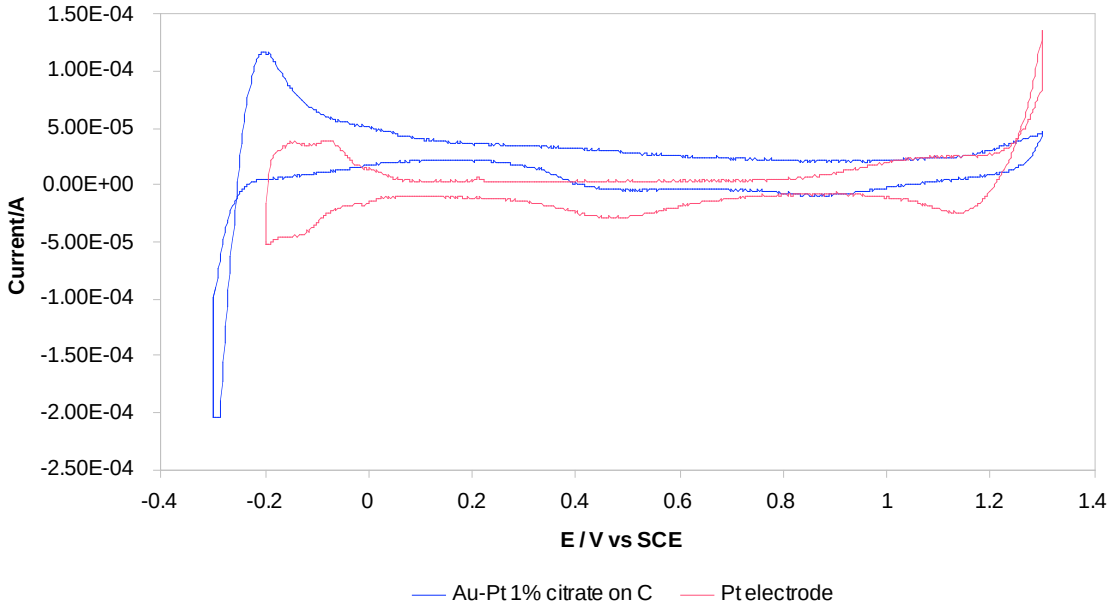

Cyclic voltammogram to show $Au_{(core)}$-$Pt_{(shell)}$ bimetallic nanoparticles with extra citrate stabiliser loaded on C and bulk polycrystalline platinum electrode in 0.05 M H_2SO_4 at a sweep rate of 0.5 V s^{-1}.

3.6.3 Discussion of. $Au_{(core)}$-$Pt_{(shell)}$ Bimetallic Nanoparticles with extra Citrate Stabiliser

The spectra of the $Au_{(core)}$-$Pt_{(shell)}$ bimetallic nanoparticles with extra citrate are different to that of the $Au_{(core)}$-$Pt_{(shell)}$ bimetallic nanoparticles discussed in section 3.3. The Pt peak has shifted to 205 nm (from 195 nm, see Figure 3.5) and a broad gold absorption is visible from 515-540 nm. This indicates that not all of the gold nanoparticle seeds are coated with platinum shells and those that are may not be completely or evenly coated. This is reflected in the cyclic voltammetry. The UV-vis spectra are similar to published data [24]. However, the spectra are not identical, possibly due to the different stabilisers used. It may be that the addition of extra stabiliser has allowed some of the platinum to nucleate and grow instead of completely coating the gold seeds.

The cyclic voltammogram of the Au-Pt bimetallic core-shell nanoparticles with 1% citrate has similarities to that of the platinum electrode, however, it only has one set of large hydrogen evolution/oxidation peaks and the oxidation peak is very small and shows both gold and platinum oxide peaks, which indicates that the gold seeds are only partially covered with platinum or forming a surface Au-Pt alloy.

3.7 $Au_{(core)}$-$Pd_{(shell)}$ Bimetallic Nanoparticles with extra Citrate Stabiliser

These $Au_{(core)}$-$Pd_{(shell)}$ bimetallic nanoparticles were formed according to method 3 (section 2.6). Extra sodium citrate solution was added to the reaction solution, at the time of the metals being mixed, to stabilise the nanoparticles as they were unstable under the electron microscope beam. It was also hoped that the additional stabiliser would prevent agglomeration of the sample. These particles were analysed by UV-vis spectroscopy.

3.7.1 UV-vis spectroscopy analysis of $Au_{(core)}$-$Pd_{(shell)}$ Bimetallic Nanoparticles with extra Citrate Stabiliser

The UV-vis spectra for the $Au_{(core)}$-$Pd_{(shell)}$ bimetallic nanoparticles in Figure 3.24 shows no visible peak at 520 nm, which is consistent with the gold core's being covered with palladium shells. This spectrum is very similar to that of the $Au_{(core)}$-$Pd_{(shell)}$ bimetallic nanoparticles with no additional citrate stabiliser. There is a shoulder of a peak at 210 nm. Unlike published data, these spectra show a peak at about 200 nm, which is associated with the palladium.

Figure 3.24

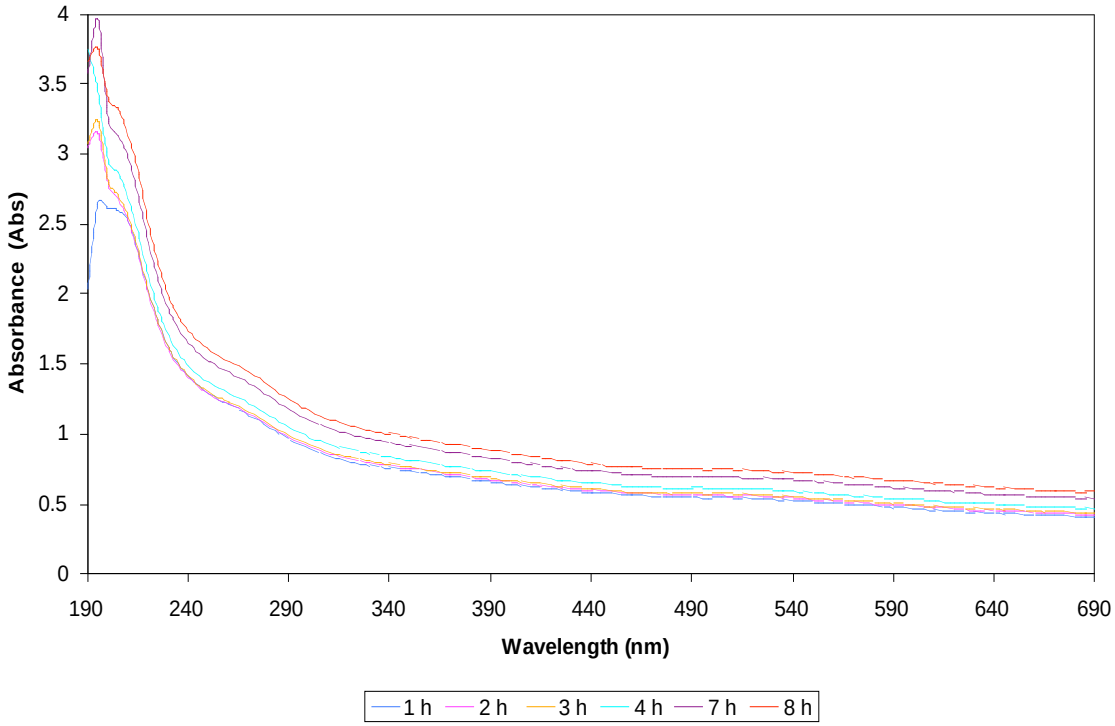

UV-vis spectra of $Au_{(core)}$-$Pd_{(shell)}$ bimetallic nanoparticles with extra citrate stabiliser.

3.7.2 Discussion of $Au_{(core)}$-$Pd_{(shell)}$ Nanoparticles with extra Citrate Stabiliser

The $Au_{(core)}$-$Pd_{(shell)}$ bimetallic nanoparticles discussed in section 3.5 had a tendency to form long chains. In this experiment, citrate solution was added in an attempt to stabilise the nanoparticles and agglomeration of the sample. The spectra of the sample without citrate stabiliser (Figure 3.19) is very similar to that of the $Au_{(core)}$-$Pd_{(shell)}$ bimetallic nanoparticles with extra stabiliser (Figure 3.24), which implies that 1% citrate stabiliser does not have much of an effect on the nanoparticle system. Further analysis of these samples with electron microscopy would give a clearer picture as to the extent of agglomeration of the sample.

3.8 $Au_{(core)}$-$Pd_{(shell)}$ Bimetallic Nanoparticles (1:4 Au:Pt and 10% Citrate Stabiliser)

These $Au_{(core)}Pd_{(shell)}$ bimetallic nanoparticles were produced according to method 4 (section 2.7). This is similar to how the particles from method 3 were produced, however, a four times more concentrated solution of palladium was used and the amount of citrate stabiliser was increased from 1% to 10%. Also, the amount of reducing agent was increased to ensure all of the palladium was reduced onto the gold cores. This was to further improve the nanoparticle stability under the electron microscope beam and to improve the monodispersity of the particles within the sample. It was also anticipated that the increased amount of palladium solution would result in a thicker palladium shell, making the core-shell structure easier to observe with the electron microscope. These $Au_{(core)}Pd_{(shell)}$ bimetallic nanoparticles were characterised by UV-vis spectroscopy analysis, AFM and HAADF analysis.

3.8.1 UV-vis Spectroscopy Analysis of $Au_{(core)}$-$Pd_{(shell)}$ Bimetallic Nanoparticles (1:4 Au:Pt and 10% Citrate Stabiliser)

The spectra for the $Au_{(core)}$-$Pd_{(shell)}$ bimetallic nanoparticles from method 4 shown in show no plasmon band at 520 nm, which indicates that the gold nanoparticle seed cores are covered with palladium shells. The sample heated for 1.5 hours shows a shoulder at 220 nm which appears to have shifted to the right with increased reaction duration; the sample heated for 5 hours shows a peak at 225 nm, the sample heated for 10 hours shows a peak at 230 nm and the samples heated for 15 and 20 hours show a peak at 235 nm. This indicated that the shell is changing

slightly with increased heating time. The spectra of the $Au_{(core)}$-$Pd_{(shell)}$ bimetallic nanoparticles are consistent with the published data [33, 34].

3.8.2 HAADF Analysis of $Au_{(core)}$-$Pd_{(shell)}$ Bimetallic Nanoparticles (1:4 Au:Pt and 10% Citrate Stabiliser)

Figures 3.36-3.31 show HAADF images of $Au_{(core)}$-$Pd_{(shell)}$ Bimetallic Nanoparticles (1:4 Au:Pt and 10% citrate stabiliser). The samples that were investigated by HAADF analysis were the $Au_{(core)}$-$Pd_{(shell)}$ bimetallic nanoparticles heated for 1.5, 5 and 20 hours. Some of the samples (1.5 and 20 hours) were diluted to see if this gave a better image, as it would decrease clustering. However, the cluster dispersion is not improved by dilution. The clusters appear to aggregate at the edges of the TEM carbon grids.

The particles form small chains. There is visible Z contrast (Au: 79 and Pd: 46). No individual particles are visible, which implies that a higher concentration of citrate does not cause increased steric hindrance or repulsion between particles; in fact quite the opposite has occurred. With increased reaction duration (for example, 20 hours compared with 1.5 hours) larger groups of chains are formed. The increased reaction duration and larger cluster density has caused the clusters to grow into dendritic crystals (Figures 3.29 and 3.30). The sample that was heated for 5 hours has an identified core-shell structure (see Figures. 3.27 and 3.28). This sample also has a better dispersion than those that were heated for 20 hours, and individual particles are visible. In Figure 3.28 the shell appears spherical but the core is misshapen. This particle is approximately 10 nm in diameter and the average particle size is 7.5 nm. The line profile shows the roughness of the particle, the arrow

is pointing to a shoulder in the profile, which is indicative of the palladium shell, however, there are two lumps of metal on top of this particle, indicated by the two peaks at approximately 9 and 13 nm. The line profile for Figure 3.29 has a more pronounced shoulder, as it has a thicker palladium shell. The palladium coatings are not consistent; some particles have a thicker shell than others. As with other samples, where the Au seeds have aggregated, the coating has covered the aggregated sections, as opposed to individual particles. This sample has thicker shells, due to the increased amount of palladium in the reaction mixture. Also the shells are more uniform than the shells on the particles produced by method 2.

Figure 3.25

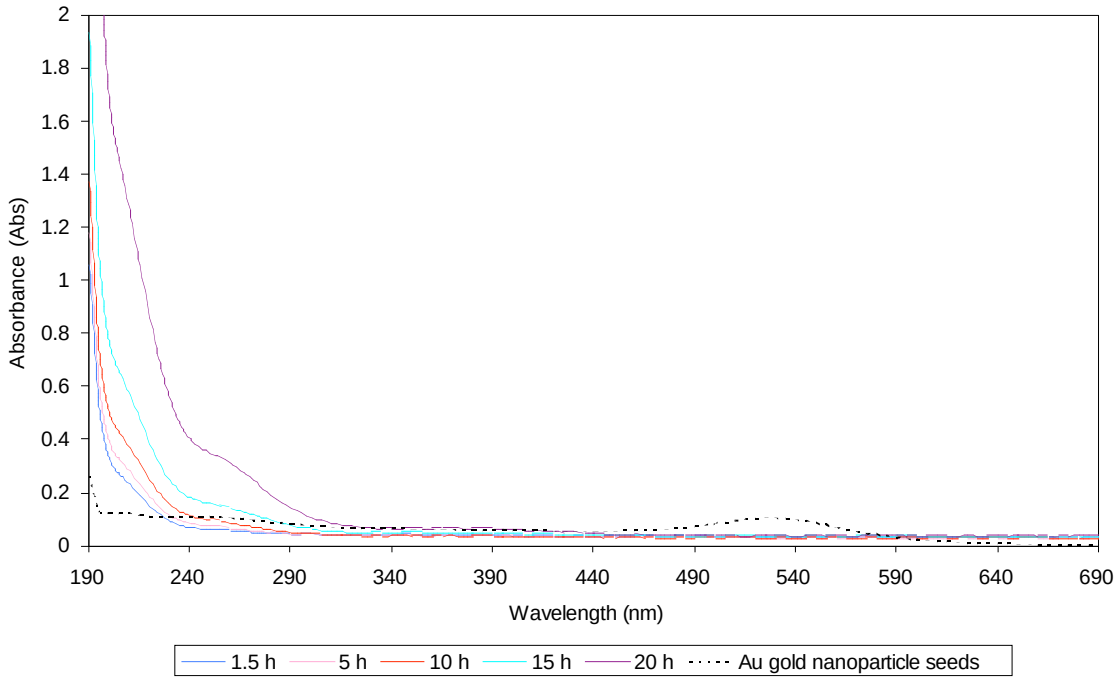

UV-vis spectra of $Au_{(core)}$-$Pd_{(shell)}$ bimetallic nanoparticles with a 1:4 metal ratio and 10% citrate stabiliser and Au nanoparticle seeds.

Figure 3.26

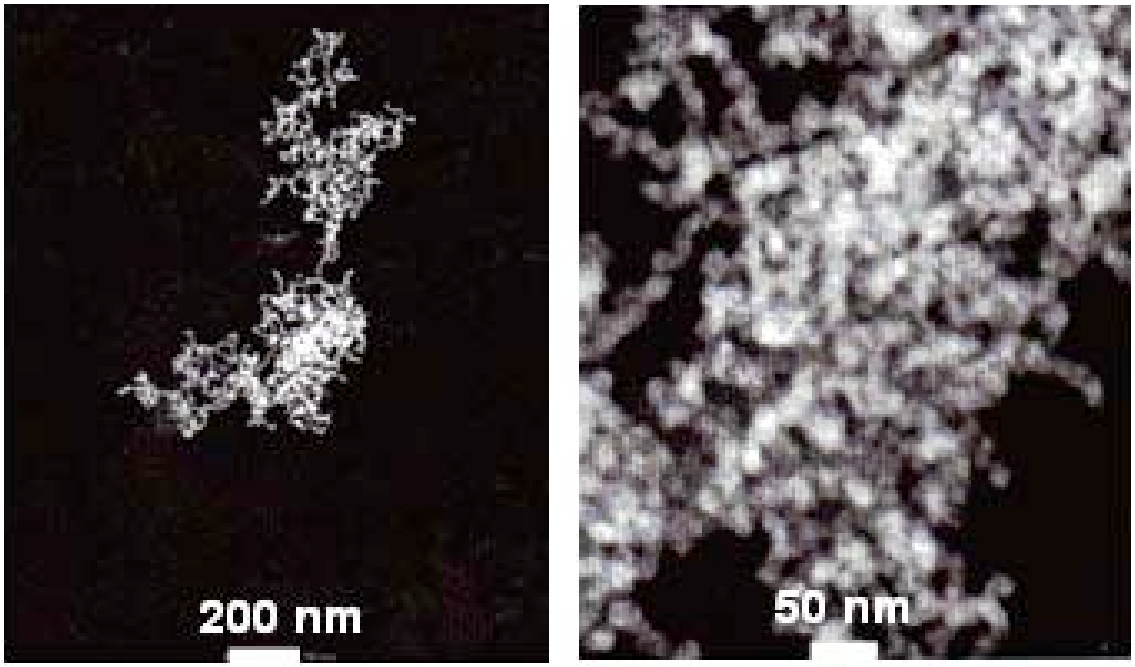

HAADF image of $Au_{(core)}$-$Pd_{(shell)}$ bimetallic nanoparticle solution, with a 1:4 metal ratio and 10% citrate stabiliser, which has been heated for 1.5 hours at 20x dilution

Figure 3.27

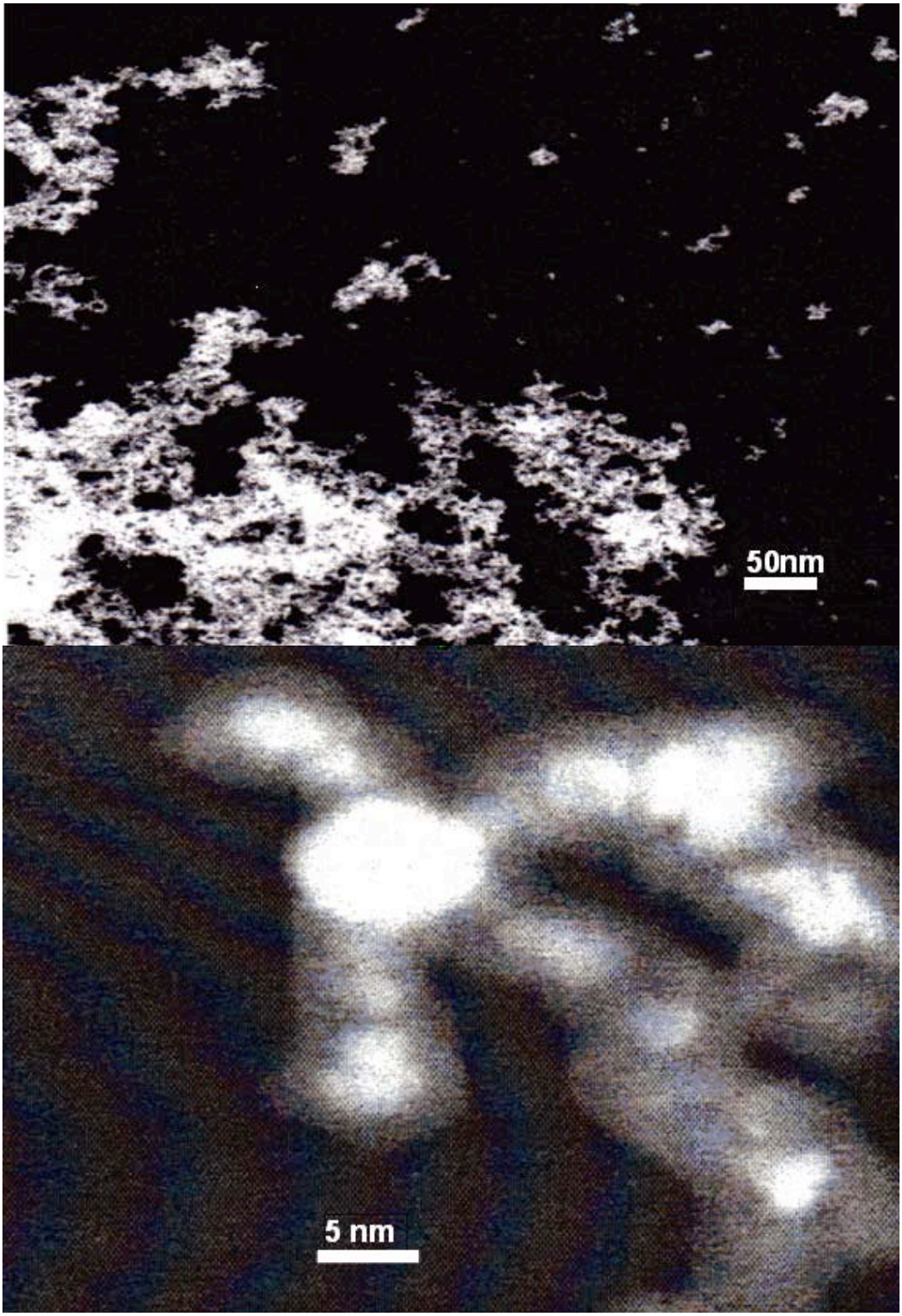

HAADF image of $Au_{(core)}$-$Pd_{(shell)}$ bimetallic nanoparticle solution, with a 1:4 metal ratio and 10% citrate stabiliser, which has been heated for 5 hours.

Figure 3.28

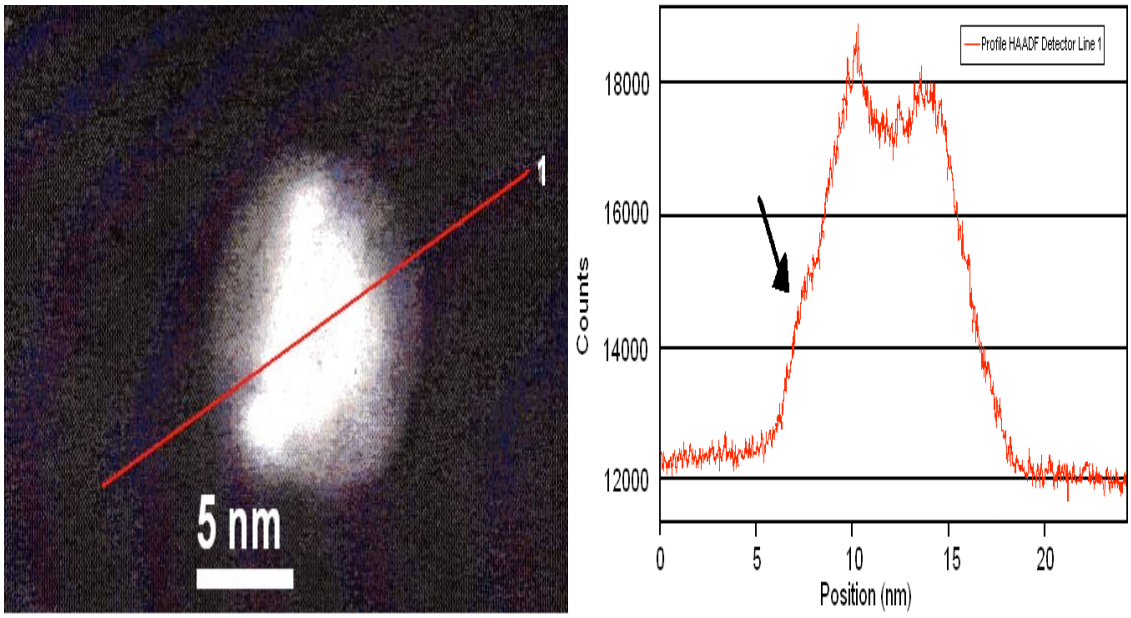

HAADF image of $Au_{(core)}$-$Pd_{(shell)}$ bimetallic nanoparticle with a 1:4 metal ratio and 10% citrate stabiliser, which has been heated for 5 hours with HAADF detector line profile.

Figure 3.29

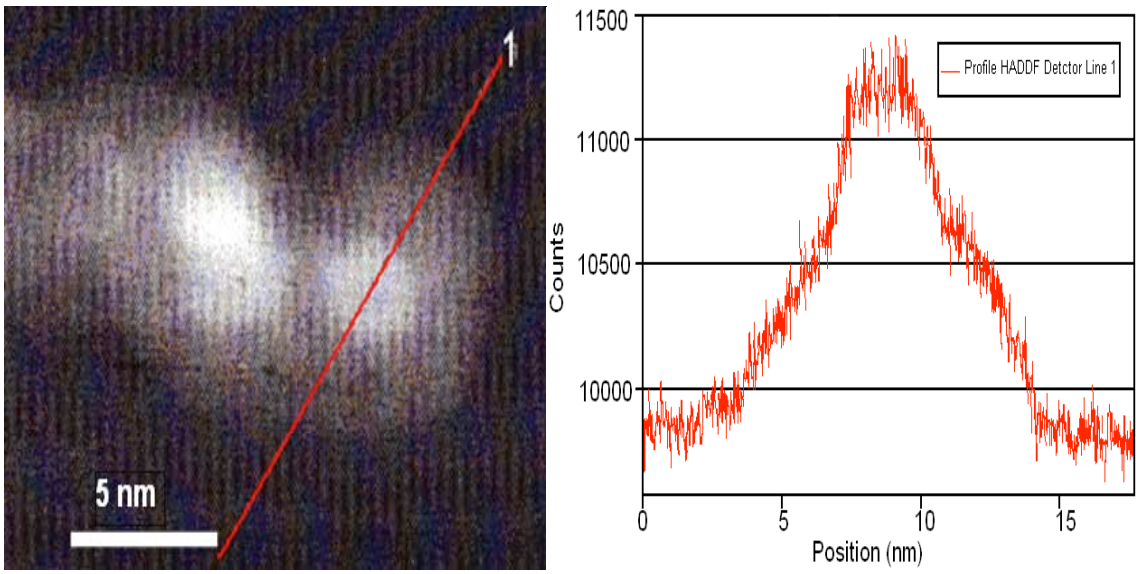

HAADF image of $Au_{(core)}$-$Pd_{(shell)}$ bimetallic nanoparticles, with a 1:4 metal ratio and 10% citrate stabiliser, which has been heated for 5 hours with HAADF detector line profile.

Figure 3.30

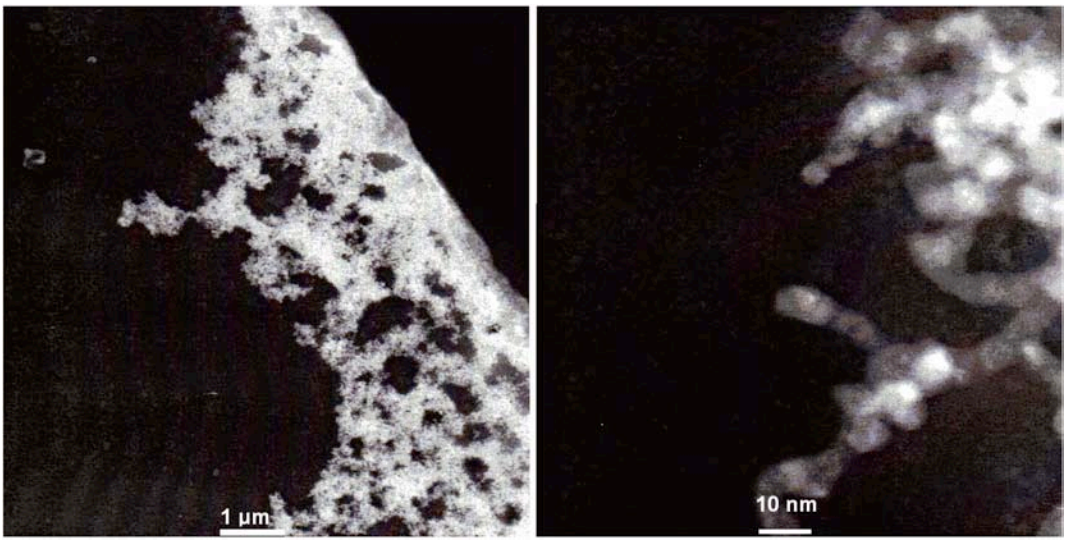

HAADF image of $Au_{(core)}$-$Pd_{(shell)}$ bimetallic nanoparticle solution, with a 1:4 metal ratio and 10% citrate stabiliser, which has been heated for 20 hours at 20x dilution.

Figure 3.31

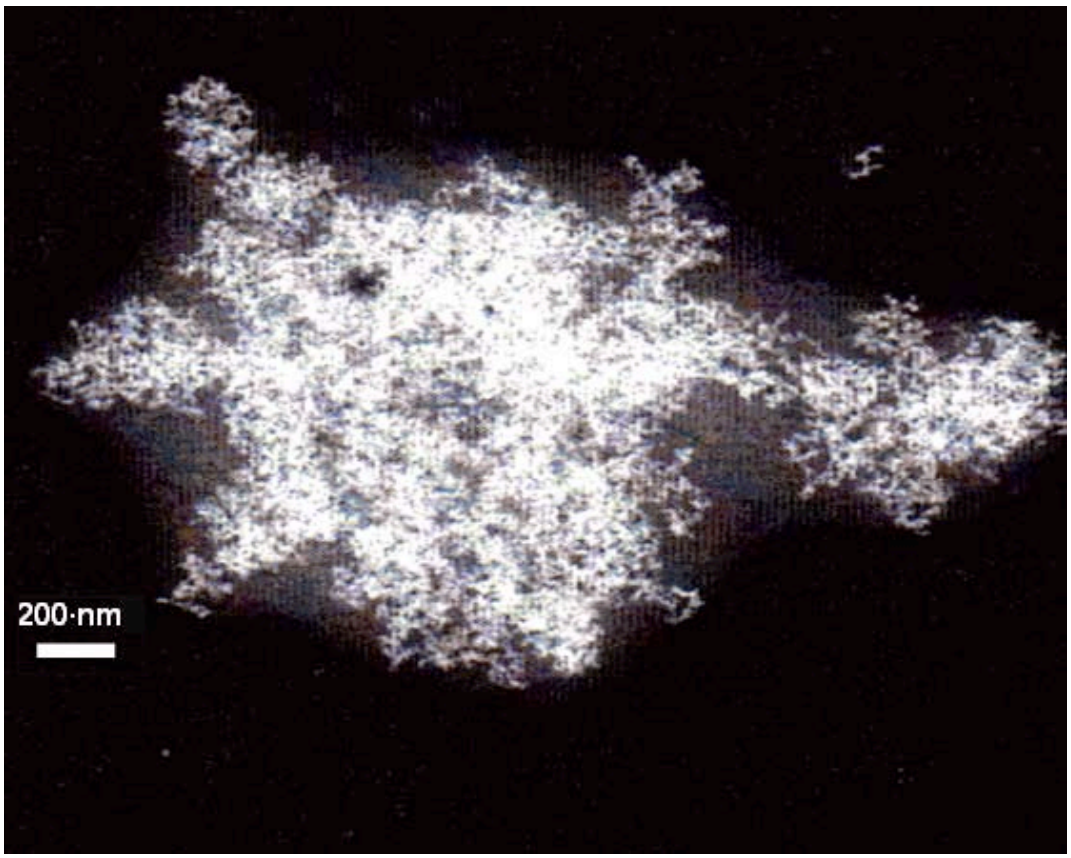

HAADF image of $Au_{(core)}$-$Pd_{(shell)}$ bimetallic nanoparticle solutions, with a 1:4 metal ratio and 10% citrate stabiliser, which has been heated for 20 hours.

3.8.3 Discussion of $Au_{(core)}$-$Pd_{(shell)}$ Bimetallic Nanoparticles (1:4 Au:Pd and 10% citrate stabiliser)

The aim of method 4 was to produce $Au_{(core)}Pd_{(shell)}$ bimetallic nanoparticles with thicker palladium shells and lower aggregation, as previous results had high rates of aggregation.

The HAADF images (Figures 3.28 and 3.29) of $Au_{(core)}$-$Pd_{(shell)}$ bimetallic nanoparticles show some particles with core-shell structure that are about 7.5 nm in diameter, but also that the increased amount of citrate stabiliser has not reduced the aggregation of the samples. The increased amount of palladium in the reaction has resulted in thicker and more even palladium shells. With the increasing reaction duration, the particles become more aggregated. This has caused the clusters to grow into dendritic crystals (Figures 3.30 and 3.31). The sample that was heated for 5 hours has a better dispersion than those that were heated for 20 hours, implying that for this reaction, 5 hours may be the optimum reaction duration. The palladium shells are uneven; this could be due to the irregular shaped gold nanoparticle seed cores. This method could be improved by possibly increasing the amount of stabiliser used, or perhaps using a stronger stabiliser. Also more spherical gold cores would improve even palladium shell deposition.

Overall this experiment was partially successful, increasing the amount of palladium available for deposition onto the gold nanoparticle core seeds does increase the palladium shell thickness. However, increasing the citrate stabiliser to 10% at the addition of the palladium to the gold nanoparticle seeds does not improve dispersity of the nanoparticles.

3.9. Discussion of Citrate-Stabilised Nanoparticles

The gold nanoparticle seeds produced according to Brown *et al*. [4] were similar in appearance to those published, however, they were of a slightly larger size (3.7 nm) The UV-vis spectroscopy analysis of the gold nanoparticle sols produced agrees with the literature [4, 29, 31]. This is a very straightforward way to produce gold nanoparticle seeds, which made them ideal to use as starting material for producing bimetallic core-shell nanoparticles. However, the unevenness of the gold particle shape has resulted in the bimetallic core-shell product's being unevenly coated.

The particles produced according to method 2 did all show bimetallic core-shell structure, as was reflected by the UV-vis spectroscopy. The UV-vis spectra of these bimetallic particle systems did not show the absorption band associated with the gold nanoparticle seeds. The HAADF analysis revealed the samples to be highly aggregated and unstable under the electron microscope beam. This led to the reaction parameters being altered to develop methods 3 and 4.The large triangular and square nanoparticles formed when producing $Au_{(core)}$-$Rh_{(shell)}$ bimetallic nanoparticles were not reproduced and it was decided to concentrate on the $Au_{(core)}$-$Pt_{(shell)}$ and $Au_{(core)}$-$Pd_{(shell)}$ nanoparticles. In method 3 additional citrate stabiliser was added at the time of mixing the two metals, to stabilise the particles. The UV-vis spectra for the $Au_{(core)}$-$Pt_{(shell)}$ bimetallic nanoparticle system produced according to method 3 showed a strong absorbance at 515-540 nm, which indicated that the gold nanoparticle seeds were not being completely coated. No further analysis was performed on the samples from method 3, and the samples from method 4 become the focus of the project. Method 4 involved the metal ratio from 1:1

Au:Pd to 1:4 Au:Pd and the amount of citrate stabiliser added at the time of the metals was mixed being increased to 10%. The particles produced using method 4 had thicker shells than those produced by method 2, indicating that increasing the amount of metal salt available for deposition increases shell thickness. However, the aggregation of the samples was not improved by the additional citrate stabiliser.

Overall, methods 2, 3 and 4 did produce bimetallic core-shell nanoparticles; however, it was felt that a better bimetallic core-shell product could be produced by using gold nanoparticle seeds with a more regular shape. This is investigated in chapter 5, which looks at using gold nanoparticle seeds stabilised with thiol instead of citrate.

CHAPTER 4 – THIOL-STABILISED NANOPARTICLES

4.1 Introduction to Thiol-Stabilised Gold Nanoparticles

After trying various experiments using citrate as a stabilizing agent, it was decided to try thiol-stabilised reactions, to see if this gave less aggregation in the bimetallic core-shell product. The method used to produce gold nanoparticle seeds is reported by Yang *et al.* [5]. This method was also adapted to see if it could be applied to other metal salts to produce different starting products and also, if it could be adapted to produce bimetallic core-shell nanoparticles.

4.2 Thiol-Stabilised Gold Nanoparticle Seeds

These seeds were made according to Yang *et al*. [5] (section 2.8 (method 5)). They are thiol-stabilised gold nanoparticles seeds with an average size of 3.1±0.26 nm. The particles produced according to method 5 were characterised using HAADF analysis and cyclic voltammetry.

4.2.1 HAADF Analysis of Thiol-Stabilised Gold Nanoparticle Seeds

Figure 4.1 shows HAADF images of the thiol-stabilised gold nanoparticles. These gold seeds are mostly spherical and well dispersed, although occasionally particles have formed small chains of 2-7 particles. The particles appear monodisperse in size. These particles have an average size of 3.6±0.68 nm, which is in reasonable agreement with the size reported (3.1±0.26 nm). These particles also

withstood the electron microscope beam far better than the citrate stabilised particles. This could be due to thiol being a better stabilizing agent than citrate.

4.2.2 Cyclic Voltammetry of Thiol-Stabilised Gold Nanoparticle Seeds

The cyclic voltammogram for the thiol stabilised gold nanoparticles adsorbed on carbon shown in Figure 4.2 has a small oxidation onset at 1 V. Hydrogen evolution is observed negative of approximately -0.4 V. The thiol-stabiliser appears not to be blocking the HER. This cyclic voltammogram it is similar to that of the citrate-stabilised gold seeds (Figure 3.3).

Figure 4.1

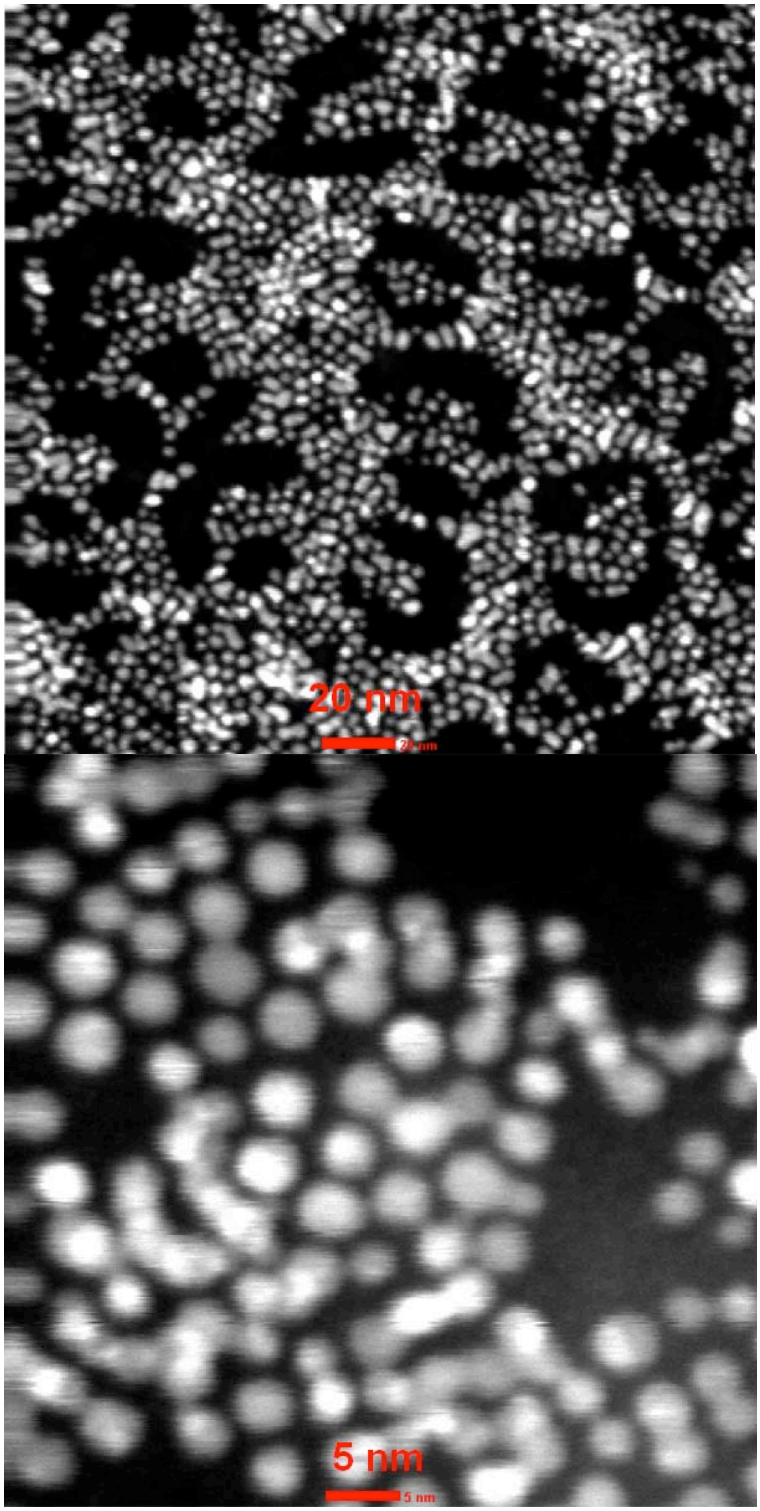

HAADF images of thiol-stabilised gold nanoparticle seeds.

Figure 4.2

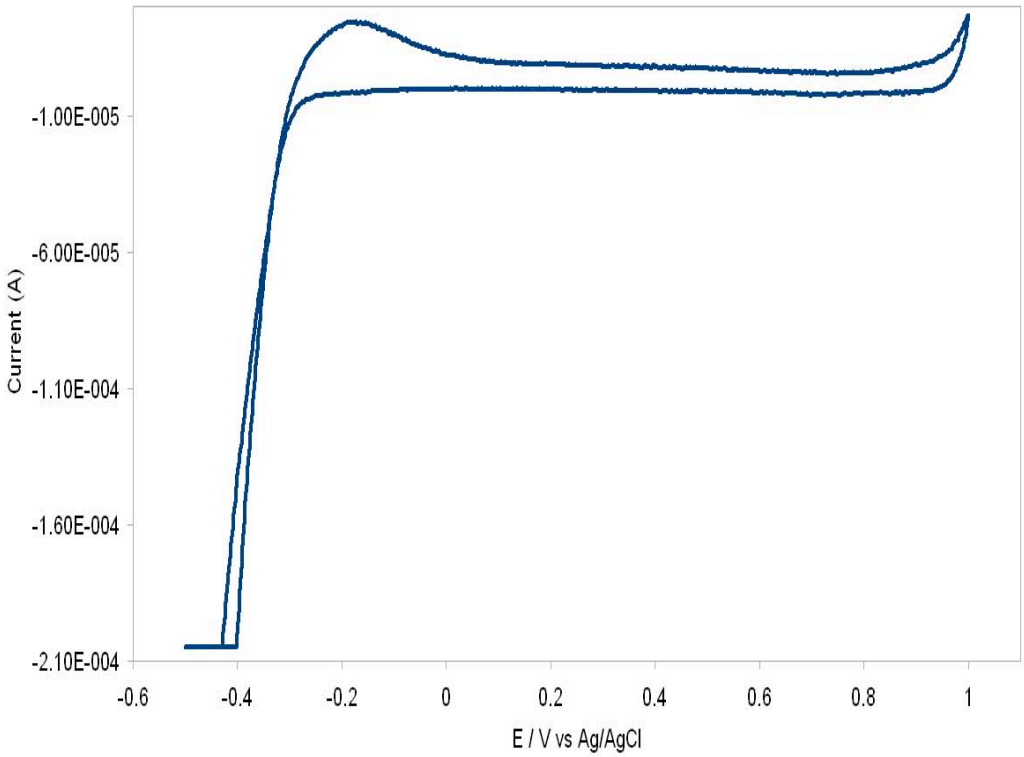

Cyclic voltammogram of thiol-stabilised gold nanoparticles in 0.05 M H_2SO_4, at a sweep rate of 0.05 V s^{-1}.

4.2.3 Discussion of Thiol-Stabilised Gold Nanoparticle Seeds

The thiol-stabilised gold nanoparticle seeds made according to method 5 are well separated; not forming clusters, and appear monodisperse in size. Most particles are spherical, however, some particles have formed small chains of 2-7 particles. These thiol-stabilised gold nanoparticles have an average size of 3.6±0.68 nm which is consistent for the published data on this method [5]. They exhibit a more regular spherical shape than those produced according to method 2.

4.3 Thiol-Stabilised $Au_{(core)}$-$Pd_{(shell)}$ Bimetallic Nanoparticles

These $Au_{(core)}$-$Pd_{(shell)}$ bimetallic nanoparticles were produced according to method 6 (chapter 2, section 2.9). These particles were investigated by UV-vis spectroscopy and HAADF analysis.

4.3.1 UV-vis Spectroscopy Analysis of Thiol-Stabilised $Au_{(core)}$-$Pd_{(shell)}$ Bimetallic Nanoparticles

The UV-vis spectrum of $Au_{(core)}$-$Pd_{(shell)}$ bimetallic nanoparticles in Figure 4.4 has an absorption band at 570 nm. This absorption peak is associated with gold nanoparticles of about 75 nm in size [22]. This could indicate that either the particles are very large, or that they are very misshapen, causing optical scattering. The peak associated with gold indicates that not all the gold nanoparticle seed are covered with palladium. The spectrum is similar to that reported by Lopez-Sanchez *et al.* [35].

4.3.2 HAADF Analysis of Thiol-Stabilised $Au_{(core)}$-$Pd_{(shell)}$ Bimetallic Nanoparticles

The HAADF images (Figure 4.5) do not show much evidence of core-shell structures, although a few core-shell particles were observed (Figure 4.6). This indicates that the palladium prefers to nucleate separately. The gold seeds that are coated in palladium have a very thin shell, which is less than 1 nm in thickness. The bimetallic $Au_{(core)}$-$Pd_{(shell)}$ nanoparticles are spherical in shape with an average size of 4 nm.

Figure 4.4

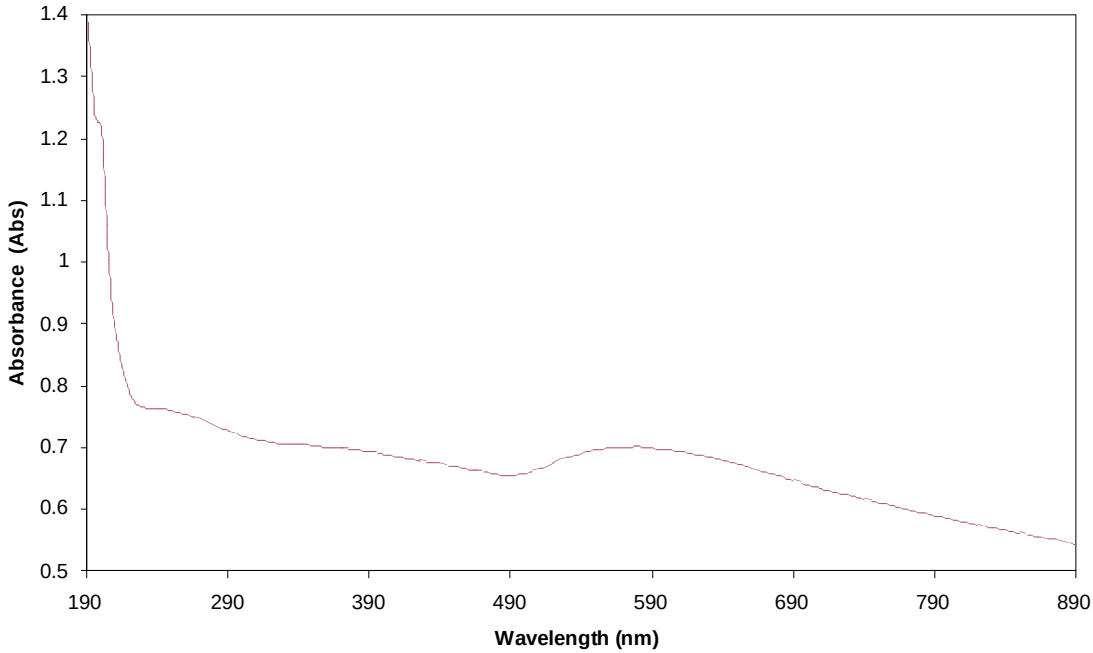

UV-vis spectrum of $Au_{(core)}$-$Pd_{(shell)}$ bimetallic nanoparticles in ethanol.

Figure 4.5

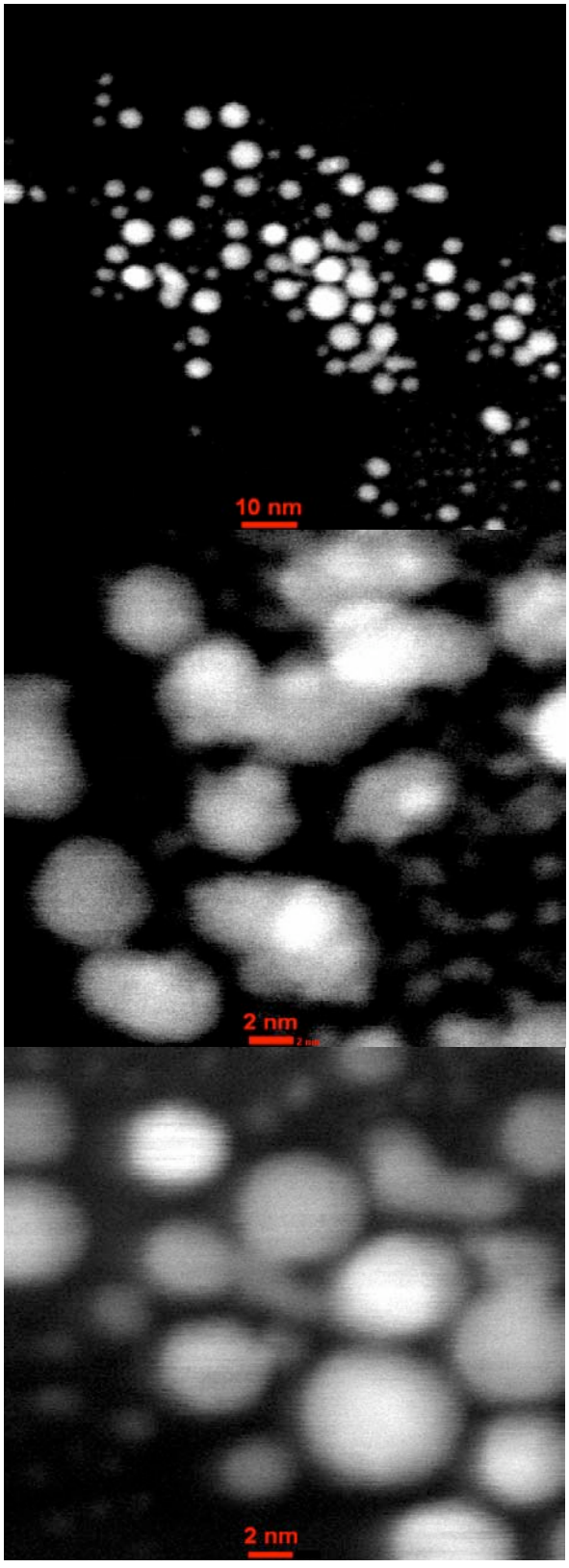

HAADF images of thiol-stabilised $Au_{(core)}$-$Pd_{(shell)}$ bimetallic nanoparticles.

Figure 4.6

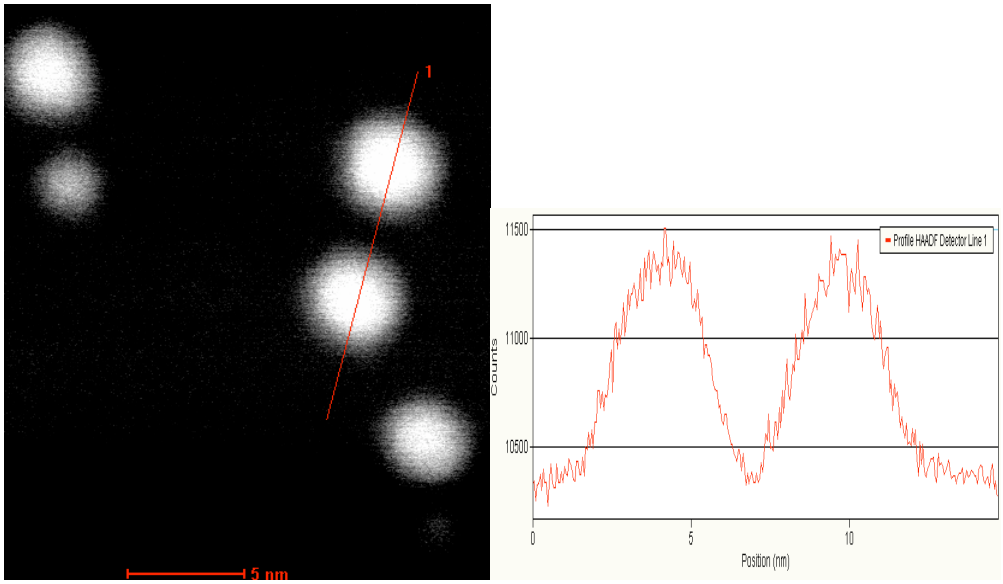

HAADF image of thiol-stabilised $Au_{(core)}$-$Pd_{(shell)}$ bimetallic nanoparticles with line profile.

Figure 4.7

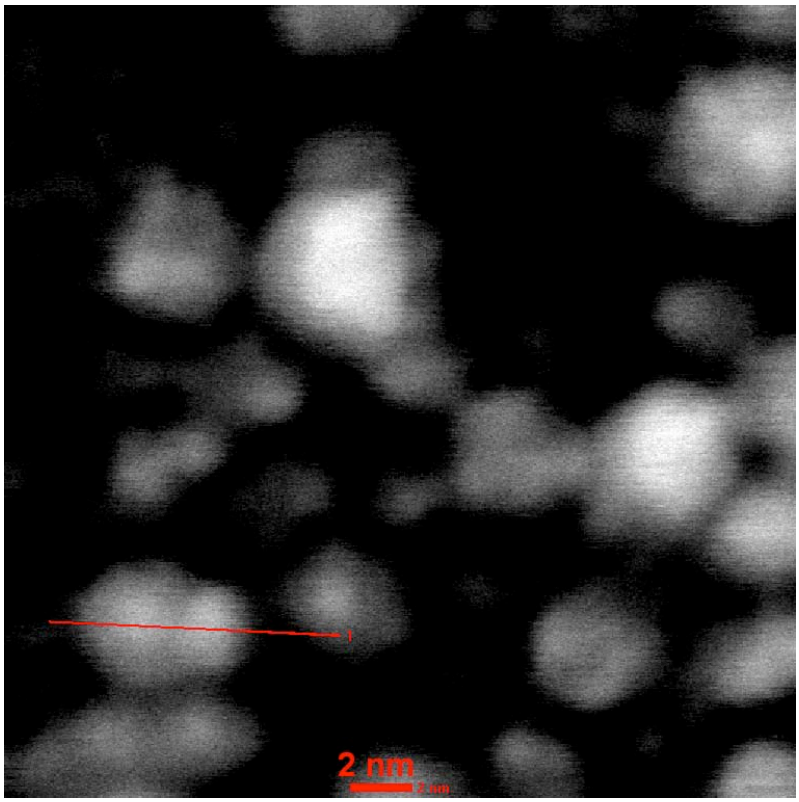

HAADF image of thiol-stabilised $Au_{(core)}$-$Pd_{(shell)}$ bimetallic nanoparticles showing core-shell structure as indicated by the line.

4.3.3 Discussion of Thiol-Stabilised $Au_{(core)}$-$Pd_{(shell)}$ Bimetallic Nanoparticles

The UV-vis spectrum for $Au_{(core)}$-$Pd_{(shell)}$ bimetallic nanoparticles has an absorption band at 570 nm associated with gold nanoparticles The broadening of the spectra could be due to polydispersity, partial aggregation or irregular-shaped particles [31].This is seen in the HAADF images. The UV-vis spectroscopy indicates that not all the gold nanoparticle seed are covered with palladium.. The spectrum of thiol-stabilised $Au_{(core)}$-$Pd_{(shell)}$ bimetallic nanoparticles is similar in appearance to that reported by Lopez-Sanchez *et al.* [35].

The HAADF analysis shows that the palladium appears to be nucleating separately, resulting in monometallic Au and Pd nanoparticles. The particles are not aggregated, and a limited amount of bimetallic core-shell behaviour is observed.

Although this method has produced bimetallic $Au_{(core)}$-$Pd_{(shell)}$ nanoparticles which are spherical in shape with an average size of 4 nm with an even shell thickness of approximately 1 nm, these particles are a minority population within the sample. The most likely explanation is that the palladium ions have difficulty diffusing between the thiol chains to deposit on the gold particle surface. The palladium is reduced before it can reach a gold seed particle and thus palladium nuclei grow to form nanoparticles.

4.4 Thiol-Stabilised Rhodium Nanoparticles

These seeds are produced according to method 7 (chapter 2, section 2.10). This is the same method as was used for the gold particles (method 5), except that the gold metal salt has been replaced with a rhodium salt. This was carried out to determine whether the gold seed production method could be adapted to other metals. If this method had been successful, the rhodium particles would have been used as core material in a bimetallic core-shell nanoparticle system. These particles were analysed using UV-vis spectroscopy and HAADF analysis.

4.4.1 UV-vis Spectroscopy Analysis of Thiol-Stabilised Rhodium Nanoparticles

Figure 4.8 shows the UV-vis spectra of these particles, which shows a strong absorption at 205 nm. The calculated spectra for rhodium nanoparticles only shows only a rather broad absorption continuum which extends throughout the visible-near ultraviolet range [31]. The observed spectrum has red shift compared with the calculated spectra. This could be due to polydispersity, partial aggregation or irregular-shaped particles [31].

4.4.2. HAADF Analysis of Thiol-Stabilised Rhodium Nanoparticles

The HAADF analysis (Figure 4.9) shows some small nanoparticles of about 6 nm in diameter dispersed amongst background material that could be left over reagents from the reaction. The nanoparticles have a low density. A large population of particles approximately 1 nm in diameter can be found under the larger aggregated rhodium particles.

Figure 4.8

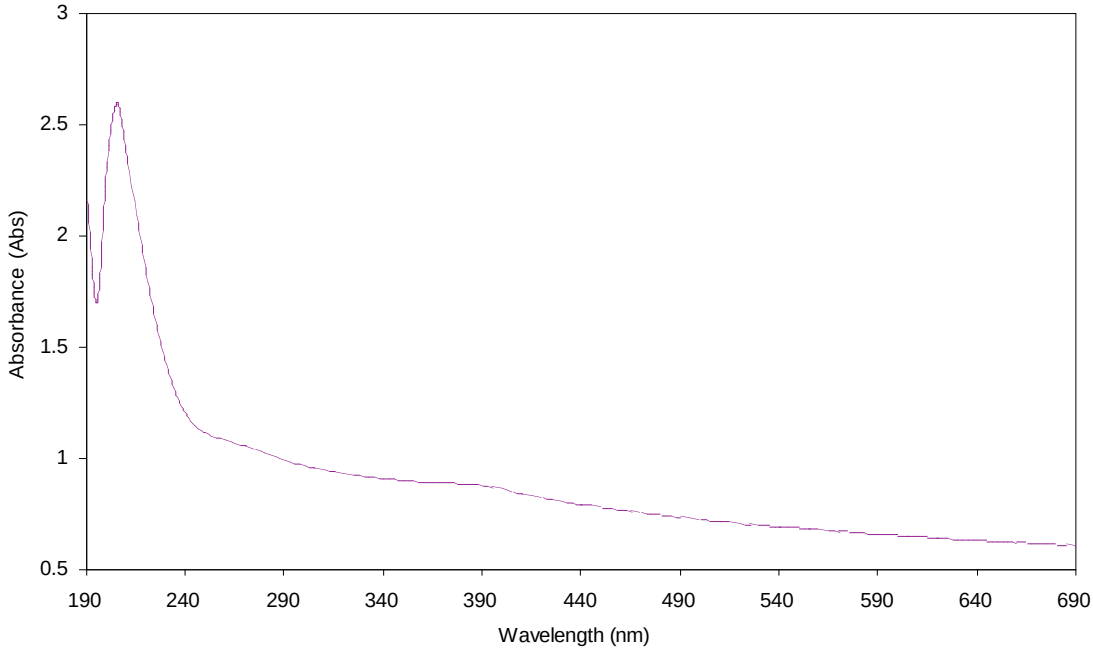

UV-vis spectrum of thiol stabilised Rh nanoparticles.

Figure 4.9

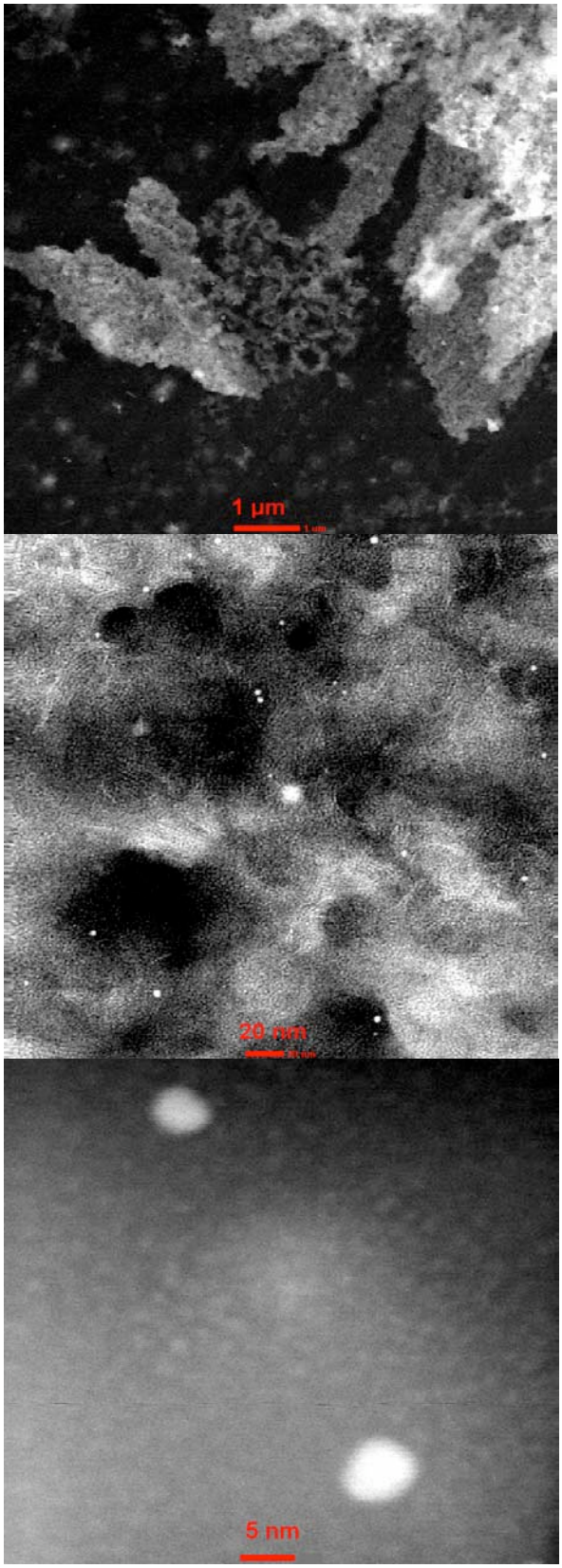

HAADF images of thiol-stabilised rhodium nanoparticles.

4.4.3 Discussion of Thiol-Stabilised Rhodium Nanoparticles

The UV-vis spectroscopy analysis of these particles shows a strong absorption at 205 nm, red shifted compared to the calculated spectra. This could be due to polydispersity, partial aggregation or irregular-shaped particles [31].

The HAADF analysis (figure 4.9) shows some small nanoparticles of about 6 nm in diameter. However, these are a minority population that are scattered against background material

This method is not suited for the production of rhodium nanoparticles, due to the poor particle separation and dispersion.

4.5 Thiol-Stabilised Platinum Nanoparticles

These seeds are produced according to method 7 (chapter 2, section 2.10). This experiment was carried out simultaneously with the thiol-stabilised rhodium experiment, the goal of which was to determine whether the gold seed production method could be adapted to other metals. These particles were analysed using UV-vis spectroscopy and HAADF analysis.

4.5.1 UV-vis Spectroscopy Analysis of Thiol-Stabilised Platinum Nanoparticles

The UV-vis spectroscopic analysis (Figure 4.10) of these platinum nanoparticles shows a strong peak at 225 nm. The published data for platinum nanoparticle sol UV-vis spectroscopic analysis mostly shows only a rather broad absorption continuum which extending throughout the visible-near ultraviolet range [31]. Henglein reported a broad absorption band at 215 nm for platinum nanoparticles of 12 nm [24]. The spectrum for the thiol-stabilised platinum nanoparticles is what could be expected for larger particles, as absorption bands for nanoparticles have been known to red-shift when the particle size is increased [4].

4.5.2 HAADF Analysis of Thiol-Stabilised Platinum Nanoparticles

The HAADF analysis of the thiol-stabilised platinum nanoparticles (Figure 4.11) reveals large areas of aggregated particles; these nanoparticles have a low density. A large population of particles approximately 1 nm in diameter can be found under the larger aggregated platinum particles.

Figure 4.10

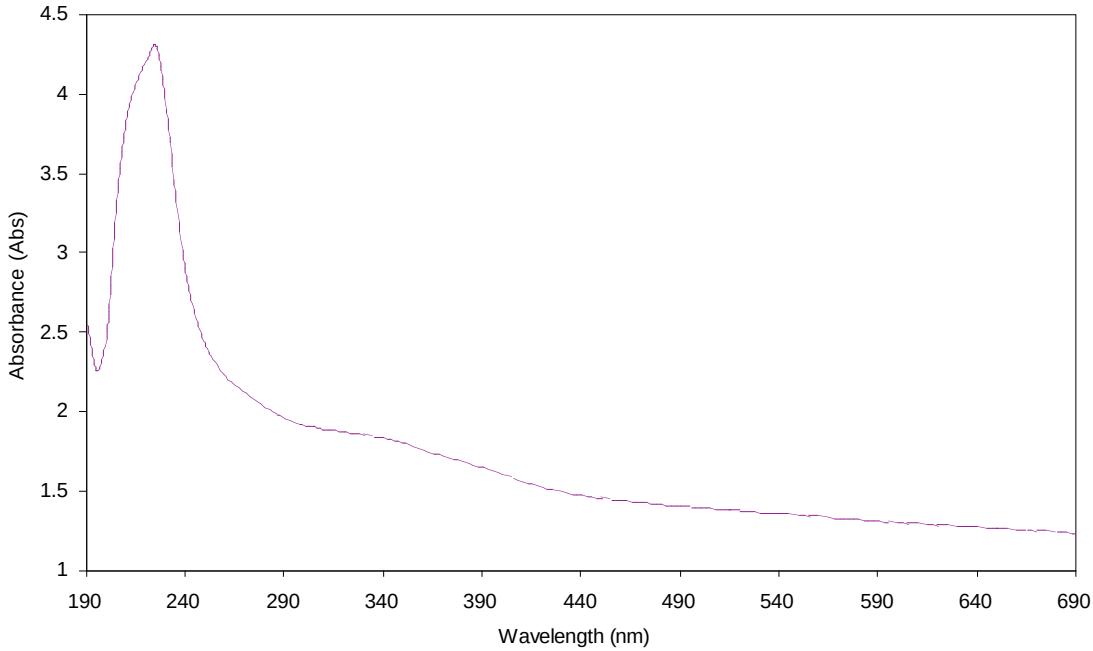

UV-vis spectrum of thiol stabilised platinum nanoparticles.

Figure 4.11

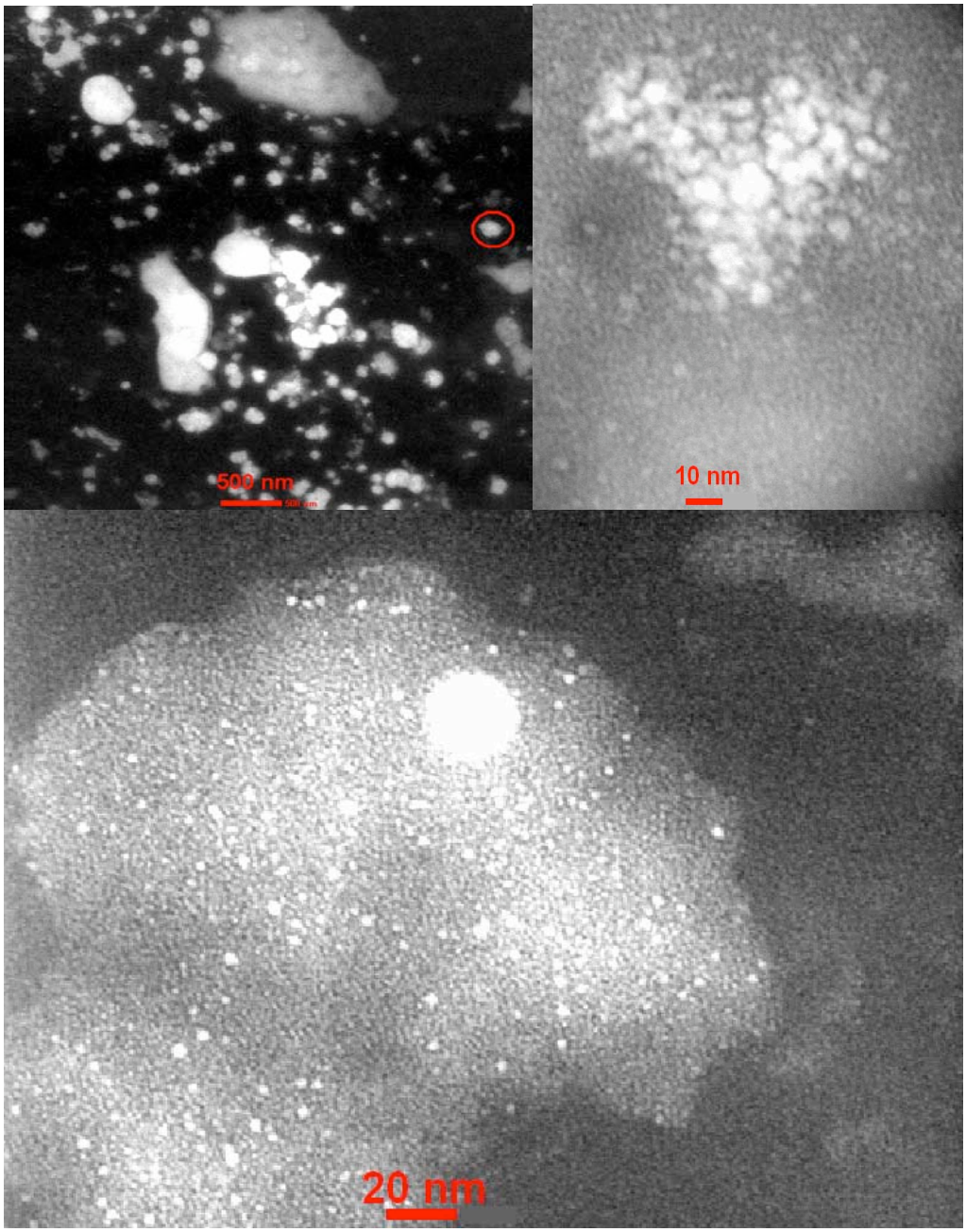

HAADF images of thiol-stabilised platinum nanoparticles.

4.5.3 Discussion of Thiol-Stabilised Platinum Nanoparticles

The UV-vis spectroscopic analysis of these platinum nanoparticles shows a strong peak at 225 nm. The spectra is similar to reported data, [24] however, it is what could be expected for larger platinum nanoparticles, as absorption bands for nanoparticles have been known to red-shift then the particle size is increased [4].

The HAADF analysis of the thiol-stabilised platinum nanoparticles reveals large areas of aggregated particles. A high density of particles approximately 1 nm in diameter can be found under the platinum nanoparticles.

Overall, method 7 has not produced nanoparticles similar to those of method 5 in shape and dispersion. Method 5 as reported by Yang *et al.* [5] is not suitable for adapting to all transition metals.

4.6 Discussion of Thiol-Stabilised Nanoparticles

The thiol-stabilised gold nanoparticles were very similar in appearance to those reported by Yang *et al*. [5]. This method has proven not to be transferable for platinum and rhodium. It is possible that by varying the reaction parameters, these methods could become more viable for platinum and rhodium nanoparticle production.

The thiol-stabilised $Au_{(core)}$-$Pd_{(shell)}$ bimetallic nanoparticle experiment was marginally more successful than the monometallic experiments, as some evidence was seen of bimetallic core-shell behaviour. However, this method would also benefit from a change in reaction parameters.

4.6.1 Comparison of Thiol-Stabilised Au Nanoparticles with Citrate-Stabilised Au Nanoparticles

The thiol stabilised particles withstood the electron microscope beam far better than the citrate stabilised particles. In comparison with the citrate stabilised gold seeds, the thiol stabilised gold seeds are more monodisperse and better separated, also the yield appears higher. Both sets of particles are similar in size, with the citrate stabilised particles having a mean size of 3.02 nm and the thiol stabilised particles having a mean size of 3.6±0.68 nm.

However, it may be possible, by adjusting the reaction parameters, that this method (7) could be used to produce other metal nanoparticles. Methods that could achieve this include: leaving out or changing the relative amount of thiol stabiliser, using a different thiolated stabiliser, or increasing the amount of metal salt available for reduction.

CHAPTER 5 – ELECTROCHEMICAL DEPOSITION OF PLATINUM ONTO GOLD NANOPARTICLES

5.1 Introduction to Electrochemical Deposition of Platinum onto Gold Nanoparticles

This chapter discusses the results of depositing platinum onto gold particles via galvanic displacement technique as reported by Kumar and Zou [11], who used this technique to coat colloidal gold with a platinum film. This method was chosen to see if it could be possible to generate bimetallic core-shell particles. This technique is shown to deposit onto both the citrate and the thiol-stabilised gold nanoparticles.

5.2 Electrochemical Deposition of Platinum onto Citrate-Stabilised Gold Nanoparticle Seeds

The cyclic voltammogram in Figure 5.1,of the citrate stabilised gold nanoparticles has a small oxidation onset at 1 V and a hydrogen evolution reaction at -0.5 V. After the sample was loaded onto the glassy carbon electrode substrate, it was then subjected to Cu underpotential deposition (UPD) and deposition of platinum by the galvanic replacement technique in accordance with method 9. Although the cyclic voltammogram for the gold seeds is not as expected, the Cu UPD is very similar to that reported by Mrozek *et al*. [14].

The platinum has deposited onto the gold seeds well, it is clear to see that with each successive sweep, more platinum is deposited onto the gold nanoparticles. This is consistent with the published data [11, 14]. Also as the potential is increased negatively, a more definitive platinum cyclic voltammogram is seen. The platinum

cyclic voltammograms are similar in appearance to those reported by Marković *et al*. [39].

Figure 5.1

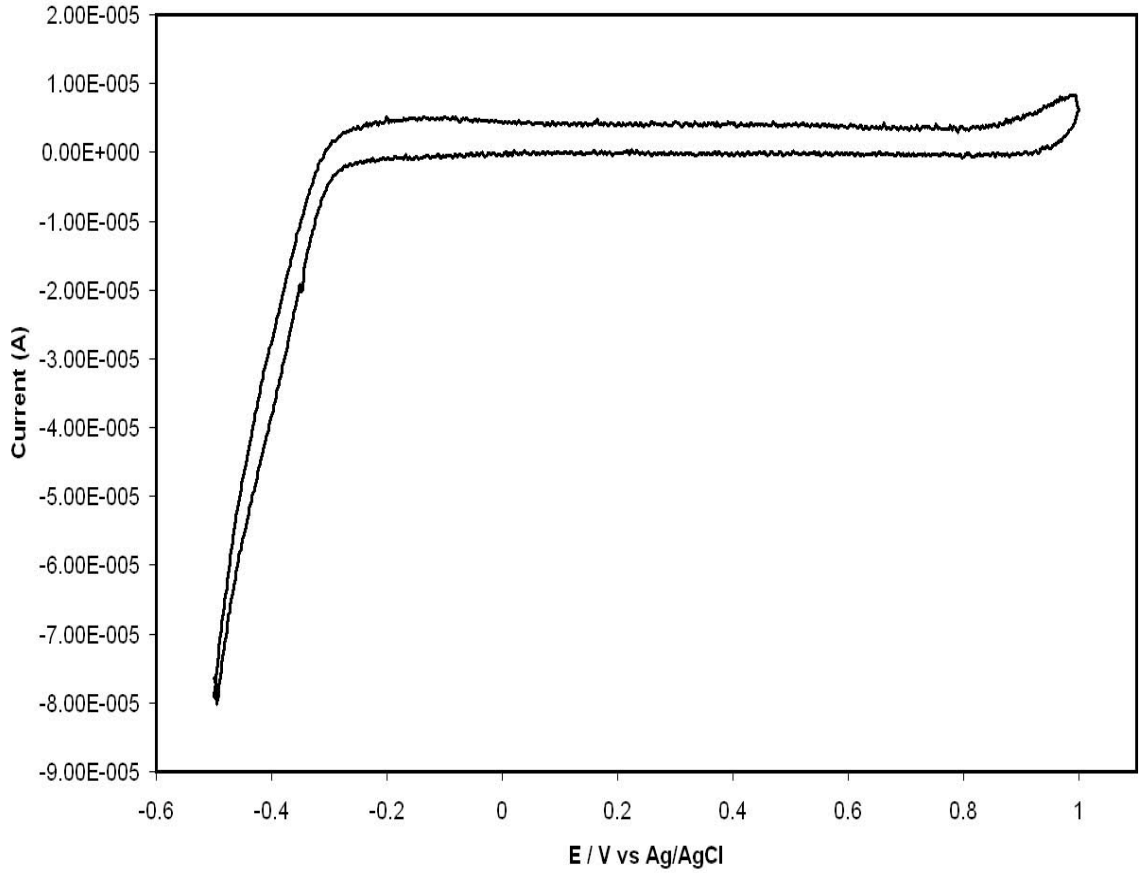

Cyclic voltammogram of citrate stabilised gold in 0.05 M H_2SO_4, scan rate: 0.05 V s^{-1}.

Figure 5.2

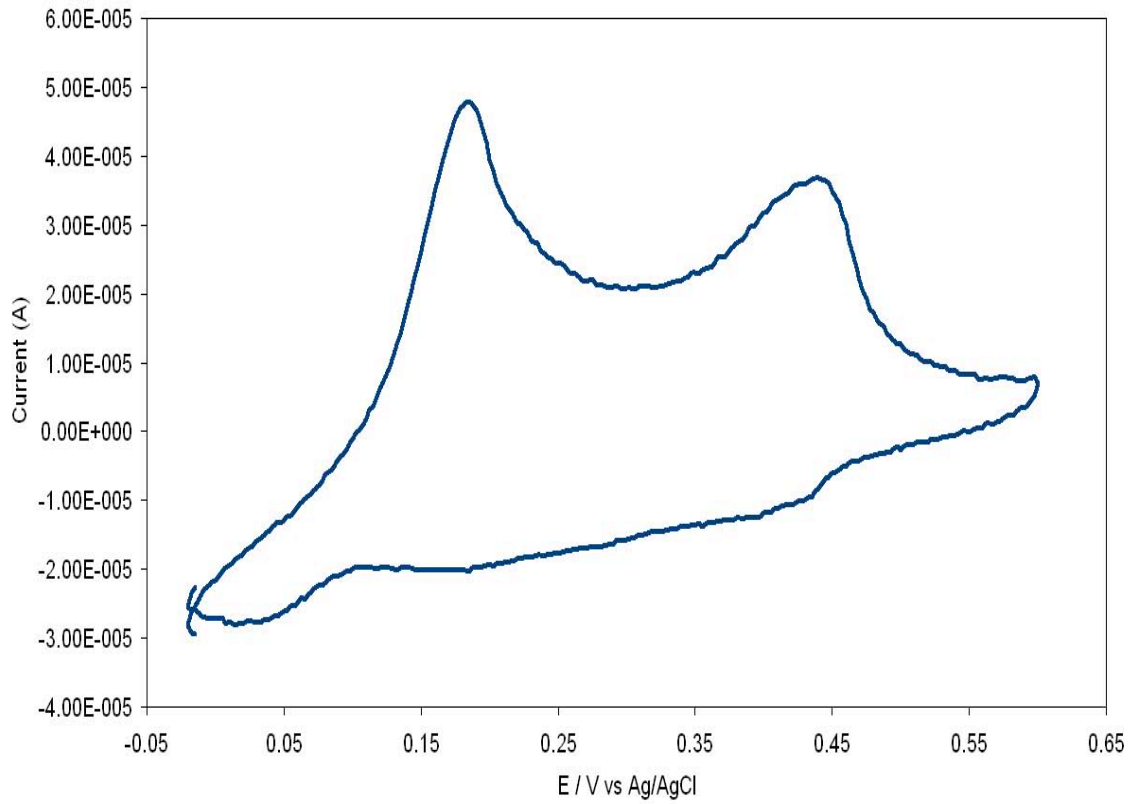

Cyclic voltammogram of citrate stabilised gold after Cu UPD in 1 mM $CuSO_4$ + 0.1 M H_2SO_4 after holding at -0.2 V for 2 minutes. Sweep rate: 0.1 V s^{-1}.

Figure 5.3

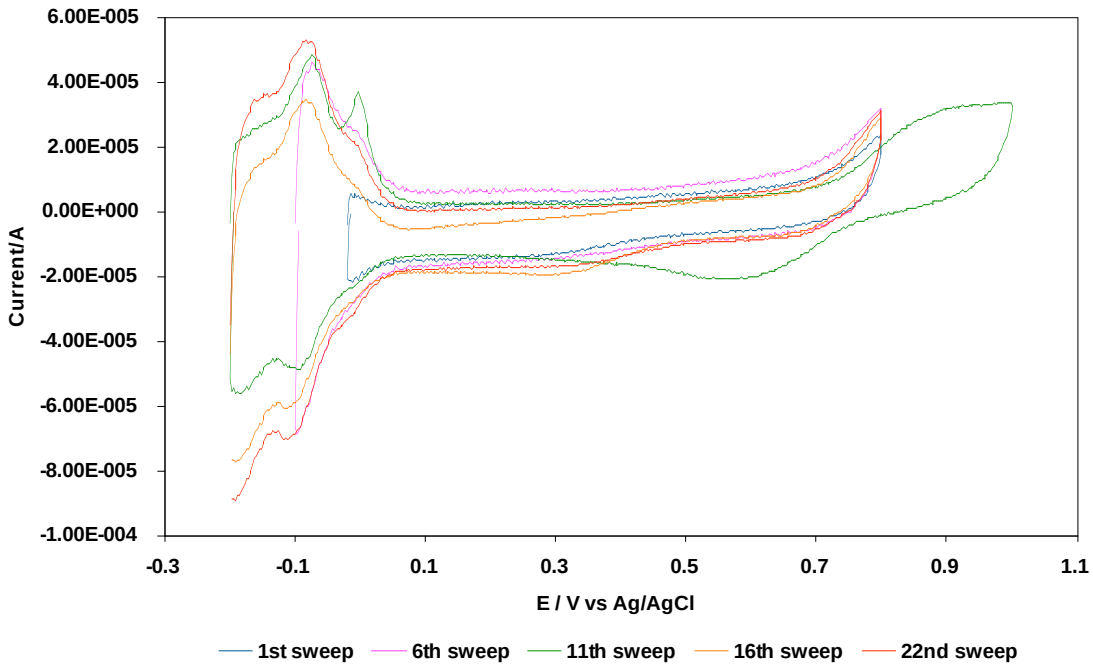

Cyclic voltammogram of citrate-stabilised gold nanoparticle seeds after platinum deposition, in 5 mM K_2PtCl_4 + 0.1 M $HClO_4$, increasing number of potential cycles

5.2.1 Discussion of Electrochemical Deposition of Platinum on to Citrate-Stabilised Gold Nanoparticle Seeds

The cyclic voltammogram for citrate stabilised gold nanoparticles was not what was expected. This result is not similar to any observed in the literature. This could be due to the citrate stabiliser interacting with the electrolyte. Although the initial cyclic voltammogram was unusual, the Cu UPD and platinum deposition cyclic voltammograms are much more like those reported in the literature [11, 14]. This is a fast, efficient way to coat gold seeds with platinum, and the progress of the platinum deposition can be observed in real time, which is very informative when compared with sol methods.

CHAPTER 6 - CONCLUSIONS

The aim of this project was to design a synthesis route for producing monodisperse bimetallic core-shell nanoparticles in the size region 2-10 nanometres. I feel that I have successfully achieved the aims of this project, especially concerning the citrate-stabilised $Au_{(core)}$-$Pd_{(shell)}$ bimetallic nanoparticles with 10% citrate stabiliser and a 1:4 metal ratio, for which the HAADF analysis clearly shows a core-shell structure.

Unfortunately, due to time constraints I was unable to investigate the catalytic properties of the particles that were produced. Also there have been some issues concerning equipment, the STEM has not always been operational and the AFM small scanner is currently unavailable, rendering the AFM useless for the work that I wished to undertake.

The particles that have been produced have been successfully characterised using AFM, HAADF imaging, UV-vis spectroscopy and cyclic voltammetry. These methods have produced information on the initial gold seeds used and any shell that was produced around the core.

This project has shown that the galvanic displacement technique for coating gold particles or surfaces with platinum is very easy to achieve. This could potentially be applied to other metals. Also the project has shown that methods previously

applied to a solid substrate, for example, an ITO glass slide [11], can also be performed in solution.

Unfortunately, attempting to use Yang *et al's.* [5] method of gold seed growth to produce either metal seeds or bimetallic core-shell systems was not very successful. Although some core-shell structure was seen in the Au-Pd system (fig 4.6), these were a very limited number in the sample. Also some particles were found in the Pt and Rh seed systems, these too were lacking in quantity and were mixed in with larger aggregates, as well as showing poor monodispersity and irregular shapes. However, by adjusting reaction parameters, such as: stabiliser, stabiliser concentration, metal concentration, reducing agent concentration and heating times, it could be possible to manipulate this method into a new technique.

The citrate-stabilised $Au_{(core)}$-$Pd_{(shell)}$ bimetallic nanoparticle system was the most focussed on as the initial results of $Au_{(core)}$-$Rh_{(shell)}$, $Au_{(core)}$-$Pt_{(shell)}$ and $Au_{(core)}$-$Pd_{(shell)}$ bimetallic nanoparticles, the $Au_{(core)}$-$Pd_{(shell)}$ bimetallic nanoparticle system had the least aggregation and showed the most evidence of core-shell structure (fig 3.21). It was because of this that the $Au_{(core)}$-$Pd_{(shell)}$ bimetallic nanoparticle system was chosen for the 1:4 metal ratio and 10% citrate stabiliser experiment (method 4). This is also the reason for palladium being chosen to attempt to cover the thiol-stabilised gold seeds, as it was felt that this system would be the most likely to succeed.

The focus with the $Au_{(core)}$-$Rh_{(shell)}$ bimetallic nanoparticle system was to see if the large triangular and square nanoparticles seen in the 30 minute sample (fig 3.12) were reproducible and if they were bimetallic in structure. Although this was not a part of the project initially, it seemed worthy of investigation. Henceforth, a rhodium control experiment was run exactly as the initial sample was prepared, with the exception of the gold metal salt being present, to see if the rhodium nucleated on its own to form these large particles. A second batch of samples was made in the same condition as the first experiment to see if the large particles would be visible in this second batch. However, it would appear that these large particles were a one-time phenomenon, and were not seen again. One reason for this could be contamination.

In conclusion, the project has been successfully completed, as a synthesis route for a bimetallic core-shell nanoparticle system has been produced. However, there is still the potential for more work to be carried out on these particles concerning kinetics and catalytic activity.

6.1 Future Work

There are many more investigations that could be carried out concerning the particles that have been produced in the course of this project. Firstly, more work could be done involving the citrate-stabilised bimetallic nanoparticle systems. It would be interesting to see if the Au-Pt and the Au-Rh system react in the same way as the Au-Pd system if treated with 10% citrate stabiliser and a1:4 metal ratio. Also, work could be undertaken citrate stabiliser, to find the optimum concentration and to investigate if aggregation of the samples can be further reduced.

The particles produced could be tested to see how catalytically active they are. In theory, the particles should be efficient catalysts as they could have synergistic effects from combining to metals together in the nanoscale, also the metals used are good catalysts [7, 11, 17, 24].

The Au-Pt systems produced by galvanic displacement need further characterisation, preferably by HAADF, as the UV-vis analysis did confirm the metals present. However, it did not give information on characteristics such as particle size. HAADF analysis would reveal whether the particles had a bimetallic core-shell configuration. However, it would be difficult to image electrode surfaces with HAADF analysis without damaging them and AFM in practice could be well suited for this purpose. These samples also need testing for catalytically activity.

Concerning the citrate-stabilised systems, kinetics work could be carried out within the first 30 minutes of reaction time to find out when the shells are formed. The UV-vis spectroscopic analysis carried out shows that the shells are formed after 30 minutes and do not change with extended reaction times. This could be preliminarily carried out with UV-vis spectroscopy, followed up with HAADF analysis.

LIST OF REFERENCES

[1] *Catal. Today*, T. Akita, T. Hiroki, S. Tanaka, T. Kofima, M. Kohyama, A. Iwase and F. Hori, 2008. **131**(1-4): p. 90.
[2] *J. Phys. Chem.*, *A*, Mohamed, M.B., Z.L. Wang, and M.A. El-Sayed, 1999. **103**(49): p. 10255.
[3] *Faraday Discuss.*, J. P. Li, F. Wilcoxon, Y. Yin, R. E. Chen, R. E. Palmer and R. L. Johnston. 2007. **138**: p. 363.
[4] *Chem. Mater.*, K. R. Brown, D.G. Walter, and M.J. Natan. 2000. **12**(2): p. 306.
[5] *Nanotechnology*, Y. Yang, Y. Yan, W. Wang and J. Li. 2008. **19**(17): p. 175603.
[6] *Chem. Rev.*, C. Burda, X. Chen, R. Narayanan and M. A. El-Sayed. 2005. **105**(4): p. 1025.
[7] *Faraday Discuss*, J. Jellinek. 2008. **138**: p. 11.
[8] *Angew. Chem. Int. Ed.*, D. Zhao and B-Q Xu. 2006. **45**(30): p. 4955.
[9] *Chem. Rev.*, R Ferrando, J. Jellinek, and R.L. Johnston. 2008. **108**(3): p. 845.
[10] *Chem. Mater.*, Z. Liang, A. Susha and F. Caruso. 2003. **15**(16): p. 3176.
[11] *Langmuir*, S. Kumar and S. Zou. 2007. **23**(13): p. 7365.
[12] *Chem. Mater.*, M. R. Knecht, M. G. Weir, A. I. Frenkel and R. M. Crooks. 2008. **20**(3): p. 1019.
[13] *J. Colloid and Interface Sci.*, C-S. Lin, M. K. Khan and S. D. Lin. 2006. **299**(2): p. 678.
[14] *Anal. Chem.*, M. F. Mrozek, Y. Xie and M. J. Weaver. 2001. **73**(24): p. 5953.
[15] *Discuss. of the Faraday Soc.*, J. Hiller, P. Stevenson and J. Turkevich. 1951. **11**: p. 55.
[16] *J. Chem. Soc., Chem. Comm.*, M. Brust, M. Walker, D, Bethell, D. J. Schiffrin and R. Whyman. 1994: p. 801.
[17] *Small*, J. Rin and R. D. Tilley. 2007. **3**(9): p. 1508.
[18] *J. Chem. Soc., Faraday Trans. 1*, N. Furlong, A. Launikonis and W. H. F. Sasse. 1984. **80**(3): p. 571.
[19] *J. Res. Inst. for Catal., Hokkaido Uni.*, Turkevich, S. Namba, I. Okura, L. L. Ban and K. Aika. 1976. **24**(1): p. 54.
[20] *J. Phys. Chem.*, A. Henglein, B.G. Ershov, and M. Malow. 1995. **99**(38): p. 14129.
[21] *Mater. Letts.*, Y. Luo and X. Sum. 2007. **61**(10): p. 2015.
[22] *Chem. Mater.*, J. H. Kim, H.W. Chung, and T.R. Lee. 2006. **18**(17): p. 4115.
[23] *Chem. Mater.*, L. Cao, L. Tong, P. Diao, T. Zhu and Z. Liu. 2004. **16**(17): p. 3239.
[24] *J. Phys. Chem. B*, A. Henglein. 2000. **104**(10): p. 2201.
[25] Morita, S., R. Wiesendanger, and E. Meyer, eds. *Noncontact Atomic Force Microscopy*. 1st ed. Nanoscience and Technology, ed. P. Avouris, et al. 2002, Springer.
[26] *http://www.chembio.uoguelph.ca/educmat/chm729/afm/details.htm*, D. Thomas, Editor. 1997.
[27] *http://www.chembio.uoguelph.ca/educmat/chm729/afm/introdn.htm*, D. Thomas, Editor. 1997.
[28] *http://www.chembio.uoguelph.ca/educmat/chm729/afm/operate.htm*, D. Thomas, Editor. 1997.

[29] *Sensors and Actuators B: Chem.*, Y. Joseph, B. Guse, A. Yasuda and T. Vossmeyer. 2004. **98**(2-3): p. 188.
[30] *Philos. Trans.*, M. Faraday. 1857. **147**: p. 145.
[31] *J. Chem. Soc., Faraday Trans.,* J. A. Creighton and D. G. Eadon. 1991. **87**(24): p. 3881.
[32] Ann. Phys., G. Mie. 1908. **25**: p. 329.
[33] *J. Colloid Sci. Suppl.*, J.Turkevich, G. Garton and P. C. Stevenson. 1954. **9**: p. 26.
[34] *Langmuir*, A. Henglein. 1999. **15**(20): p. 6738.
[35] *Phys. Chem. Chem. Phys.*, J. A. Lopez-Sanchez, N. Dimitratos, P. Mieleziak, E. Ntainjua, J. K .Edwards, D. Morgan, A. F. Carley, R. Tiruvalam, C. J. Kiely and G. J. Hutchings. 2008. **10**: p. 1921.
[36] *Nano Letts*., D. Ferrer, A. Torres-Castro, X. Gao, S. Sepúlveda-Guzman, U. Ortiz-Mendez & M. José-Yacamán. 2007. **7**(6): p. 1701.
[37] *Surf. Sci.*, S. R. Brankovic, J.X. Wang, and R.R. Adžić. 2001. **474**(1-3): p. L173.
[38] *Surf. Sci.*, O. Cavalleri, O., S.E. Gilbert, and K. Kern. 1997. **377-379**: p. 931.
[39] Marković, N.M., V.R. &, and J. P. N. Ross, eds. *Weickowski: Synthetic Coordination and Organometallic Chemistry*. 2001, Marcel Dekker Inc.